Fossil Record 29 (2) 2026, 611–674 | DOI 10.3897/fr.29.195537

PENSOFT

MUSEUM FÜR NATURKUNDE BERLIN

Osteology, paleoecology, and phylogenetic relationships of the carettochelyid turtle *Allaeochelys crassesculpta* from the middle Eocene Konservat-Lagerstätte of Messel, Germany

Yann Rollot[1,2,3], Marcus Zuber[4], Elias Hamann[4], Walter G. Joyce[1]

1 *Department of Geosciences, University of Fribourg, 1700 Fribourg, Switzerland*
2 *Denver Museum of Nature & Science, Denver, CO 80205, USA*
3 *Department of Biomedical Sciences, Heritage College of Osteopathic Medicine, Ohio University, Athens, OH 45701, USA*
4 *Institute for Photon Science and Synchrotron Radiation, Karlsruhe Institute of Technology, 76344 Eggenstein-Leopoldshafen, Germany*

https://zoobank.org/DFC1F821-E887-4AE4-B1B8-4EABC5F7CE00

Corresponding author: Yann Rollot (yann.rollot@gmail.com)

Academic editor: Florian Witzmann ♦ **Received** 14 April 2026 ♦ **Accepted** 15 July 2026 ♦ **Published** 14 August 2026

Abstract

Allaeochelys crassesculpta is a carettochelyid turtle from the middle Eocene Messel Pit, near Messel, Germany. The species is known by one of the richest fossil records among turtles consisting of dozens of specimens, of which most represent near-complete and articulated skeletons. Despite this richness, the osteology of *Allaeochelys crassesculpta* is only known superficially as its anatomy was never described in detail. Here, we use micro-computed laminography and tomography to investigate the anatomy of the skull, shell, and appendicular skeleton and provide high-resolution 3D reconstructions of the cranium, mandible, and fore- and hindlimb. *Allaeochelys crassesculpta* exhibits an interesting mosaic of features, which are typical of early branching carettochelyids (e.g. a deeper and larger antrum postoticum, a foramen posterius canalis carotici interni located more anteriorly) and more advanced taxa (e.g. presence of a maxilla-quadratojugal contact below the jugal, complete loss of carapace and plastral scutes). We assemble and analyze a new phylogenetic matrix to test the impact of recent anatomical works on the evolutionary history of carettochelyids. We also provide evidence that *Allaeochelys crassesculpta* was capable of 'synchronous rowing,' the unique locomotor mode employed by the extant pig-nosed turtle *Carettochelys insculpta* and suggest that the acquisition of this peculiar trait may have occurred during the Late Cretaceous to Paleocene.

Key Words

Anatomy, *Carettochelyidae*, laminography, Lutetian, palaeoecology, phylogeny, tomography, *Trionychia*

Introduction

Carettochelyidae is a clade of aquatic cryptodiran turtles with a single living taxon, the pig-nosed turtle *Carettochelys insculpta*, that lives as a relict species in the southern part of New Guinea and the Northern Territory of Australia (Ramsay 1887; Joyce 2014; TTWG 2025). The fossil record of carettochelyids is moderately rich with 21 valid species currently known from the late Early Cretaceous to middle Miocene (Joyce 2014; Havlik et al. 2014; Godinot et al. 2018; Carbot-Chanona et al. 2020; White et al. 2023; Hutchison and Westgate 2024; Kim et al. 2025; Rollot et al. 2025). The earliest representatives of the group are from the Cretaceous of Asia, in particular *Byeoljubuchelys yeosuensis* from the Aptian–Albian of South Korea (Kim et al. 2025), *Kizylkumemys khoratensis* from the Aptian of Thailand (Tong et al. 2005), and *Kizylkumemys schultzi* from the Cenomanian of Uzbekistan (Nessov 1976), and the group is, therefore, deemed to have originated in Asia, plausibly during the Late Jurassic (Joyce et al. 2013; Joyce 2014; Pereira et al. 2017; Thomson et al. 2021). A notable peak of diversity occurred during the Eocene, as about half of extinct taxa are known from that time, including

Copyright *Yann Rollot et al.* This is an open access article distributed under the terms of the Creative Commons Attribution License (CC BY 4.0), which permits unrestricted use, distribution, and reproduction in any medium, provided the original author and source are credited.

Allaeochelys crassesculpta from the middle Eocene Messel Pit of Germany (Joyce 2014).

While most fossil carettochelyids are known from fragmentary and incomplete remains, *Allaeochelys crassesculpta* stands out by being known by more than 100 fossils from Messel, of which most represent near-complete articulated skeletons (Harrassowitz 1922; Joyce 2014; Cadena et al. 2018). Harrassowitz (1922) originally established two distinct species, *Anosteira crassesculpta* and *Anosteira gracilis*, but the latter is now considered to be a junior synonym of *Allaeochelys crassesculpta* (Gramann 1956; Joyce 2014). Skeletons of *Allaeochelys crassesculpta* found as pairs were even shown to represent the first record of copulating fossil vertebrates (Joyce et al. 2012). *Allaeochelys crassesculpta* is, therefore, not only a remarkable taxon among carettochelyids, but also among turtles in general. Although this species is known from such rich material, it was described initially based on relatively incomplete specimens by Harrassowitz (1922), with only minor additions from Weitzel (1949), Groessens-Van Dyck (1978) and Joyce et al. (2012). It is otherwise commonly figured in books on Messel (e.g., Schaal and Ziegler (1992); Smith et al. (2018)).

As part of a project that aims to provide new insights into the evolutionary history of carettochelyids, we here provide a detailed analysis of the anatomy, paleoecology, and phylogenetic relationships of *Allaeochelys crassesculpta*. We use micro-computed laminography and tomography to provide high-resolution 3D reconstructions of the cranium, mandible, and appendicular skeleton, and document the osteology of *Allaeochelys crassesculpta* using more than 50 specimens. Our 3D reconstruction of a complete forelimb also allows us to explore for the first time the locomotor mode of *Allaeochelys crassesculpta*. We hereby show that *Allaeochelys crassesculpta* was plausibly as well-adapted to swimming as *Carettochelys insculpta* and that the unique way of swimming of carettochelyids ("synchronous rowing"; Rivera et al. 2013; Krahl 2021) likely evolved relatively early in the evolutionary history of the group. Finally, we also assembled a new morphological matrix that includes all valid carettochelyid taxa as well as all the micro-computed tomography-based anatomical insights provided in the last years with our project (Rollot et al. 2024a, 2024b, 2025), which we analyzed using both parsimony and Bayesian Inference.

Institutional abbreviations

AMNH, American Museum of Natural History, New York, USA; **ANSP**, Academy of Natural Sciences of Drexel University, Philadelphia, USA; **BMNH**, Natural History Museum London, London, UK; **BSPG**, Bayerische Staatssammlung für Paläontologie und Geologie, Munich, Germany; **FHM**, Fossilien- und Heimatmuseum Messel, Messel, Germany; **FMNH**, Field Museum of Natural History, Chicago, USA; **HLMD**, Hessisches Landesmuseum Darmstadt, Darmstadt, Germany; **IRSNB**, Institut Royal des Sciences Naturelles de Belgique, Brussels, Belgium; **IVPP**, Institute of Vertebrate Paleontology and Paleoanthropology, Beijing, China; **KU**, University of Kansas, Biodiversity Institute and Natural History Museum, Lawrence, USA; **MAGNT**, Museum and Art Gallery of the Northern Territory, The Gardens, Australia; **NHMUK**, Natural History Museum, London United Kingdom; **PCHP**, Turtle Conservancy, Ojai, USA; **PMOL**, Paleontological Museum of Liaoning, Shenyang, China; **SDZ**, San Diego Zoo, San Diego, USA; **SMF**, Senckenberg Naturmuseum, Frankfurt, Germany; **SMNK**, Staatliches Museum für Naturkunde Karlsruhe, Karlsruhe, Germany; **TMM**, Texas Science & Natural History Museum, Austin, USA; **YPM**, Yale Peabody Museum, New Haven, USA.

Material and methods

Selection of specimens

Allaeochelys crassesculpta is known from more than a hundred specimens from the middle Eocene Messel Pit (early Lutetian, MP11) that often represent nearly complete articulated skeletons preserved in volcanic maar lake deposits. For an extensive summary of the geology and dating of Messel Pit, please refer to Smith et al. (2018). We here mostly focus on the material housed at HLMD and SMF as these two public collections hold the most extensive and best prepared collections. Three juvenile skeletons were included from IRSNB and FHM, while one articulated specimen and one disarticulated specimen with a nicely preserved mandible were added to the sample from SMNK. We only figure the most complete and best-preserved specimens but provide pictures of the other specimens studied at the HLMD and SMF in a supplementary file (see Suppl. material 1). All specimens used in our study are listed in Table 1.

A large number of specimens include skulls that superficially look to be well-preserved. We subjected a selection of specimens (HLMD Me7592, HLMD Me14997, SMF Me611, SMF Me3004, and SMF Me3566) to X-ray micro-computed laminography (μCL) and tomography (μCT, see below) only to conclude that all specimens are heavily crushed internally. We thus here only provide complete segmentation for the best-preserved skull, SMF Me3004, but supplement our descriptions with observations obtained from all μCL data, though without figures.

Scanning, segmentation, and digital reconstruction

Scanning of material was performed at the Institute for Photon Science and Synchrotron Radiation of the Karlsruhe Institute of Technology, Germany using a custom-designed setup for computed laminography and tomography. For all scans, a flat panel detector (XRD

Table 1. List of specimens of *Allaeochelys crassesculpta* from the middle Eocene Messel Pit selected for the present study.

Specimen number	Comments	Figures
SMF Me3004	Cranium	Figs 1–10
SMNK Pal45053	Skeleton, incomplete and disarticulated, including mandible	Fig. 11
HLMD Be158	Skeleton, nearly complete	Fig. 12
HLMD Be159	Skeleton, nearly complete	Fig. 13
HLMD Me1461	Shell, nearly complete	Fig. 14
HLMD Me4282	Skeleton, nearly complete	Fig. 15
HLMD Me7428	Carapace, posterior half	Fig. 16
HLMD Me7429	Carapace, nearly complete	Fig. 17
HLMD Me13721	Skeleton, nearly complete	Fig. 18
HLMD Me15012	Skeleton, nearly complete	Fig. 19
HLMD Me15956	Skeleton, nearly complete	Fig. 20
SMF Me611	Skeleton, nearly complete	Figs 21, 30, 31, 32
SMF Me1794	Skeleton, including shell and right humerus	Fig. 22
SMF Me2449	Pair of skeletons, nearly complete	Fig. 23
SMF Me3018	Skeleton, nearly complete	Fig. 24
SMF Me3566	Skeleton, nearly complete	Figs 25, 26
SMF Me3783	Skeleton, incomplete, including most of the carapace, damaged right half of plastron, right fore- and both hindlimbs, and damaged skull	Fig. 27
SMF Me11418	Skeleton, incomplete, with heavily eroded and damaged plastron, and lacking most of the hindlimbs	Fig. 28
SMNK Pal986	Skeleton, nearly complete	Fig. 29
IRSNB MeR007	Skeleton, juvenile	Fig. 33
IRSNB MeR015	Skeleton, juvenile	Fig. 33
HLMD Be169	Skeleton, juvenile	Fig. 33
SMF Me11381	Skeleton, juvenile	Fig. 33
HLMD Be217	Skeleton, crushed	Suppl. material 1: fig. S1.1
HLMD Me4000	Carapace, incomplete	Suppl. material 1: fig. S1.2
HLMD Me4283	Skeleton, including fragmentary carapace and nearly complete plastron	Suppl. material 1: fig. S1.3
HLMD Me4353a	Skeleton, including the skull, anterior half of the carapace, and plastron	Suppl. material 1: fig. S1.4
HLMD Me5001	Carapace, incomplete	Suppl. material 1: fig. S1.5
HLMD Me7427	Skeleton, crushed	Suppl. material 1: fig. S1.6
HLMD Me7592	Skeleton, nearly complete	Suppl. material 1: fig. S1.7
HLMD Me7593	Pair of skeletons, nearly complete	Suppl. material 1: fig. S1.8
HLMD Me7599	Skeleton, incomplete	Suppl. material 1: fig. S1.9
HLMD Me7892	Skeleton, nearly complete but greatly damaged, except the plastron	Suppl. material 1: fig. S1.10
HLMD Me9722	Skeleton, nearly complete	Suppl. material 1: figs S1.11, S1.12
HLMD Me9795	Skeleton, nearly complete	Suppl. material 1: figs S1.13, S1.14
HLMD Me10375	Skeleton, heavily crushed	Suppl. material 1: fig. S1.15
HLMD Me13397	Skeleton, fragmentary and disarticulated	Suppl. material 1: fig. S1.16
HLMD Me13436	Skeleton, nearly complete	Suppl. material 1: figs S1.17, S1.18
HLMD Me13484	Skeleton, nearly complete	Suppl. material 1: fig. S1.19
HLMD Me14919	Skeleton, nearly complete but folded	Suppl. material 1: fig. S1.20
HLMD Me14920	Skeleton, nearly complete	Suppl. material 1: figs S1.21, S1.22
HLMD Me14997	Skeleton, nearly complete but disarticulated	Suppl. material 1: fig. S1.23
HLMD Me14998	Skeleton, nearly complete	Suppl. material 1: figs S1.24, S1.25
HLMD Me14999	Skeleton, incomplete	Suppl. material 1: figs S1.26, S1.27
HLMD Me15273	Skeleton, incomplete	Suppl. material 1: fig. S1.28
HLMD Me15563	Skeleton, damaged and disarticulated	Suppl. material 1: fig. S1.29
HLMD Me15660	Carapace, incomplete and damaged, including appendicular elements	Suppl. material 1: fig. S1.30
HLMD Me42827	Skeleton, incomplete	Suppl. material 1: fig. S1.31
SMF Me2010	Skeleton, nearly complete but fragmented	Suppl. material 1: figs S1.32, S1.33
SMF Me2606A & B	Skeleton, incomplete	Suppl. material 1: figs S1.34, S1.35
SMF Me3779	Skeleton, incomplete, including partial parts of the carapace, plastron, skull, and appendicular elements	Suppl. material 1: figs S1.36, S1.37
FHM 45	Skeleton, nearly complete	Suppl. material 1: fig. S1.38
FHM 46	Skeleton, juvenile	Suppl. material 1: fig. S1.39
HLMD Be235	Skeleton, nearly complete	Not figured (HLMD exhibition)
HLMD Me15372	Skeleton, nearly complete	Not figured (HLMD exhibition)

1621 CN14 ES, PerkinElmer, Waltham, USA) with a physical pixel size of 200 µm and a DRZ+ scintillator and a microfocus X-ray tube (XWT-225, X-RAY WorX, Garbsen, Germany) were employed. The 3D volumes were reconstructed from the recorded projection images using the ufo/tofu toolkit (Faragó et al. 2022). The most suitable parameters for the X-ray tube, spectrum filtration, detector and scanning geometries were selected for sampled specimens. The different geometries are described in Zuber et al. (2017). A µCL configuration was set up to scan several anatomical areas of interest of SMF Me611, the mandible of SMNK Pal45053, and the skulls of HLMD Me7592, HLMD Me14997, and SMF Me3566, which are preserved in epoxy plates, while a µCT configuration was used to scan SMF Me3004, an isolated crushed cranium. SMF Me611 is a nearly complete skeleton that preserves most of the animal's body, including the left fore- and hindlimb, which were subjected to scanning. Scanning of the left fore- and hindlimb was performed using a voltage of 180 kV, a target power of 15 W, 2048 projections, and a 1 mm copper filter. Both scanning sessions resulted in 1104 horizontal slices with a voxel size of 36.5 µm. Scanning of the skulls of HLMD Me7592, HLMD Me14997, and SMF Me3566 was performed using a voltage of 180 kV, a target power of 15 W, 2048 projections, and a 1 mm copper filter. Each scanning session resulted in 1104 horizontal slices with a voxel size of 36.5 µm. Scanning of the cranium SMF Me3004 was performed using a voltage of 180 kV, a current of 110 µA, 4476 projections, and a 0.1 mm copper filter. The scanning resulted in 2640 coronal slices with a voxel size of 25 µm. Scanning of the mandible of SMNK Pal45053 was performed using a voltage of 180 kV, a target power of 35 W, 4096 projections, and a 0.5 mm copper filter. The scanning resulted in 400 horizontal slices with a voxel size of 40 µm.

All datasets were segmented using Mimics Innovation Suite 25 (https://www.materialise.com/en/healthcare/mimics-innovation-suite) with the lasso and interpolation tools. All segmented bones were exported as .ply files. The 3D models were imported into Blender 4.2 (https://www.blender.org) to create the illustrations and figures. We also used Blender 4.2 to manually reassemble the crushed cranium SMF Me3004, which consists of 151 bony elements that are sufficiently complete, well-preserved, and minimally displaced to allow their identification and to reassemble the left fore- and hindlimb of SMF Me611, to provide a reconstruction of the limbs that reflects the life posture of the appendicular skeleton. To provide the best possible and accurate reconstruction of the cranium, we compared SMF Me3004 to other crania of *Allaeochelys crassesculpta* available to us and also used figures and illustrations from the literature that document the cranial anatomy of carettochelyids (*Anosteira maomingensis*: Danilov et al. (2017a); *Anosteira pulchra*: Joyce et al. (2018); *Allaeochelys libyca*: Rollot et al. (2024a); *Allaeochelys meylani*: Rollot et al. (2025); *Carettochelys niahensis*: White et al. (2023); and *Carettochelys insculpta*: Rollot et al. (2024b)). All datasets and 3D models are available on MorphoSource (https://www.morphosource.org/projects/000839347).

Measurement of limb proportions and paleoecological inferences

To investigate the paleoecology of *Allaeochelys crassesculpta*, we followed the protocol and method implemented by Joyce and Gauthier (2004) to study the paleoecology of turtles based on limb proportions. We measured the length of the humerus from the preaxial process to the distal articular surface, the total length of the ulna along its lateral margin, and the combined length of metatarsal III and digit III in the segmented forelimb of SMF Me611. Measurements were taken to the tenth of a millimeter in Mimics, based on the 3D models obtained from our segmentations. We then calculated the ratio of each measurement relative to the entire limb length (obtained from the addition of the lengths of the humerus, ulna, metatarsal III and digit III) and plotted our results into a ternary diagram with the original data and habitat preferences as defined by Joyce and Gauthier (2004). Our measurements and calculations are listed in Table 2.

Table 2. Measurements and ratios in the left forelimb of SMF Me611.

Bones measured	Length (mm)	Ratio relative to full limb length
humerus	29	29.32%
ulna	17.9	18.10%
metatarsal and digit III	52	52.58%
total length	**98.9**	**100.00%**

Phylogenetic analysis

The phylogenetic relationships of *Allaeochelys crassesculpta* and carettochelyids were investigated using a newly assembled morphological matrix. This new matrix is primarily based on that of Joyce (2007) and all subsequent matrices that were based on the latter to study carettochelyid relationships (Havlik et al. 2014; Danilov et al. 2017a; Carbot-Chanona et al. 2020; Kim et al. 2025). All characters that depict carettochelyid anatomy in these matrices were selected, with the addition of a few characters useful for pan-trionychian relationships in general, as *Adocus lineolatus* and *Lissemys punctata* were included in our sample of taxa. The matrix newly includes *Anosteira crowcreekensis* from the late Eocene of Arkansas, USA (Hutchison and Westgate 2024), *Allaeochelys rouzilhacensis* from the early-middle Eocene of France (Godinot et al. 2018), *Eulalichelys labarrerei* from the early-middle Eocene of France (Godinot et al. 2018), *Carettochelys niahensis* from the Late Oligocene of Malaysia (White et al. 2023), and *Allaeochelys meylani* from the Early

Miocene of Egypt (Rollot et al. 2025), which had not yet been included in previous phylogenetic analyses of carettochelyid relationships. We also include *Anosteira shantungensis* from the Early Miocene of China (Cheng 1961). This taxon was previously suggested to be a junior synonym of *Anosteira mongoliensis* based on its similar morphology and presumably similar age (Late Eocene-Early Oligocene; Joyce (2014)), but more recent studies suggest a middle middle Eocene age for the correlated Ulan Shireh and Irdin Manha Formations (Wang et al. 2012; Bai et al. 2018; Wang et al. 2019), from which *Anosteira mongoliensis* was collected, and an Early Miocene age for the Niushan Formation (Sun et al. 2002; He et al. 2011; Yu et al. 2021), which yielded the partial skeleton of *Anosteira shantungensis*. We, therefore, consider these two turtles to be distinct taxa and scored them separately in our matrix. Twenty-nine new characters were phrased (characters 2, 3, 5, 8, 10, 11, 15, 16, 17, 18, 19, 20, 30, 32, 33, 34, 36, 38, 40, 41, 42, 45, 46, 47, 48, 53, 54, 55, and 62) based on recent works on carettochelyid anatomy and the review of historical material and data from the literature. Twenty characters form morphoclines that can be ordered (characters 5, 8, 11, 19, 24, 26, 29, 31, 39, 41, 42, 48, 51, 54, 55, 56, 58, 59, 63, and 66). The final matrix consists of 24 taxa and 66 characters: 42 for the cranium, six for the mandible, 15 for the shell, and three for the appendicular skeleton. The character list, including illustrations and figures for each character, are provided in Suppl. material 2, the Mesquite matrix for parsimony analysis in TNT is available in Suppl. material 3, and the matrix for Bayesian tip-dating analysis in MrBayes in Suppl. material 4. The list of carettochelyid taxa considered valid in the present study is available below (Table 3).

Table 3. List of carettochelyid taxa considered valid in the present study, sorted by stratigraphic age from oldest to youngest.

Valid taxa	References and additional specimens studied
Kizylkumemys khoratensis	Tong et al. (2005)
Byeoljubuchelys yeosuensis	Kim et al. (2025)
Kizylkumemys schultzi	Nessov (1977, 1986, 1987); Danilov and Obraztsova (2015); Danilov et al. (2017b)
Allaeochelys lingnanica	Young and Chow (1962)
Allaeochelys rouzilhacensis	Godinot et al. (2018)
Eulalichelys labarrerei	Godinot et al. (2018)
Anosteira ornata	Leidy (1873; Hay (1906, 1908) AMNH 6132; ANSP 9846
Allaeochelys crassesculpta	Harrassowitz (1922); this study
Anosteira manchuriana	Zangerl (1947) FMNH P15102
Anosteira mongoliensis	Gilmore (1931) AMNH 6666; AMNH 6697
Allaeochelys delheidi	Dollo (1886); Jiménez Fuentes (1992); Alonso Santiago and Alonso Andrés (2005); Alonso Santiago et al. (2008) BMNH 12778; BMNH 38965; BMNH 38953; BMNH 40099; IRSNB R19
Anosteira pulchra	Clark (1932); Joyce et al. (2018); Adrian et al. (2020) TMM 41576-27; YPM PU16317; YPM PU16318
Allaeochelys parayrei	Noulet (1867); de Stefano (1902); Bergounioux (1931); Broin (1977)
Allaeochelys magnifica	Hutchison et al. (2004)
Anosteira maomingensis	Chow and Liu (1955); Tong et al. (2010); Danilov et al. (2017a) IVPP V816; PMOL AR6
Anosteira crowcreekensis	Hutchison and Westgate (2024)
Carettochelys niahensis	White et al. (2023)
Anosteira shantungensis	Cheng (1961) IVPP V2585
Allaeochelys liliae	Carbot-Chanona et al. (2020)
Allaeochelys meylani	Rollot et al. (2025)
Allaeochelys libyca	Rollot et al. (2024a)
Carettochelys insculpta	Walther (1922); Evers et al. (2022); Hermanson et al. (2024); Rollot et al. (2024b) AMNH 85893; AMNH 92674; BMNH 1903.7.10.1; PCHP 14; PCHP 3116; PCHP 4800; SDZ unnumbered; TMM M18053

The first round of phylogenetic analyses was performed under parsimony in TNT 1.6 (Goloboff and Morales 2023). As the matrix is small, a traditional search analysis was conducted under equal-weighting with characters ordered and one thousand random addition sequences, followed by a round of tree bisection reconnection, and 100 trees saved per replication. Trees suboptimal by 10 steps and with a relative fit difference of 0.1 were retained as part of the first search. A tree collapsing rule was implemented with a minimum length of 0. *Adocus lineolatus* was chosen as the outgroup.

We also performed a Bayesian tip-dating analysis using MrBayes 3.2.7 (Ronquist et al. 2009) on the online platform CIPRES (https://www.phylo.org; Miller et al. (2010)), with *Adocus lineolatus* as the outgroup. *Lissemys punctata* was constrained as sister-taxon to carettochelyids as the relationships between pan-trionychian subclades are well-established and because the monophyly of *Carettochelyidae* is not disputed. Characters 5, 8, 11, 19, 24, 26, 29, 31, 39, 41, 42, 48, 51, 54, 55, 56, 58, 59, 63, and 66 were treated as ordered, as in the parsimony analysis. We defined three character partitions, one for the skull (characters 1–48), one for the shell (characters 49–63), and one for the postcranium (characters 64–66). We used fixed age priors for extant taxa and uniform age priors for fossil taxa. Uniform age priors for the fossils were modelled around the first and last known appearance dates of the latter, based on the geological formations or stratigraphic ages associated with the fossils. The Mkv-model of Lewis (2001) was chosen as the substitution model and includes an ascertainment bias correction for morphological data. Rate variation across characters in the model is drawn from a gamma distribution. We applied an Independent Gamma Rates (IGR) relaxed-clock model (Lepage et al. 2007), with the gamma distribution set to have a variance following an exponential (10) distribution (Zhang 2016) and defined the clock rate prior to follow a normal distribution with a mean of 0.001 and a variance of 0.01 (Ezcurra et al. 2020). Divergence times were estimated under a fossilized birth-death (FBD) model, for which we used default settings

for the priors on the speciation (exponential 10 distribution), extinction (beta distribution with values of 1 and 1), and fossilization (beta distribution with values of 1 and 1) rates. The sampling proportion was set to 0.056 (2/36, based on extant trionychians according to TTWG 2025) and we specified a diversified sampling strategy. The tree age prior was specified using an offset exponential function, with the mean set to be 175 Ma and the minimum set to be 130 Ma. The analysis was performed using Markov Chain Monte Carlo (MCMC) with four runs of six chains each. Temperature of the heated chains was set to 0.005 and the number of attempted chain swaps was set to 3. Chains were run for 20,000,000 generations, with trees sampled every 500 generations. The first 25% of sampled trees were discarded as burn-in. Convergence diagnostics were examined to ensure adequate mixing and stationarity. The Estimated Sample Size (EES) values for all parameters clearly exceeded 200 in each run individually and the Potential Scale Reduction Factor (PSRF) values for all parameters reached 1.000 to 1.001. Topological convergence between runs was indicated by the average standard deviation of split frequencies dropping below 0.01, with a finishing value of 0.0025 after 20,000,000 generations.

Systematic palaeontology

Testudines Batsch, 1788
Cryptodira Cope, 1868
***Trionychia* Baur, 1891**
***Carettochelyidae* Gill, 1889**
***Allaeochelys* Noulet, 1867**

Allaeochelys crassesculpta (Harrassowitz, 1922)

= *Anosteira gracilis* Harrassowitz, 1922. (for the full taxonomic history, see Joyce (2014))

Type material. • HLMD 4353 (specimen no. 3 of Harrassowitz (1922)), syntype, a poorly-preserved shell (Harrassowitz 1922, pl. 2.2; Suppl. material 1: fig. S1.4); • HLMD 4283 (specimen no. 4 of Harrassowitz (1922)), syntype, hyoplastra, hypoplastra and xiphiplastra (Harrassowitz 1922, pl. 6.4; Suppl. material 1: fig. S1.3); • HLMD 1461 (specimen no. 6 of Harrassowitz (1922)), syntype, nearly complete skeleton embedded in a concretion (Harrassowitz (1922), pl. 6.1; Fig. 14).

Referred material. This list comprises all specimens from Messel Pit that are, to our knowledge, available in public collections and that can be undoubtedly referred to *Allaeochelys crassesculpta*, but we suspect there are many more. For figures, please consult Table 1 and Suppl. material 1. BSPG 1982 I 74, a nearly complete skeleton; FHM 45, a nearly complete skeleton; FHM 46, a nearly complete juvenile skeleton; HLMD Be158, a nearly complete skeleton; HLMD Be159, a nearly complete skeleton; HLMD Be169, a juvenile skeleton; HLMD Be217, a crushed and folded skeleton; HLMD Be 235, a nearly complete skeleton; HLMD Me3173, a partial skeleton; HLMD Me3377, a fragmentary skeleton; HLMD Me4000, a partial carapace (syntype of *Allaeochelys gracilis*, specimen no. 5 of Harrassowitz (1922)); HLMD Me4282 (syntype of *Allaeochelys gracilis*, specimen no. 1 of Harrassowitz (1922)), a nearly complete skeleton (Harrassowitz 1922; pl. 1.3, pl. 4.2, pl. 4.4, pl. 6.5, pl. 6.6); HLMD Me5001, a partial carapace; HLMD Me7427, a nearly complete, but folded shell; HLMD Me7428, posterior half of carapace; HLMD Me7429, a nearly complete carapace; HLMD Me7592, a nearly complete skeleton; HLMD Me7593, a nearly complete pair of skeletons; HLMD Me7599, a partial skeleton; HLMD Me7892, a partial skeleton; HLMD Me9722, a nearly complete skeleton; HLMD Me9795, a nearly complete skeleton; HLMD Me10375, a partial skeleton; HLMD Me13397, a fragmentary skeleton; HLMD Me13432, a costal; HLMD Me13436, a nearly complete skeleton; HLMD Me13484, a nearly complete skeleton; HLMD Me13721, a nearly complete skeleton; HLMD Me14919, a nearly complete, folded skeleton; HLMD Me14920, a nearly complete skeleton; HLMD Me14997, a nearly complete skeleton; HLMD Me14998, a nearly complete skeleton; HLMD Me14999, a nearly complete skeleton; HLMD Me15012, a nearly complete skeleton; HLMD Me15273, a partial skeleton; HLMD Me15372, a nearly complete skeleton; HLMD Me15563, a partial skeleton; HLMD Me15660, a fragmentary skeleton; HLMD Me15956, a nearly complete skeleton; HLMD Me42827, a nearly complete skeleton; IRSNB MeR001, a nearly complete skeleton; IRSNB MeR002, a nearly complete skeleton; IRSNB MeR006, a nearly complete skeleton; IRSNB MeR007, a juvenile skeleton; IRSNB MeR010, a nearly complete pair of skeletons; IRSNB MeR011, a nearly complete skeleton; IRSNB MeR012, a nearly complete, but crushed cranium; IRSNB MeR014, a nearly complete skeleton; IRSNB MeR015, a juvenile skeleton; IRSNB MeR018, a nearly complete skeleton; IRSNB MeR020, a nearly complete skeleton; IRSNB MeR022, a nearly complete skeleton; IRSNB MeR024, a nearly complete skeleton; IRSNB MeR025, a juvenile skeleton; IRSNB MeR029, a nearly complete skeleton; IRSNB MeR030, a nearly complete skeleton; IRSNB MeR031, a nearly complete skeleton; IRSNB MeR032, a nearly complete skeleton; IRSNB MeR034, a nearly complete skeleton; SMF Me373, a nearly complete skeleton; SMF Me436, a partial skeleton; SMF Me441, a partial skeleton; SMF Me514, a nearly complete skeleton; SMF Me611, a nearly complete skeleton; SMF Me718, a partial shell; SMF Me938, partial posterior part of carapace; SMF Me1444, a nearly complete skeleton; SMF Me1794, a complete shell; SMF Me1808, a partial skeleton; SMF Me1809, a nearly complete skeleton; SMF Me2009, a partial skeleton; SMF Me2010, a partial skeleton; SMF Me2034, a partial pair of skeletons; SMF Me2449, a nearly complete skeleton; SMF Me2606, a partial skeleton; SMF Me3004, an isolated and crushed cranium; SMF Me3018, a nearly complete skeleton; SMF Me3566, a nearly complete pair of skeletons;

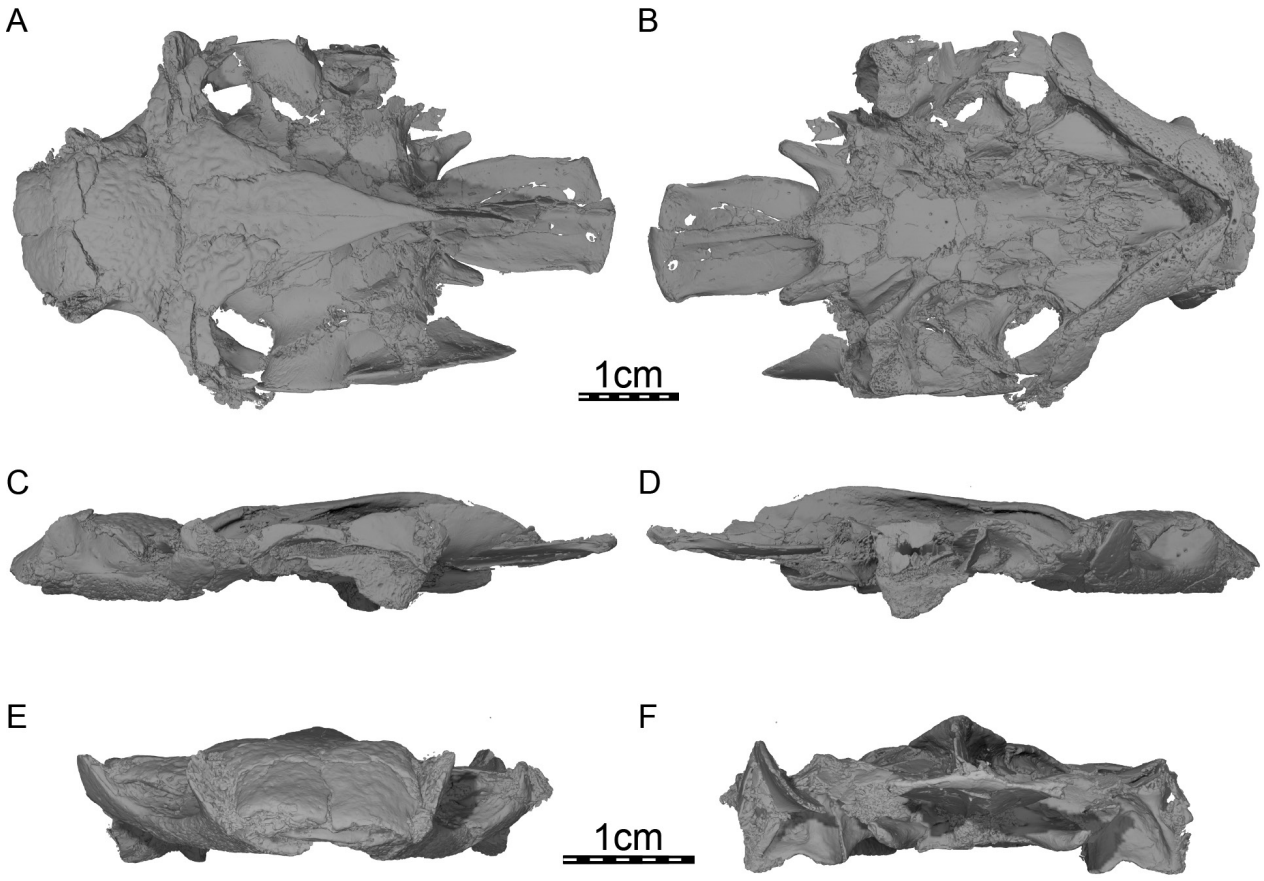


Figure 1. Three-dimensional renderings of a cranium of *Allaeochelys crassesculpta* (SMF Me3004). **A.** Dorsal view; **B.** Ventral view; **C.** Left lateral view; **D.** Right lateral view; **E.** Anterior view; **F.** Posterior view.

SMF Me3775, a partial skeleton; SMF Me3779, a partial skeleton; SMF Me3783, a partial skeleton; SMF Me3787, a partial skeleton; SMF Me11381, a juvenile skeleton; SMF Me11418, a partial skeleton; SMF Me11573, a partial skeleton; SMNK Pal986, a nearly complete skeleton; SMNK Pal45053, a fragmentary skeleton.

Type locality and horizon. Messel Pit, near the village of Messel, State of Hesse, Germany (Harrassowitz 1922: fig. 6); MP11, early Lutetian (ca. 47 Ma), middle Eocene (Joyce et al. 2012).

Amended diagnosis. *Allaeochelys crassesculpta* can be diagnosed as a representative of *Carettochelyidae* by a bone surface ornamentation consisting of thick ridges separated by equally-sized grooves, presence of a quadrate fossa, presence of a midline keel on the dorsal surface of the carapace, a single suprapygal, presence of a lip formed on the visceral side of the posterior peripherals and pygal, plastral kinesis, a triangular entoplastron, and reduction of plastral scutes. *Allaeochelys crassesculpta* can be diagnosed as a member of Carettochelyinae by the presence of a maxilla-quadratojugal contact below the jugal, absence of a contact between the quadratojugal and squamosal, presence of elongate tubercula basioccipitale, complete loss of carapace and plastral scutes, and an equilateral entoplastron. *Allaeochelys crassesculpta* can be differentiated from other carettochelyines by having a straight labial margin of the maxilla, an anteroposteriorly short postorbital, a moderately deep quadrate fossa, a large antrum postoticum, a foramen posterius canalis carotici interni located close to the parabasisphenoid-pterygoid suture at about mid-length of the parabasisphenoid, a pterygoid fossa ventrally open and not covered by an enfolded ridge of the pterygoid, a supraoccipital excluded from the skull roof, and a flat ventral surface of the basioccipital.

Description.

Cranium

General comments. SMF Me3004 is a crushed, flattened cranium (Fig. 1). After segmentation and reconstruction, it appears that none of the bones is completely preserved.

All reconstructed bones are incomplete. The prefrontals, frontals, premaxilla, maxillae, jugals, quadrates, and parabasisphenoid are fairly well-preserved, whereas the vomer, pterygoids, and opisthotics are highly incomplete (Fig. 2). As the cranium is heavily compressed dorsoventrally, the secondary wall of the braincase is the area that suffered most. In the μCT dataset, we were not able to identify any pieces in that area as belonging to either bone forming the secondary braincase wall of other carettochelyids and most of the material that can visually be attributed to bone and not matrix was either too crushed or too small to be identified with confidence. These fragments were, thus, omitted from the segmentations and reconstructions. Consequently, most anatomical structures located in that area, such as the foramen nervi

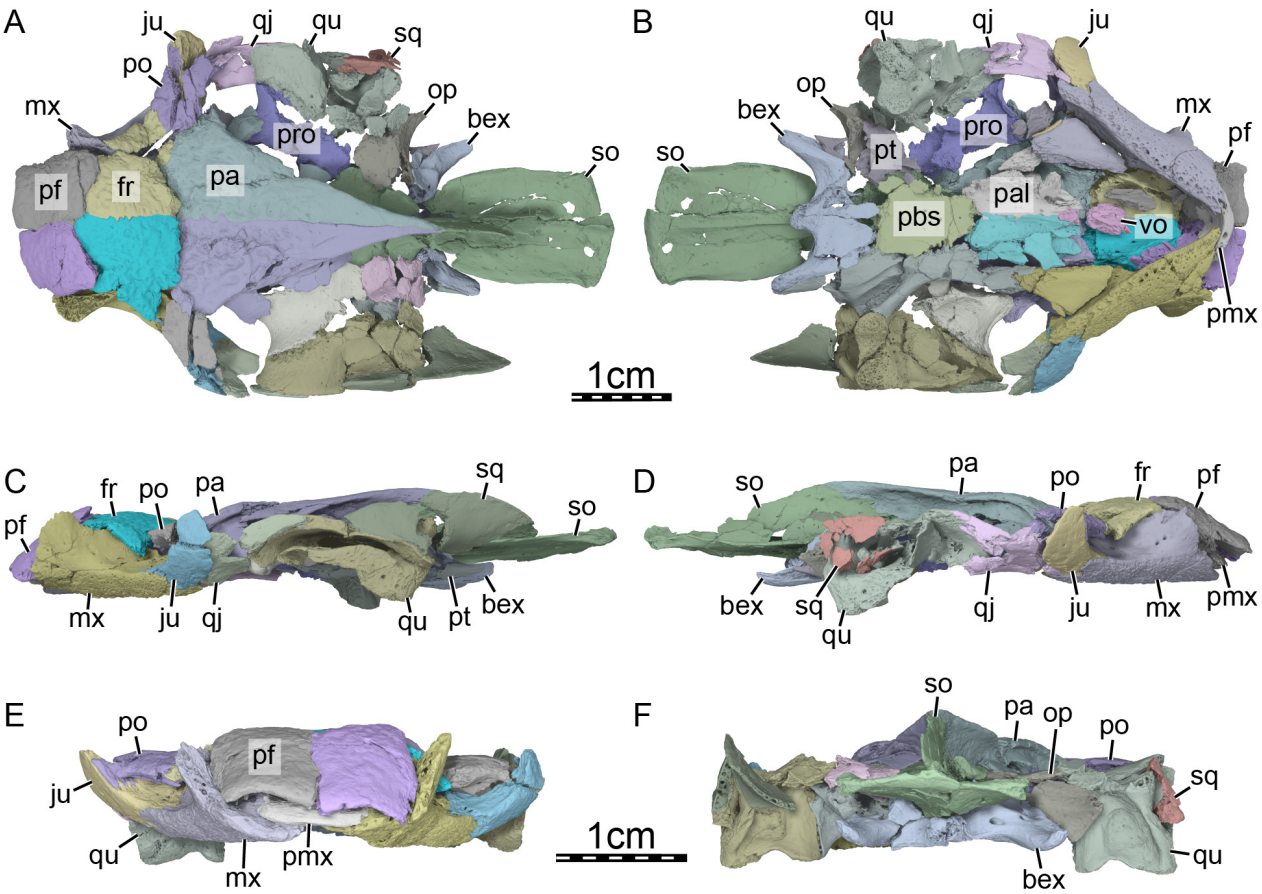


Figure 2. Three-dimensional renderings of a segmented cranium of *Allaeochelys crassesculpta* (SMF Me3004). **A.** Dorsal view; **B.** Ventral view; **C.** Left lateral view; **D.** Right lateral view; **E.** Anterior view; **F.** Posterior view. Abbreviations: bex, basioccipital-exoccipital complex; fr, frontal; ju, jugal; mx, maxilla; op, opisthotic; pa, parietal; pal, palatine; pbs, parabasisphenoid; pf, prefrontal; pmx, premaxilla; po, postorbital; pro, prootic; pt, pterygoid; qj, quadratojugal; qu, quadrate; so, supraoccipital; sq, squamosal; vo, vomer.

trigemini or cavum labyrinthicum, are either incomplete or missing completely. Likewise, the epipterygoids, which were likely present by reference to other pan-trionychians, could not be segmented and described as they were completely crushed and destroyed.

SMF Me3004 preserves the typical surface ornamentation of carettochelyids, which is made of thick ridges separated by equally-sized grooves that are mostly visible on the prefrontals, frontals, and parietals (Figs 2, 3). The surface ornamentation of the cranium, however, is less pronounced than on the shell. As in all carettochelyids (Waite 1905; Walther 1922; Havlik et al. 2014; Joyce 2014; Danilov et al. 2017a; Joyce et al. 2018; White et al. 2023; Rollot et al. 2024a, 2024b, 2025), the cranium has a deep upper temporal emargination, a posteriorly expanded supraoccipital crest that ventrally forms a broad horizontal plate, an incisura columella auris that is fully enclosed by the quadrate, a quadrate fossa, a low mandibular condyle, and a contact between the palatines and parabasisphenoid that prevents the pterygoids from contacting one another medially (Figs 2, 3).

Nasal. Nasals are absent in *Allaeochelys crassesculpta*, as in all carettochelyids (Waite 1905; Walther 1922; Danilov et al. 2017a; Joyce et al. 2018; White et al. 2023; Rollot et al. 2024a, 2025).

Prefrontal. The prefrontals of SMF Me3004 are generally well-preserved and only damaged ventrally at the level of their descending process, of which only two small pieces remain preserved on the right side (Figs 2A–E, 3A–E). The prefrontal contacts the maxilla ventrolaterally along its ascending process and the frontal posteriorly (Figs 2A–E, 3A–E). The dorsal plate of the prefrontal forms the dorsal margin of the apertura narium externa. The rim of the apertura narium externa, which is otherwise also formed by the maxilla and premaxilla, is thin (Figs 2E, 3E), as in most carettochelyids (Havlik et al. 2014; Danilov et al. 2017a; Joyce et al. 2018; White et al. 2023; Rollot et al. 2024a), except for *Allaeochelys delheidi* (YR, pers. obs. on NHMUK PAL PV OR 38953) and *Allaeochelys meylani* (Rollot et al. 2025) in which the bones forming the aperture are greatly thickened. The prefrontal also forms the anterodorsal margin of the orbit and roofs the fossa nasalis. The dorsal plate of the prefrontal is rectangular and longer than wide, as in *Anosteira pulchra* (Joyce et al. 2018) and *Carettochelys insculpta* (Rollot et al. 2024b), which contrasts with the prefrontal of *Allaeochelys libyca* (Havlik et al. 2014; Rollot et al. 2024a) and *Allaeochelys meylani* (Rollot et al. 2025), where the dorsal plate is about as long as wide. The descending process of the prefrontal of SMF Me3004

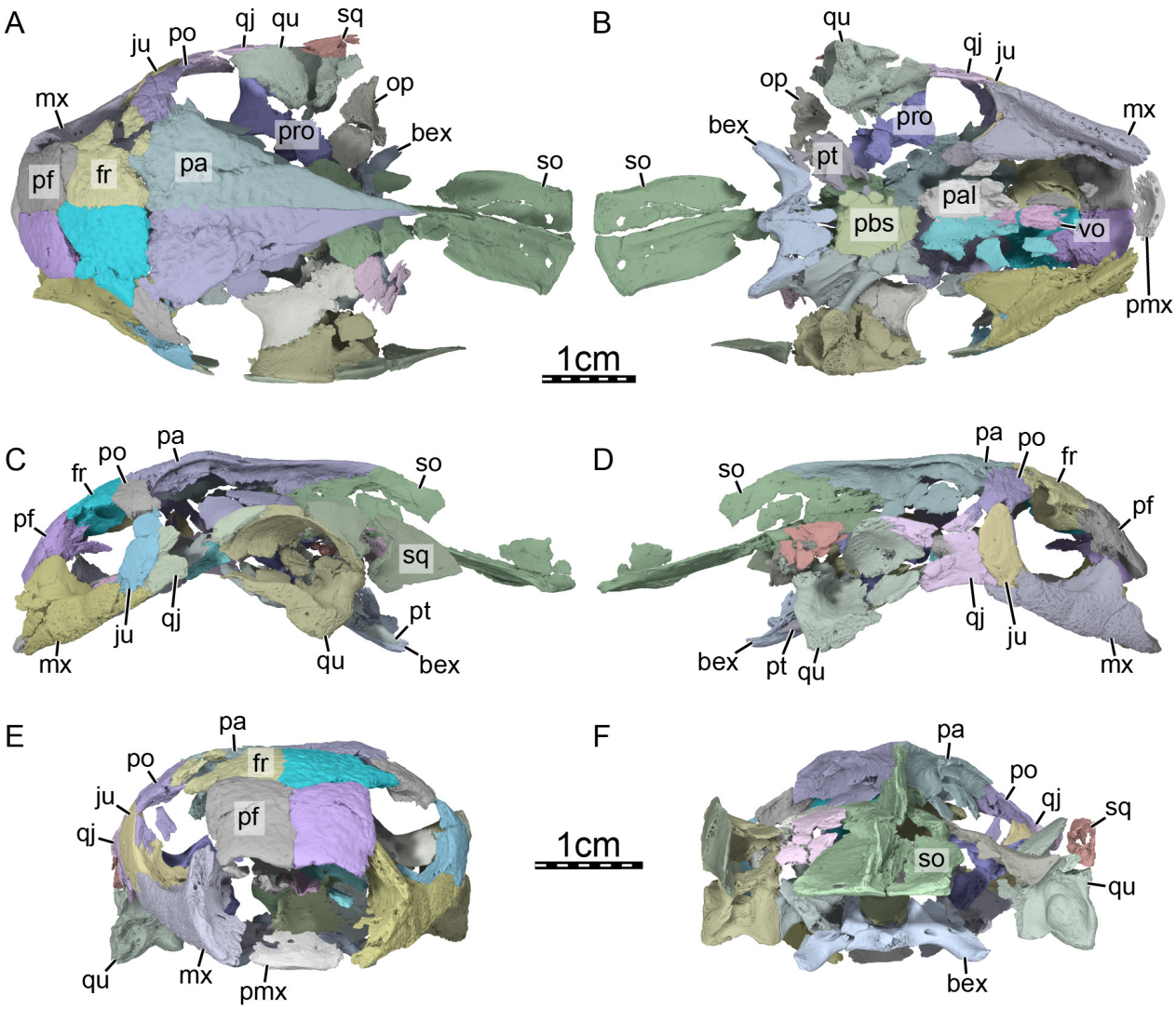


Figure 3. Three-dimensional renderings of a segmented and reconstructed cranium of *Allaeochelys crassesculpta* (SMF Me3004). **A.** Dorsal view; **B.** Ventral view; **C.** Left lateral view; **D.** Right lateral view; **E.** Anterior view; **F.** Posterior view. Abbreviations: bex, basioccipital-exoccipital complex; fr, frontal; ju, jugal; mx, maxilla; op, opisthotic; pa, parietal; pal, palatine; pbs, parabasisphenoid; pf, prefrontal; pmx, premaxilla; po, postorbital; pro, prootic; pt, pterygoid; qj, quadratojugal; qu, quadrate; so, supraoccipital; sq, squamosal; vo, vomer.

is almost completely lacking on both sides (Fig. 3C, D). Only two small pieces are preserved on the right side. The larger of these two pieces corresponds to the end of the posterior process of the descending process of the prefrontal, which contacts the vomer ventromedially. The dorsal surface of this element is smooth, suggesting that a contact with the crista cranii of the frontal is absent. This is confirmed by specimens HLMD Me7592 and HLMD Me14997, in which most of the posterior process is preserved. *Allaeochelys crassesculpta* thus lacks an ophthalmic foramen, but possesses an ophthalmic slit instead, as in *Anosteira pulchra* (Joyce et al. 2018) and *Carettochelys insculpta* (Rollot et al. 2024b).

Frontal. The two frontals of SMF Me3004 are nearly complete, albeit broken into several pieces that had to be reassembled for the reconstruction of the cranium (Figs 2A, 3A). The frontal contacts the prefrontal anteriorly, the postorbital posterolaterally, the parietal posteriorly, and its counterpart medially (Figs 2A, C, D, 3A, C–E, 4). The frontal slightly protrudes anteromedially between the prefrontals by means of a short process. The process is particularly well-developed on the left frontal, which contacts the two prefrontals, whereas the right frontal process only contacts the right prefrontal. The frontal forms the dorsal margin of the orbit margin (Figs 2A, D, 3A, C–E, 4). The contribution of the frontal to the orbit margin is large as in *Anosteira maomingensis* (Danilov et al. 2017a), *Anosteira pulchra* (Joyce et al. 2018), and *Carettochelys niahensis* (White et al. 2023) and contrasts with the moderate contribution seen in *Allaeochelys libyca* (Havlik et al. 2014) and the small contribution seen in *Allaeochelys meylani* (Rollot et al. 2025). In the extant *Carettochelys insculpta*, the contribution of the frontal to the orbit margin appears to vary from small to moderate, but these differences might be linked to ontogeny, as small specimens have a moderate contribution, whereas large specimens exhibit a small one (Waite 1905; Walther 1922; Rollot et al. 2024b). Ventrally, the frontal of SMF

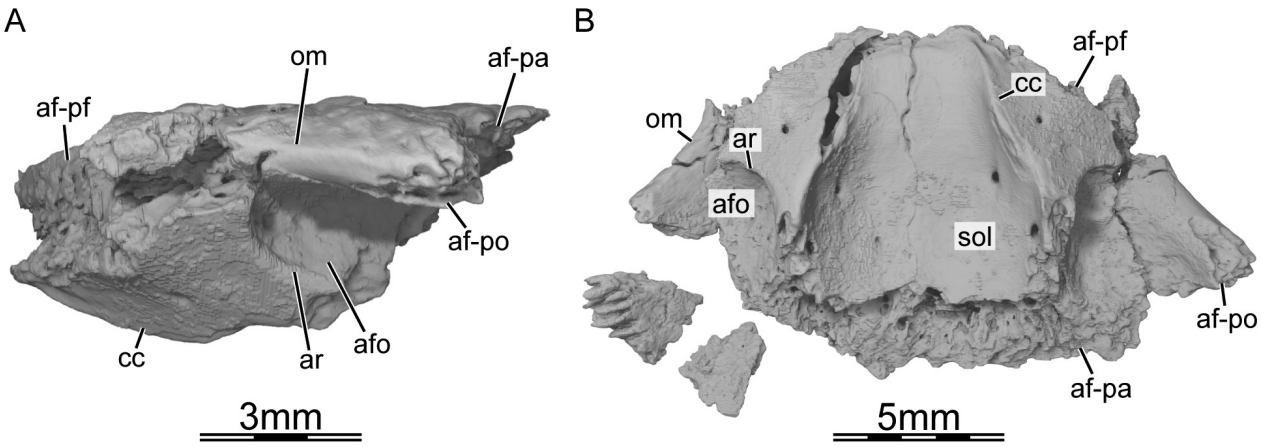


Figure 4. Three-dimensional renderings of the reconstructed frontals of *Allaeochelys crassesculpta* (SMF Me3004). **A.** Lateral view of left frontal; **B.** Ventral view of left and right frontals. Abbreviations: af-pa, articulation facet for parietal; af-pf, articulation facet for prefrontal; af-po, articulation facet for postorbital; afo, accessory fossa; ar, accessory ridge; cc, crista cranii; om, orbit margin; sol, sulcus olfactorius.

Me3004 forms a robust and well-developed crista cranii (Fig. 4). The crista cranii posteriorly forms an articular facet on both frontals, showing that a contact was present with the descending process of the parietal along the entire height of the crista, likely constricting the foramen interorbitale dorsally. Ventral contact of the crista cranii with the dorsal aspect of the descending process of the prefrontal is absent, as explained above (see Prefrontal; Fig. 4). Additional evidence to postulate the absence of this foramen is visible on the left crista cranii of SMF Me3004, as the ventral edge of the crista cranii does not form an articular facet, in contrast to carettochelyids that exhibit this structure (Fig. 4). In *Allaeochelys meylani* (Rollot et al. 2025), *Allaeochelys libyca* (Rollot et al. 2024a), and *Carettochelys niahensis* (White et al. 2023), the crista cranii forms a broad, flat central plateau that is developed as a well-defined articular surface for articulation with the prefrontal. This is clearly absent in SMF Me3004. These observations are backed up by the morphology of the crista cranii of HLMD Me7592, which is identical to that of SMF Me3004. The crista cranii forms the lateral wall of the sulcus olfactorius, which is notably broad (Fig. 4) as in *Allaeochelys libyca* (Rollot et al. 2024a), *Carettochelys niahensis* (White et al. 2023) and *Carettochelys insculpta* (Rollot et al. 2024b). Posteriorly, along the lateral surface of the crista cranii, the frontal of SMF Me3004 forms a low, curved ridge that extends anterodorsolaterally and forms the anterior and medial margin of a relatively deep and large fossa, whose posterior half is formed by the parietal (Fig. 4A).

Parietal. The dorsal plate of both parietals is completely preserved in SMF Me3004, but the processus inferior parietalis is almost completely lacking on both elements (Figs 2A, C, D, 3A, C–E). The length of each parietal clearly exceeds the combined width of the two elements (Fig. 3A). On the skull roof, the dorsal plate of the parietal contacts the frontal anteriorly, the postorbital anterolaterally, the supraoccipital posteriorly, and its counterpart medially (Figs 2A, 3A). The dorsal plate of the parietal also forms the anteromedial and medial margin of the deep upper temporal emargination, as in all carettochelyids (Waite 1905; Walther 1922; Havlik et al. 2014; Joyce 2014; Danilov et al. 2017a; Joyce et al. 2018; White et al. 2023; Rollot et al. 2025). The processus inferior parietalis is only preserved on both sides by a few isolated pieces that belong to the most dorsal aspect of the process, just below the dorsal plate of the parietal (Fig. 3C). It is clear that the processus inferior parietalis had an elongate contact laterally with the prootic, as in other carettochelyids (Walther 1922; Havlik et al. 2014; Danilov et al. 2017a; Joyce et al. 2018; White et al. 2023; Rollot et al. 2025). However, a contact between the parietal and opisthotic appears to have been absent, prevented by a clear contact between the prootic and supraoccipital, as in *Allaeochelys libyca* (Havlik et al. 2014) and *Allaeochelys meylani* (Rollot et al. 2025), but contrasting *Anosteira maomingensis* (Danilov et al. 2017a) and *Anosteira pulchra* (Joyce et al. 2018), in which a small contact is present. In *Carettochelys insculpta*, the contact is variably present or absent (Walther 1922; Joyce 2014; Rollot et al. 2024b). In SMF Me3004, the processus inferior parietalis is anteriorly continuous with the tall crista cranii of the frontal, to which it is tightly sutured (see Frontal above). Anteroventrolaterally, the parietal bears a ridge that extends anterolaterally from the processus inferior parietalis and forms the posterolateral rim of a large fossa formed by the frontal and parietal in the posterodorsomedial corner of the orbit. The ridge extends further on the inner, medial surface of the postorbital, forming a broad bony wall posterior to the orbit (Fig. 3E). The ridge likely extended to the jugal, as the latter bone appears to be medially expanded, but the complete extent of the posterior orbit wall cannot be fully determined because of damage to the jugal. A similar, mediolaterally expanded wall posterior to the orbit is also present in *Allaeochelys meylani* (Rollot et al. 2025) and maybe *Carettochelys niahensis* (White et al. 2023) and is reminiscent of the septum orbitotemporale seen in pleurodires and trionychids (Gaffney et al. 2006). In the extant *Carettochelys insculpta*, a similar ridge is present, but a

mediolateral thickened postorbital wall is not apparent (Rollot et al. 2024b). Anterolaterally, the braincase is greatly enlarged and contained broad cerebral hemispheres, as in *Allaeochelys libyca* (Havlik et al. 2014), *Allaeochelys meylani* (Rollot et al. 2025), *Carettochelys niahensis* (White et al. 2023), and *Carettochelys insculpta* (Rollot et al. 2024b).

Postorbital. The postorbitals of SMF Me-3004 are overall well-preserved on both sides, with damage mostly affecting the ventral part of the postorbital wall, which is partially missing (Figs 2A, C–E, 3A, C–E). The postorbital is a small bone that forms the posterior margin of the orbit and the anterior margin of the upper temporal emargination (Figs 2A, 3A, C–E). The postorbital is anteroposteriorly short (Fig. 3A, C, D), as seen in *Anosteira pulchra* (Joyce et al. 2018), but which contrasts with the elongate postorbital seen in *Anosteira maomingensis* (Danilov et al. 2017a), *Allaeochelys libyca* (Havlik et al. 2014), *Allaeochelys meylani* (Rollot et al. 2025), *Carettochelys niahensis* (White et al. 2023), and *Carettochelys insculpta* (Walther 1922; Rollot et al. 2024b). On the external skull surface of SMF Me3004, the postorbital contacts the frontal anteromedially, the parietal posteromedially, the jugal ventrally, and the quadratojugal posteroventrally (Figs 2A, C–E, 3A, C–E). Medially, the postorbital is greatly expanded, forming a broad wall posterior to the orbit (Fig. 3E), as in *Allaeochelys meylani* (Rollot et al. 2025) and, likely, *Carettochelys niahensis* (White et al. 2023). An anteroventral contact with the maxilla is prevented in SMF Me3004 by the contribution of the jugal to the orbit margin (Fig. 3C–E), as in all carettochelyids (Waite 1905; Walther 1922; Danilov et al. 2017a; Joyce et al. 2018; White et al. 2023; Rollot et al. 2024b, 2025).

Jugal. The jugals of SMF Me3004 show good preservation on both sides, with damage only affecting their medial process (Figs 2B–E, 3C–E). The jugal is a small bone that forms the posteroventral margin of the orbit and the anterior margin of the lower temporal emargination (Fig. 3C–E). The contribution of the jugal to the orbit margin is broad (Fig. 3C–E), as in all other carettochelyids (Waite 1905; Walther 1922; Danilov et al. 2017a; Joyce et al. 2018; White et al. 2023; Rollot et al. 2024b), except *Allaeochelys meylani* (Rollot et al. 2025), where this contribution is greatly reduced. On the external skull surface, the jugal contacts the maxilla anteroventrally, the quadratojugal posteriorly and posteroventrally, and the postorbital dorsally (Figs 2C–E, 3C–E). The jugal is prevented from contributing to the upper temporal emargination by a short contact between the postorbital and quadratojugal posterodorsally (Fig. 3D). The jugal is also prevented from contributing to the cheek emargination by a contact between the maxilla and quadratojugal ventrally (Fig. 3C, D), as in *Allaeochelys meylani* (Rollot et al. 2025), *Carettochelys niahensis* (White et al. 2023), and *Carettochelys insculpta* (Waite 1905; Walther 1922; Rollot et al. 2024b), but not *Anosteira maomingensis* (Danilov et al. 2017a) and *Anosteira pulchra* (Joyce et al. 2018). Within the fossa orbitalis, the jugal anteriorly contacts the maxilla and deeply protrudes within the latter, giving the suture a V-shaped appearance. The medial process of the jugal is damaged, but the preserved portion shows that the process was well-developed and contributed to the broad, but likely thin, postorbital wall (Fig. 3E), as in *Allaeochelys meylani* (Rollot et al. 2025) and likely *Carettochelys niahensis* (White et al. 2023). Posteromedially, the jugal of SMF Me3004 likely contacted the pterygoid, as both bones are extremely close to one another in both the original and reassembled 3D reconstructions. A medial contact with the palatine is less certain, as the jugal and palatine appear to be prevented from contacting one another by a contact between the maxilla and pterygoid, but the great degree of incompleteness of the palatines anterolaterally makes this determination uncertain.

Quadratojugal. The quadratojugals of SMF Me3004 are both damaged (Figs 2B–D, 3B–D). The right element is fairly complete, but lacks its central portion and its posteroventral process, whereas the left element only consists of the most anterior part and the posterodorsal process. The quadratojugal is a small, plate-like bone that forms the anterolateral margin of the upper temporal emargination and the dorsal and posterior margins of the reduced cheek emargination (Fig. 3C, D). The quadratojugal contacts the jugal anteriorly, the postorbital anterodorsally, the maxilla anteroventrally, and the quadrate posteriorly along a tall, concave suture (Figs 2B–D, 3B–D). The contact between the quadratojugal and postorbital is only slightly shorter than that between the jugal and postorbital (Fig. 3D), which contrasts with the condition of *Anosteira maomingensis* (Danilov et al. 2017a) and *Allaeochelys meylani* (Rollot et al. 2025), in which it is greatly reduced. Posteriorly, the quadratojugal of SMF Me3004 contributes to the anterior margin of the cavum tympani (Fig. 3C, D), as in *Anosteira maomingensis* (Danilov et al. 2017a), *Anosteira pulchra* (Joyce et al. 2018), *Allaeochelys libyca* (Rollot et al. 2024a), and *Carettochelys insculpta* (Walther 1922; Rollot et al. 2024b), but contrary to *Allaeochelys meylani* (Rollot et al. 2025). Posterodorsally, the quadratojugal of SMF Me3004 forms an elongate process that extends over the anterodorsal margin of the cavum tympani (Figs 2C, D, 3C, D). Contact between the quadratojugal and squamosal is absent as in *Allaeochelys libyca* (Rollot et al. 2024a), *Allaeochelys meylani* (Rollot et al. 2025), and *Carettochelys insculpta* (Walther 1922; Rollot et al. 2024b), which contrasts with *Anosteira maomingensis* (Danilov et al. 2017a) and *Anosteira pulchra* (Joyce et al. 2018), in which a quadratojugal-squamosal contact is present.

Squamosal. The squamosals of SMF Me3004 are damaged (Figs 2A–D, F, 3A–D, F). The right element is highly incomplete and the few, disarticulated elements that remain preserved only allow reconstructing portions of the anterior third of the element, which contacts the quadrate anteroventrally just posterodorsal to the cavum tympani (Figs 2D, 3D, F). The left squamosal is more complete, but lacks a substantial part of its central aspect,

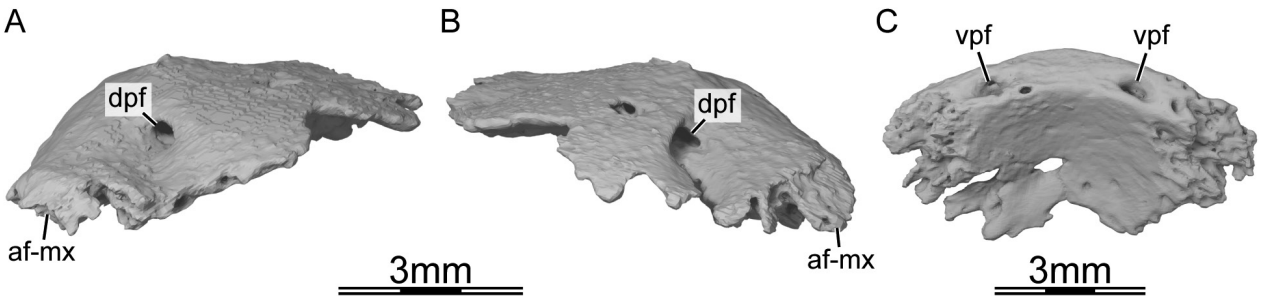


Figure 5. Three-dimensional renderings of the fused premaxillae of *Allaeochelys crassesculpta* (SMF Me3004). **A.** Left posterolateral view; **B.** Right posterolateral view; **C.** Ventral view. Abbreviations: af-mx, articulation facet for maxilla; dpf, dorsal premaxillary foramen; vpf, ventral premaxillary foramen.

which prevents direct assessment of the presence of an antrum postoticum (Figs 2C, 3C, F; but see Quadrate). In HLMD Me14997 and SMF Me3566 (female individual), however, this portion of the right squamosal and right quadrate and squamosal, respectively, are preserved and show the presence of a large antrum postoticum. A large antrum postoticum is otherwise present in *Kizylkumemys schultzi* (Nessov 1977) and *Anosteira pulchra* (contra Joyce et al. (2018); pers. obs. by YR on the µCT data of FMNH PR 966), while a shallow antrum postoticum is present in *Anosteira maomingensis* (Danilov et al. 2017a) and *Allaeochelys libyca* (Havlik et al. 2014) and the antrum is absent in adult *Carettochelys insculpta*, but present in juveniles (Rollot et al. 2024b). The squamosal of SMF Me3004 forms the posterolateral margin of the upper temporal emargination (Figs 2A, 3A). The only preserved contact of the squamosal is with the quadrate anteroventrally (Fig. 3C, D). A contact with the quadratojugal is absent (Figs 2A, C, 3A, C), as in *Allaeochelys libyca* (Rollot et al. 2024a), *Allaeochelys meylani* (Rollot et al. 2025), and *Carettochelys insculpta* (Walther 1922; Rollot et al. 2024b), but not *Anosteira maomingensis* (Danilov et al. 2017a) and *Anosteira pulchra* (Joyce et al. 2018), where a quadratojugal-squamosal contact is present. The squamosal of SMF Me3004 does not contribute to the margin of the cavum tympani. This contribution is also lacking in *Allaeochelys libyca* (Rollot et al. 2024a) and *Carettochelys insculpta* (Rollot et al. 2024b), but is present in *Anosteira maomingensis* (Danilov et al. 2017a), *Anosteira pulchra* (Joyce et al. 2018) and, likely, *Allaeochelys meylani* (Rollot et al. 2025). The posterior portion of the squamosal of SMF Me3004 forms a mediolaterally thin, but anteroposteriorly elongate posterior process (Figs 2C, F, 3C, F).

Premaxilla. The premaxilla of SMF Me3004 is well-preserved and only lacks small portions of its most posterior aspects (Figs 2B, E, 3B, E, 5). The premaxilla is a single, small bone that forms the anteroventral tip of the snout (Figs 2B, E, 3B, E). The premaxilla forms the ventral margin of the apertura narium externa, which is thin (Figs 2E, 3E), as in most carettochelyids (Havlik et al. 2014; Danilov et al. 2017a; Joyce et al. 2018; White et al. 2023; Rollot et al. 2024b), except for *Allaeochelys delheidi* (YR, pers. obs. on NHMUK PAL PV OR 38953) and *Allaeochelys meylani* (Rollot et al. 2025), which have greatly thickened bones forming the aperture. The premaxilla of SMF Me3004 floors the anterior part of the fossa nasalis and likely formed the anterior margin of the foramen intermaxillaris. The only preserved contact of the premaxilla is with the maxilla laterally (Figs 3E, 5), but comparisons with other carettochelyids suggest that no other contacts were present (Walther 1922; Danilov et al. 2017a; Rollot et al. 2024b, 2025). There are two pairs of foramina in the premaxilla. The first pair of foramina pierces the premaxilla along its dorsal surface and each foramen is located at about one-third of the bone's width (Fig. 5A, B). Each foramen leads into a very short canal that extends anteromedially and anastomoses with its counterpart. At about the same level, a canal branches off from each side of the anastomosis and extends ventrally to join the anteroventral surface of the premaxilla, where the premaxilla forms a second pair of foramina (Fig. 5C). These foramina and canals are reminiscent of the premaxillary canal of other turtles, in which the premaxillary canal serves for the passage of a branch of the anterior nasal artery (Tada et al. 2025). A closer look at µCT data and 3D models of *Carettochelys insculpta* (Rollot et al. 2024b) demonstrated that similar foramina and canals are also present in the latter taxon.

Maxilla. The maxillae of SMF Me3004 are dislocated, but almost completely preserved and could, thus, be reconstructed with ease (Figs 2B–E, 3B–E). The maxillae are only slightly damaged along the anterior part of the ascending process and along the suture with the premaxilla (Figs 2B–E, 3B–E). The maxilla forms the anteroventral portion of the snout, the lateral margin of the apertura narium externa, the lateral wall of the fossa nasalis, the anterior and ventral margin of the orbit, the anteroventral margin of the reduced cheek emargination, and the lateral margin of the foramen intermaxillaris (Figs 2B–E, 3B–E). The rim of the external nares, which is formed by the prefrontal, maxilla, and premaxilla, is thin as in most carettochelyids (Havlik et al. 2014; Danilov et al. 2017a; Joyce et al. 2018; White et al. 2023; Rollot et al. 2024b), except in *Allaeochelys delheidi* (YR, pers. obs. on NHMUK PAL PV OR 38953) and *Allaeochelys meylani* (Rollot et al. 2025), in which the rim is greatly thickened. On the external skull surface of SMF Me3004, the maxilla contacts the premaxilla

anteromedially, the prefrontal dorsally along an elongate suture for all the length of its ascending process, the jugal posteriorly, and the quadratojugal posteriorly just below the jugal (Figs 2C–E, 3C–E). A maxilla-quadratojugal contact is also present in *Allaeochelys meylani* (Rollot et al. 2025), *Carettochelys niahensis* (White et al. 2023), and *Carettochelys insculpta* (Waite 1905; Walther 1922; Rollot et al. 2024b), but not in *Anosteira maomingensis* (Danilov et al. 2017a) and *Anosteira pulchra* (Joyce et al. 2018). The labial margin of SMF Me3004 is nearly straight (Fig. 3C, D), as in *Anosteira pulchra* (Joyce et al. 2018), which contrasts with the more sinuous margin seen in *Allaeochelys meylani* (Rollot et al. 2025) and *Carettochelys insculpta* (Waite 1905; Walther 1922; Rollot et al. 2024b). Within the fossa nasalis of SMF Me3004, just medial to the anteroventral corner of the orbit, the maxilla forms a relatively large foramen alveolare superius. The foramen alveolare superius leads into a large, unnamed canal that extends anteroventrolaterally within the maxilla and merges with the canalis alveolaris superior. In the floor of the fossa orbitalis, the maxilla forms at about mid-length the foramen supramaxillare, which leads into the large canalis infraorbitalis. The canalis infraorbitalis extends anteriorly through the maxilla and merges with the canalis alveolaris superior. The canalis alveolaris superior seems to form in the most posterior part of the maxilla by the successive merging of multiple small canals that connect to the lateral and triturating surfaces of the maxilla. The posterior portion of the canalis alveolaris superior is fairly small and the canal extends anteriorly through the maxilla to merge with the canalis infraorbitalis slightly anterolateral to the level of the foramen supramaxillare. The resulting canal, which retains the name canalis alveolaris superior (Albrecht 1967; Gaffney 1972), is extremely large and extends anteriorly through the maxilla, while giving off multiple small branches. At the level of the anterior wall of the orbit, the canalis alveolaris superior merges with the unnamed canal that extends from the foramen alveolaris superior and the resulting canal continues to extend anteriorly through the maxilla. The path of the canal is difficult to follow, as it gives off numerous small to large canals along its way that connect to the lateral, medial, and triturating surfaces of the maxilla. One canal, however, extends anteriorly straight through the maxilla and exits the cranium by means of a foramen formed by the maxilla, along the ventrolateral margin of the external nares. The location of this foramen is reminiscent of the maxillary foramen described in *Allaeochelys meylani* (Rollot et al. 2025) and *Carettochelys insculpta* (Rollot et al. 2024b), which transmits a branch of the superior alveolar artery that may be linked to proboscis blood supply (Rollot et al. 2025). In SMF Me3004, just posterodorsal to the foramen alveolare superius, the edge of the maxilla is developed as a thin ridge that likely forms the anteroventral margin of the foramen orbito-nasale. Within the fossa orbitalis, the maxilla contacts the jugal posteriorly along a V-shaped suture, the pterygoid posteromedially, and palatine medially. In ventral view, the triturating surface is moderately broad and progressively expands mediolaterally towards the posterior (Fig. 3B). The labial margin is nearly straight and anteriorly continuous with the anteroventral edge of the premaxilla (Fig. 3B). The morphology of this area is, therefore, similar to that of *Anosteira maomingensis* (Danilov et al. 2017a) and *Anosteira pulchra* (Joyce et al. 2018), but greatly contrasts with that of *Allaeochelys meylani* (Rollot et al. 2025) and *Carettochelys insculpta* (Rollot et al. 2024b). In the latter two taxa, the labial ridge forms a short process medially that separates the triturating surface posteriorly from a half-cup fossa anteriorly formed by the maxilla and premaxilla. This fossa is large in *Allaeochelys meylani* (Rollot et al. 2025), small in *Carettochelys insculpta* (Rollot et al. 2024b), and completely absent in *Anosteira maomingensis* (Danilov et al. 2017a), *Anosteira pulchra* (Joyce et al. 2018), and *Allaeochelys crassesculpta*. In SMF Me3004, the maxilla forms an elongate articular facet posteromedially for about one third of its length, which corresponds to a suture shared with the palatine medially and pterygoid posteromedially and posteriorly. As the articular surface is uninterrupted for its entire length, we postulate that the maxilla had no contribution to the foramen palatinum posterius, as some part of the maxilla would otherwise be smooth and highlight the position of the foramen palatinum posterius. Bony contributions to the foramen palatinum posterius are variable among carettochelyids and the foramen is formed by the maxilla, palatine, and pterygoid in *Anosteira maomingensis* (Danilov et al. 2017a), by the maxilla and palatine in *Allaeochelys meylani* (Rollot et al. 2025), and only by the palatine in *Anosteira pulchra* (Joyce et al. 2018) and adult *Carettochelys insculpta* (Rollot et al. 2024b).

Palatine. The palatines are overall well-preserved in SMF Me3004, but the anterolateral aspect of both elements is damaged and dislocated (Figs 2B, 3B). The palatine contacts the vomer anteromedially, the maxilla anterolaterally, the pterygoid posterolaterally, the parabasisphenoid posteriorly, and its counterpart medially (Figs 2B, 3B). The posterior contact of the palatine with the parabasisphenoid prevents the pterygoids from contacting one another along the midline, as in all carettochelyids (Waite 1905; Walther 1922; Danilov et al. 2017a; Joyce et al. 2018; Rollot et al. 2024a, 2024b). Dorsally, at about mid-length, the palatine forms a tall ascending process (Fig. 6), as in all trionychians (Meylan 1987; Joyce 2014). The posterior half of the ascending process is much lower than the anterior half. This difference is only minimally due to breakage, as µCT scans of SMF Me3004 show that most of the dorsal aspect of the preserved portion corresponds to an articular facet. This facet likely articulated with the parietal and epipterygoid, but the corresponding portions of the latter two bones are not preserved and we are not able to identify the actual limits of the contacts. Anteriorly, on its dorsal surface, the palatine forms a low, but relatively broad ridge that extends posteriorly and posterolaterally and

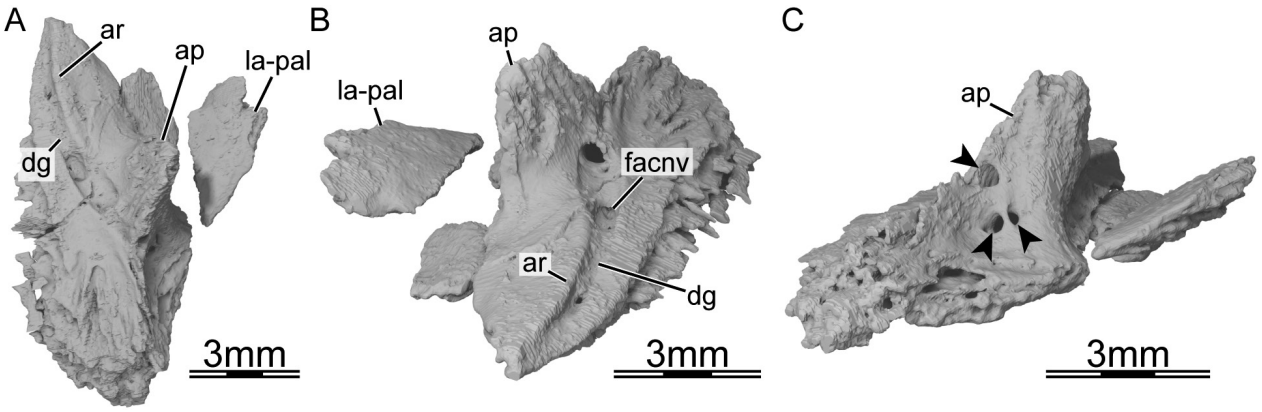


Figure 6. Three-dimensional renderings of the reconstructed right palatine of *Allaeochelys crassesculpta* (SMF Me3004). **A.** Dorsal view; **B.** Anteromedial view; **C.** Posterolateral view. Abbreviations: ap, ascending process; ar, accessory ridge; dg, dorsal groove; facnv, foramen anterius canalis nervi vidiani; la-pal, lateral aspect of palatine. Black arrowheads show the various foramina along the posteroventral part of the ascending process of the palatine.

that forms the lateral wall of a shallow groove (Fig. 6A, B). This groove extends posteriorly and posterolaterally and connects to a large foramen located at the medial base of the ascending process of the palatine. The foramen leads into a canal that extends posteriorly for a short distance and connects to other canals that cross the ascending process of the palatine. Various foramina linked to this network of canals are visible on the lateral surface of the ascending process of the palatine, just posterior to its tallest extent (Fig. 6C). At about two-thirds of the anteroposterior length of the dorsal groove, the palatine forms a small fossa, which posteriorly ends in a small foramen. This foramen leads into a canal that extends posteriorly through the palatine. The location of the foramen and path of the canal are identical to that of the foramen anterius canalis nervi vidiani and canalis nervus vidianus in *Carettochelys insculpta* (Rollot et al. 2021, 2024b) and we, therefore, identify the foramen and canal as such in SMF Me3004 (Fig. 6B). Anterolaterally, the left palatine preserves a small piece of which the two longest sides have a smooth surface. Given the orientation of this bony piece, its location in the original specimen, and the morphology of this area in other carettochelyids (Danilov et al. 2017a; Joyce et al. 2018; Rollot et al. 2024b), we interpret this element as being the anterolateral end of the palatine, with the smooth side facing anteromedially corresponding to the posterior or posterolateral margin of the foramen orbito-nasale and the smooth side facing posterolaterally corresponding to the anteromedial margin of the foramen palatinum posterius (Fig. 3B).

Vomer. The vomer of SMF Me3004 lacks its anterior and anterolateral ends, is eroded on its ventral surface, and broken into four pieces (Figs 2B, 3B). The vomer contacts the prefrontal anterolaterally and the palatine posterolaterally and posteriorly. Although the anterior and anterolateral sides of the vomer are damaged, the premaxilla and maxilla are sufficiently complete to ascertain that there is no contact of the vomer with the latter two bones, as in other carettochelyids (Walther 1922; Danilov et al. 2017a; Joyce et al. 2018; Rollot et al. 2024b). Dorsolaterally, the vomer forms low processes for articulation with the descending process of the prefrontal (Fig. 3B). Dorsally, the vomer forms a narrow, but deep sulcus vomeri that extends anteroposteriorly for all the length of the element. Ventrally, along its posterior end, the vomer forms an elongate fossa that is open posteriorly and delineated by a thin, curved ridge anteriorly and laterally, just at the level of contact with the palatine (Figs 2B, 3B).

Pterygoid. The pterygoids are moderately damaged in SMF Me3004 (Figs 2B, 3B). The left element is the most complete of the two, preserving the anterior end of the anterior process and most of the central and posterior portions of the pterygoid, although substantial parts of its dorsal surface are eroded (Figs 2B, 3B, 7). Most of the right element, however, is missing, as it only preserves the anterior tip of the anterior process and damaged portions of the posteromedial part of the bone (Figs 2B, 3B). The anterior half of the pterygoid is developed as an elongate process that contacts the maxilla anteriorly, the palatine medially, and the parabasisphenoid posteromedially (Fig. 3B). Anterolaterally, the anterior process forms a small and low, but elongate processus pterygoideus (Fig. 7D), as in *Carettochelys insculpta* (Rollot et al. 2024b). Contact of the pterygoid with its counterpart is prevented by a connection between the palatine and parabasisphenoid (Figs 2B, 3B), as in all carettochelyids (Waite 1905; Walther 1922; Danilov et al. 2017a; Joyce et al. 2018; Rollot et al. 2024a, 2024b). The posterior half of the pterygoid contacts the parabasisphenoid medially, the basioccipital-exoccipital complex posteromedially, and the quadrate laterally (Figs 3B, 7). The dorsal contacts of the pterygoid are not preserved, as the central part of the cranium is heavily damaged due to its compression. The pterygoid preserves several structures of interest on its ventral surface. The pterygoid forms the foramen posterius canalis carotici interni, which is likely entirely formed by the pterygoid, but very closely located to the parabasisphenoid, at about two-thirds of the

anteroposterior length of the pterygoid-parabasisphenoid suture (Fig. 7B, C). The position of the foramen posterius canalis carotici interni is, therefore, reminiscent of that seen in *Kizylkumemys schultzi* (Danilov and Obraztsova 2015) and *Anosteira pulchra* (Joyce et al. 2018), but differs from other carettochelyids, in which the foramen is located either more posteriorly or posterolaterally far from the pterygoid-parabasisphenoid suture (Waite 1905; Walther 1922; Havlik et al. 2014; Danilov et al. 2017a; Rollot et al. 2024a, 2024b, 2025). Given the position of the foramen posterius canalis carotici interni in SMF Me3004, the canalis caroticus internus likely extended anteriorly along the pterygoid-parabasisphenoid suture, but damage to that area precludes the description of the internal carotid artery system. Posteriorly, starting from the foramen posterius canalis carotici interni, the pterygoid forms a well-defined groove that extends posterolaterally on its ventral surface and ends close to the posterior rim of the pterygoid, which highlights the posterior path of the internal carotid artery (Figs 2B, 3B, 7B, C). Lateral to this groove, the pterygoid forms a deep pterygoid fossa (Figs 2B, 3B, 7B, C), as in *Anosteira maomingensis* (Danilov et al. 2017a), *Allaeochelys meylani* (Rollot et al. 2025), *Allaeochelys libyca* (Havlik et al. 2014; Rollot et al. 2024a), and *Carettochelys insculpta* (Waite 1905; Walther 1922), but not *Anosteira pulchra* (Joyce et al. 2018). An enfolded ridge, formed by the pterygoid that ventrally covers the pterygoid fossa when present, is absent in SMF Me3004 (Figs 2B, 3B, 7B, C), as is the case in *Kizylkumemys schultzi* (Nessov 1987; Danilov and Obraztsova 2015), *Anosteira maomingensis* (Danilov et al. 2017a) and *Anosteira pulchra* (Joyce et al. 2018), but not in *Allaeochelys meylani* (Rollot et al. 2025), *Allaeochelys libyca* (Rollot et al. 2024a), and *Carettochelys insculpta* (Walther 1922; Joyce 2014). Posteromedially, the pterygoid contributes to the elongate tuberculum basioccipitale by forming its ventrolateral part (Figs 2B, 3B, 7). Elongate tubercula basioccipitale are also present in *Allaeochelys meylani* (Rollot et al. 2025), *Allaeochelys libyca* (Havlik et al. 2014; Rollot et al. 2024a), and *Carettochelys insculpta* (Waite 1905; Walther 1922; Rollot et al. 2024b), but not in *Anosteira pulchra* (Joyce et al. 2018), where the tubercula are short. Laterally, the pterygoid has a tall suture with the quadrate that extends vertically just medial to the mandibular condyle (Fig. 7C, D). Dorsally, most of the surface of the pterygoid is eroded and damaged, preserving only a few features of interest. The dorsal surface of the posterior half of the pterygoid is intact overall and forms a low ridge at about mid-length that crosses most of the preserved element mediolaterally (Fig. 7A). This ridge is visible on both sides of the specimen and located at the same level, slightly posterior to the level of the suture between the parabasisphenoid and basioccipital-exoccipital complex. In *Allaeochelys meylani* (Rollot et al. 2025), *Allaeochelys libyca* (Rollot et al. 2024a), and *Carettochelys insculpta* (Rollot et al. 2024b), the pterygoid is slightly raised at the same level, forming either a plateau or a ridge that corresponds to the articulation facet with the processus interfenestralis of the opisthotic. Considering the morphology exhibited by these carettochelyids, we interpret the dorsal pterygoid ridge of SMF Me3004 as representing at least a portion of the articulation facet with the processus interfenestralis of the opisthotic. The area posterior to that ridge, therefore, corresponds to the floor of the recessus scalae tympani (Fig. 7A). The posterodorsal surface of the pterygoid is rough, posterior to the recessus scalae tympani. A close look at the µCT dataset shows that this surface appears to correspond to a suture, which is confirmed to be present by specimen HLMD Me7592, in which this area is partially preserved on the right side with a pterygoid-opisthotic contact (Fig. 7A, C, D). By reference to other carettochelyids, this opisthotic-pterygoid contact corresponds to the ventral contact of the secondary process of the opisthotic with the pterygoid, which restricts the fenestra postotica medially (Danilov et al. 2017a; Rollot et al. 2024a, 2024b, 2025). Just lateral to this inferred articulation facet and contact, the dorsal surface of the pterygoid is smooth and concave, forming a short groove that extends anteriorly just lateral to the recessus scalae tympani (Fig. 7A). In *Allaeochelys meylani* (Rollot et al. 2025), *Allaeochelys libyca* (Rollot et al. 2024a), and *Carettochelys insculpta* (Rollot et al. 2024b), this part of the pterygoid corresponds to the ventral margin of the fenestra postotica, which is greatly reduced in carettochelyids because of the posterior contact between the pterygoid and opisthotic. We, therefore, interpret this portion of the pterygoid in SMF Me3004 as representing the ventral margin of the fenestra postotica and the short anterior groove corresponds to the posterior floor of the cavum acustico-jugulare (Fig. 7A, C, D). In HLMD Me7592, the pterygoid forms a foramen that is located lateral to the foramen jugulare posterius, just lateral to its suture with the basioccipital-exoccipital complex and medial to its suture with the opisthotic. The foramen leads into a short canal that extends anterolaterally within the pterygoid and basioccipital-exoccipital complex and joins the recessus scalae tympani anteriorly, just lateral to the foramen that leads into the canal that posteriorly connects to the foramen jugulare posterius. The location of these structures is identical to the position of the foramen and canal for the passage of the glossopharyngeal nerve (CN IX; foramen oropharyngeale, *sensu* Evers and Al Iawati (2024)) seen in *Allaeochelys meylani* (Rollot et al. 2025), *Allaeochelys libyca* (Rollot et al. 2024a), and *Carettochelys insculpta* (Rollot et al. 2024b) and we, therefore, identify them as such in HLMD Me7592. Nevertheless, some variation in the bony contributions to these structures seems to be apparent. In HLMD Me7592, the foramen oropharyngeale is likely only formed by the opisthotic, although very closely located to the pterygoid-opisthotic suture, as observed in adult *Carettochelys insculpta* (Rollot et al. 2024b), whereas the foramen is formed by the opisthotic and pterygoid in *Allaeochelys meylani* (Rollot et al. 2025) and *Allaeochelys libyca* (Rollot et al. 2024a).

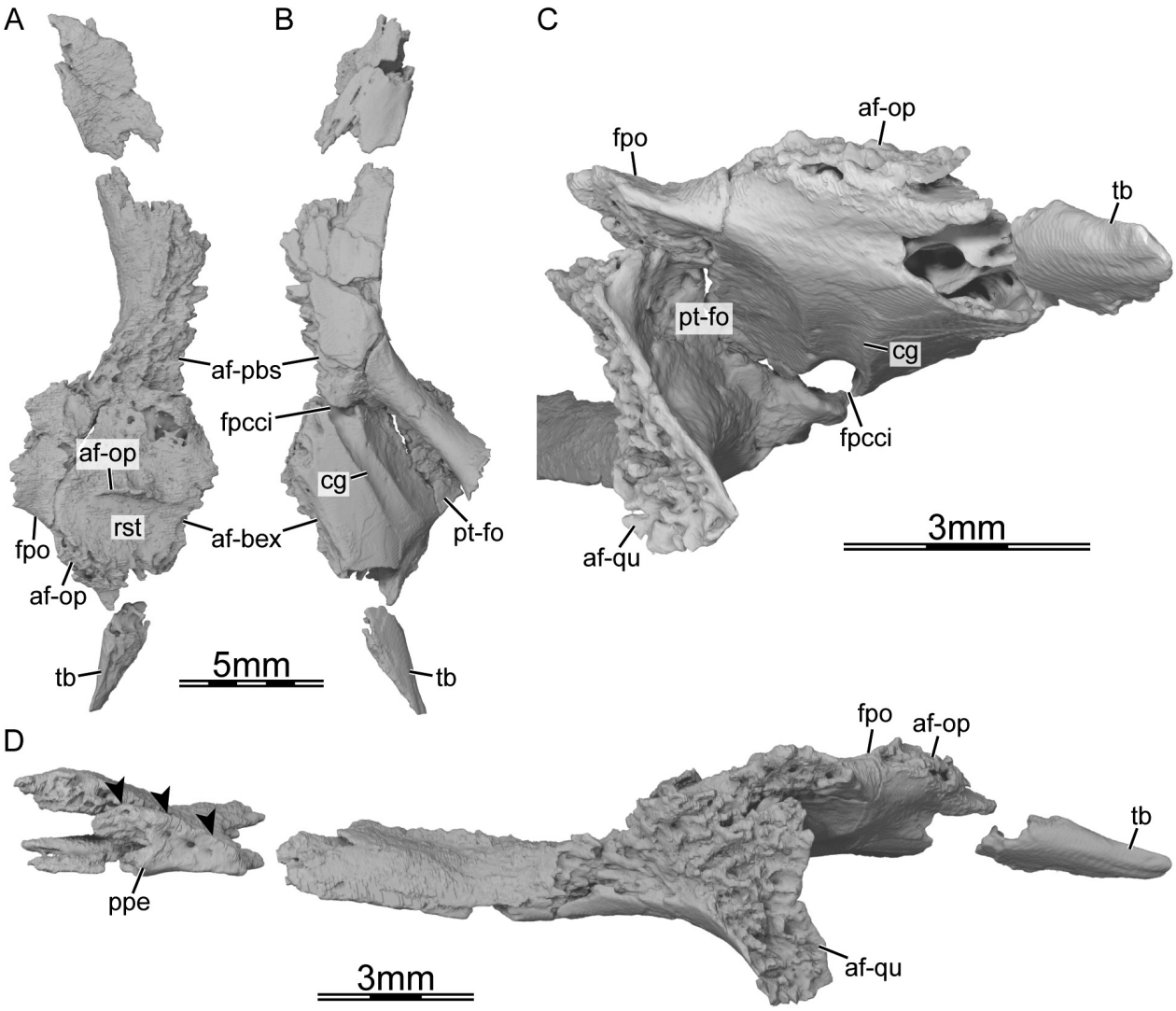


Figure 7. Three-dimensional renderings of the reconstructed left pterygoid of *Allaeochelys crassesculpta* (SMF Me3004). **A.** Dorsal view; **B.** Ventral view; **C.** Posteroventral view; **D.** Lateral view. Abbreviations: af-bex, articulation facet for basioccipital-exoccipital complex; af-op, articulation facet for opisthotic; af-pbs, articulation facet for parabasisphenoid; af-qu, articulation facet for quadrate; cg, carotid groove; fpcci, foramen posterius canalis carotici interni; fpo, fenestra postotica; ppe, processus pterygoideus externus; pt-fo, pterygoid fossa; rst, recessus scalae tympani; tb, pterygoid portion of the tubercula basioccipitale. Black arrowheads indicate the extent of the processus pterygoideus externus.

Epipterygoid. The epipterygoids are not preserved in SMF Me3004 and no insights can be obtained for other specimens.

Quadrate. The quadrates of SMF Me3004 are broken into several pieces, but most of their morphology remains preserved (Figs 2, 3, 8). The sole exception is the posterodorsal part of both elements, at the level of the antrum postoticum, which is largely missing. In lateral view, the quadrate contacts the quadratojugal along a tall, C-shaped suture and the squamosal posterodorsally (Figs 2C, D, 3C, D). The quadrate forms most of the cavum tympani, with the exception of the anterior margin, which is formed by the quadratojugal, as in *Anosteira maomingensis* (Danilov et al. 2017a), *Anosteira pulchra* (Joyce et al. 2018), *Allaeochelys libyca* (Rollot et al. 2024a), and *Carettochelys insculpta* (Walther 1922; Rollot et al. 2024b), but not *Allaeochelys meylani* (Rollot et al. 2025). The quadrate usually forms the incisura columella auris, which in carettochelyids is completely enclosed by the latter bone (Waite 1905; Walther 1922; Havlik et al. 2014; Joyce 2014; Danilov et al. 2017a; Joyce et al. 2018; Rollot et al. 2024a, 2024b, 2025), but the area is not preserved in SMF Me3004. In specimen SMF Me3566, however, the incisura columella auris is perfectly visible and completely enclosed by the quadrate. The quadrate of SMF Me3004 forms a moderately deep precolumellar fossa in the posteroventromedial corner of the cavum tympani (Figs 3D, 8A). A similar fossa, albeit shallower, is also present in *Allaeochelys meylani* (Rollot et al. 2025), but such a depression is absent in *Allaeochelys libyca* (Rollot et al. 2024a) and *Carettochelys insculpta* (Rollot et al. 2024b). Notably deep precolumellar fossae are also known in various pleurodires (Gaffney et al. 2006), but their function remains uncertain (Foth et al.

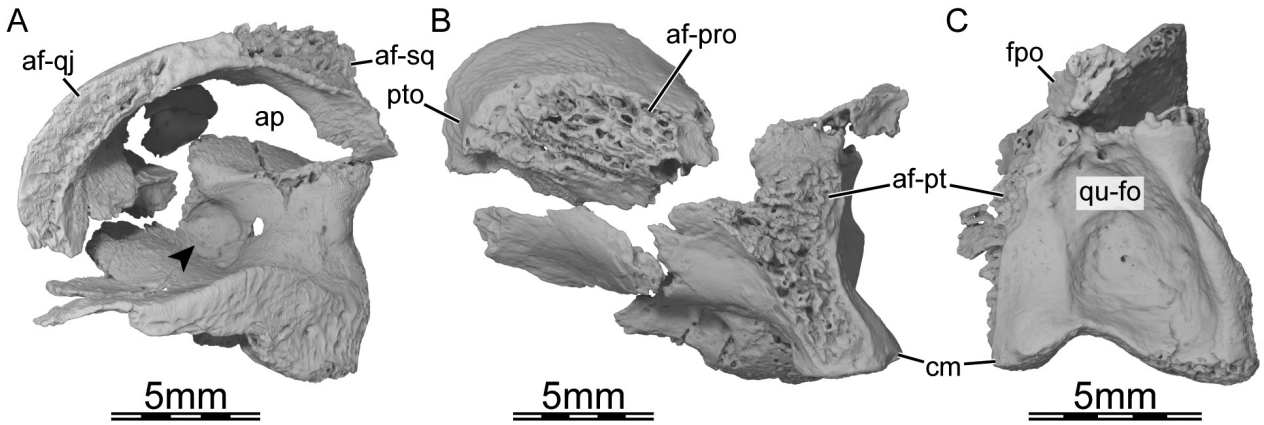


Figure 8. Three-dimensional renderings of the reconstructed quadrates of *Allaeochelys crassesculpta* (SMF Me3004). **A.** Anterolateral view of left quadrate; **B.** Medial view of right quadrate; **C.** Posterior view of right quadrate. Abbreviations: af-pro, articulation facet for prootic; af-pt, articulation facet for pterygoid; af-qj, articulation facet for quadratojugal; af-sq, articulation facet for squamosal; ap, antrum postoticum; cm, condylus mandibularis; fpo, fenestra postotica; pto, processus trochlearis oticum; qu-fo, quadrate fossa. Black arrowhead indicates the location of the precolumellar fossa within the cavum tympani.

2019). According to Harrassowitz (1922), the antrum postoticum is absent in *Allaeochelys crassesculpta*, but several specimens studied herein suggest otherwise. Indeed, a large antrum postoticum is clearly visible in the µCL scans of HLMD Me14997 and in the female individual of specimen SMF Me3566. In SMF Me3004, this area is damaged but still preserves enough of the quadrate to draw the same conclusion. Dorsal to the precolumellar fossa of the cavum tympani, the dorsal surface of the preserved quadrate forms a smooth and slightly concave surface that appears to have an anteromedial-posterolateral orientation (Figs 3C, 8A). Just anteroventral to this surface, the quadrate forms a smooth, horizontal ridge, that weakly extends above the precolumellar fossa. The morphology of this area, particularly the smooth dorsal surface of the quadrate and the low ridge anteroventral to it, is reminiscent of that of SMF Me3566 and other carettochelyids that possess an antrum postoticum, such as *Anosteira pulchra* (Joyce et al. 2018) and *Allaeochelys libyca* (Rollot et al. 2024a), but also juvenile *Carettochelys insculpta* (Rollot et al. 2024b). In dorsal view, the quadrate of SMF Me3004 contacts the quadratojugal anterolaterally, the prootic medially, the opisthotic posteromedially and the squamosal posterolaterally (Figs 2A, 3A). At about two-thirds of the anteroposterior length of the prootic-quadrate suture, the right quadrate preserves the most dorsolateral aspect of the canalis stapedio-temporalis, showing that the quadrate forms the lateral wall of that canal and the lateral margin of the foramen stapedio-temporale, as in other carettochelyids (Waite 1905; Walther 1922; Havlik et al. 2014; Danilov et al. 2017a; Joyce et al. 2018; Rollot et al. 2025). The quadrate also contributes to the processus trochlearis oticum (Figs 2B, 3B, 8B), although it only forms the most lateral part of the process, which is otherwise mostly formed by the prootic (Figs 2A, B, 3A, B). The posterior surface of the quadrate is excavated and forms a fossa (Figs 2F, 3F, 8C), as in all carettochelyids (Walther 1922; Havlik et al. 2014; Joyce 2014; Danilov et al. 2017a; Joyce et al. 2018; Rollot et al. 2024a, 2024b, 2025). The fossa in SMF Me3004 is only moderately deep, as in *Anosteira maomingensis* (Danilov et al. 2017a) and *Anosteira pulchra* (Joyce et al. 2018), which contrasts with the deeper fossa found in *Allaeochelys meylani* (Rollot et al. 2025), *Allaeochelys libyca* (Havlik et al. 2014; Rollot et al. 2024a), and *Carettochelys insculpta* (Joyce 2014; Rollot et al. 2024b). In SMF Me3004, the posterolateral edge of the quadrate protrudes posteriorly, forming a relatively broad process that folds slightly over the quadrate fossa (Figs 2F, 3F, 8C), as seen to a variable extent in other carettochelyids. This process or enfolded ridge is slightly more prominent and well-defined in SMF Me3004, *Allaeochelys libyca* (Rollot et al. 2024a) and *Carettochelys insculpta* (Rollot et al. 2024b) than in *Allaeochelys meylani*, in which it laterally delineates an additional shallow fossa (Rollot et al. 2025). In SMF Me3004, the medial surface of the quadrate is slightly concave and forms a shallow groove dorsomedially and just dorsal to the medial suture with the pterygoid. This feature is visible on both sides at the same level and, by reference to other carettochelyids (Havlik et al. 2014; Joyce 2014; Danilov et al. 2017a; Joyce et al. 2018; Rollot et al. 2024a, 2025), can be confidently identified as the lateral margin and lateral wall of the fenestra postotica and cavum acustico-jugulare, respectively (Fig. 8C). Ventrally, the quadrate forms a low and ventrally oriented mandibular condyle (Figs 2B, 3B, 8B, C), as in other carettochelyids (Waite 1905; Walther 1922; Havlik et al. 2014; Danilov et al. 2017a; Joyce et al. 2018; Rollot et al. 2025). The mandibular condyle consists of two facets, with the lateral one being about three times larger than the medial (Figs 2B, 3B). The two facets are separated by a wide and deep sulcus (Figs 2B, 3B, 8C), as seen in *Allaeochelys libyca* (Rollot et al. 2024a), which contrasts with the deep, but narrower sulcus seen in *Allaeochelys meylani* (Rollot et al. 2025) and the wide, but shallower sulcus seen in *Carettochelys insculpta* (Rollot et al. 2024b). On the anterior surface of the quadrate of SMF Me3004, just anterodorsal to the mandibular

condyle, the quadrate forms a small foramen that leads into a canal that extends dorsally within the latter bone. The path of this canal is difficult to follow as it blends into porous bone, but the position of the foramen is reminiscent of the anterior quadrate foramen seen in *Allaeochelys libyca* (Rollot et al. 2024a) and *Carettochelys insculpta* (Rollot et al. 2024b). The quadrate of carettochelyids usually contributes to various other internal structures, such as the canalis cavernosus and foramen arteriomandibulare, but these areas are neither preserved in SMF Me3004 nor any other specimen for which we acquired tomographic data.

Prootic. The prootics are incomplete in SMF Me3004 (Figs 2A, 3A). Both elements preserve most of their dorsal aspect, with that of the left prootic being almost complete and the most anterior part of the ventral process. Within the upper temporal fossa, the prootic contacts the parietal medially, the quadrate laterally, the supraoccipital posteromedially, and the opisthotic posteriorly, which clearly prevents the quadrate from contacting the supraoccipital (Figs 2A, 3A). The prootic forms most of the processus trochlearis oticum, which is developed as a relatively thin lip of bone that is strongly curved ventrally. Posterolaterally, at about two-thirds of the anteroposterior length of the prootic-quadrate suture, the prootic forms the medial margin of the left foramen stapedio-temporale, which is only visible on the left side of the specimen. Anteroventrally, the small portion of the prootic that remains preserved is anteriorly concave with a smooth, intact surface. This aspect is visible on both sides of the specimen and, by reference to the same area in other carettochelyids (Rollot et al. 2024a, 2024b, 2025), can be identified as the posterior margin of the foramen nervi trigemini *sensu stricto* (*sensu* Rollot et al. (2024a)). The preserved parts of the prootic show that it forms the anterior half of the cavum labyrinthicum and anterior half of the anterior semicircular canal. The fossa acustico-facialis, canalis nervus facialis, fenestra ovalis, and hiatus acusticus are not preserved.

Opisthotic. The opisthotic of SMF Me3004 is heavily damaged on both sides (Figs 2A, F, 3A, F). The left element only preserves the most anterior and dorsal aspects, while the right element, to which two large pieces can be attributed, preserves its anterodorsal and dorsolateral portions. The preserved parts of the opisthotic contact the supraoccipital medially, the prootic anteriorly, which prevents the supraoccipital to contact the quadrate, and the quadrate laterally (Figs 2A, F, 3A, F). The clear contact between the prootic and supraoccipital just anterior to the opisthotic also prevents the latter from contacting the parietal (Figs 2A, 3A). Internally, the opisthotic forms the posterior margin of the lateral semicircular canal, which is not fully enclosed by bone anteriorly, and the posterior margin of the posterior semicircular canal. On the right side, the most anterior portion of the paroccipital process is preserved. Ventrolaterally, the surface of the opisthotic is slightly concave and forms a very shallow groove. With reference to other carettochelyids (Rollot et al. 2024a, 2024b, 2025), this lightly concave surface likely corresponds to the medial margin of the fenestra postotica and posteromedial wall of the cavum acustico-jugulare. The ventromedial surface of the paroccipital process forms a broad, slightly concave surface, which corresponds to the roof of the recessus scalae tympani. As both opisthotics are heavily damaged, we cannot evaluate the fenestra ovalis, hiatus acusticus, fenestra perilymphatica, foramen oropharyngeale, processus interfenestralis, and canals and foramina for the glossopharyngeal nerve (CN IX). A ventral contact of the processus interfenestralis with the pterygoid can nevertheless be inferred by the presence of a raised ridge on the dorsal surface of the pterygoid and that extends mediolaterally, which is in the same position as the raised surface of the pterygoid that contacts the processus interfenestralis in other carettochelyids (see Pterygoid above; Rollot et al. (2024a, 2024b, 2025)). An additional contact of the opisthotic with the pterygoid, which corresponds to the ventral contact of the secondary process of the opisthotic with the pterygoid, is present as in other carettochelyids, based on SMF Me3004 and HLMD Me7592 (see Pterygoid above; Danilov et al. (2017a); Rollot et al. (2024a, 2024b, 2025)).

Supraoccipital. The supraoccipital is overall well-preserved in SMF Me3004 and only lacks portions of the crista supraoccipitalis and its most anteroventral aspects (Figs 2A–D, F, 3A–D, F). Within the upper temporal fossa, the supraoccipital contacts the parietal anteriorly, the prootic anterolaterally, and the opisthotic posterolaterally (Figs 2A, 3A). A posteroventral contact with the basioccipital-exoccipital complex is documented by HLMD Me14997, where the supraoccipital forms the dorsal margin of the foramen magnum and roofs the braincase posteriorly. The supraoccipital does not contribute to the foramen stapedio-temporale and canalis stapedio-temporalis, as is the case in other carettochelyids (Waite 1905; Walther 1922; Havlik et al. 2014; Danilov et al. 2017a; Joyce et al. 2018; Rollot et al. 2024a, 2025). The supraoccipital is also excluded from the skull roof (Figs 2A, 3A), which appears to be a unique feature among carettochelyids, although this contribution is generally small in members of the clade (Walther 1922; Danilov et al. 2017a; Joyce et al. 2018; Rollot et al. 2024b). Posteriorly, the supraoccipital forms an elongate crista supraoccipitalis, which is ventrally expanded into a broad, flat shelf (Figs 2A, B, F, 3A, B, F). The crista supraoccipitalis and associated flat shelf represent more than half of the length of the supraoccipital and posteriorly extend far beyond the level of the squamosal processes and appear to be slightly longer than that of *Carettochelys insculpta* (Walther 1922; Rollot et al. 2024b) and similar to the condition seen in *Anosteira maomingensis* (Danilov et al. 2017a). In SMF Me3004, the supraoccipital also roofs the braincase posteriorly and forms the posterior half of the anterior semicircular canal and anterior half of the posterior semicircular canal. Ventromedially, the surface of the supraoccipital perfectly preserves the dorsal aspect of the anterior and posterior semicircular canals. The area

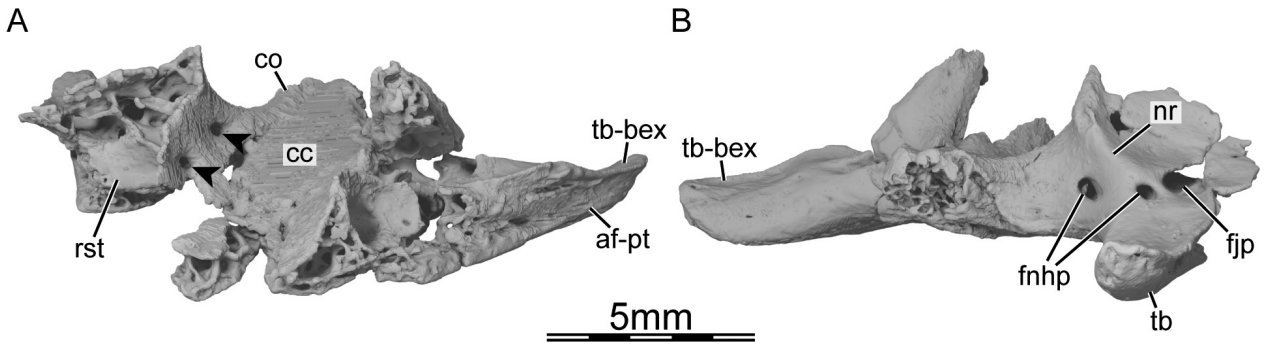


Figure 9. Three-dimensional renderings of the reconstructed basioccipital-exoccipital complex of *Allaeochelys crassesculpta* (SMF Me3004). **A.** Left anterolateral view; **B.** Right posterolateral view. Abbreviations: af-pt, articulation facet for pterygoid; cc, cavum cranii; co, condylus occipitalis; fjp, foramen jugulare posterius; fnhp, posterior foramen nervi hypoglossi; nr, neurapophyseal ridge; rst, recessus scalae tympani; tb-bex, basioccipital-exoccipital complex portion of the tubercula basioccipitale. Black arrowheads show the anterior foramina nervi hypoglossi.

between the two canals, which corresponds to the dorsal imprint of the common crus, is nearly flat and horizontally continuous with the path of the anterior and posterior semicircular canals. This morphology suggests that the dorsal embayment of the common crus was very low, if not completely absent, as seen in *Allaeochelys meylani* (Rollot et al. 2025).

Basioccipital-exoccipital complex. The basioccipital and exoccipitals are fused in SMF Me3004 (Figs 2A–D, F, 3A–D, F, 9), and we, therefore, describe these bones as a single osteological unit. Remnants of the basioccipital-exoccipital suture are visible in HLMD Me7592, but only internally in the area of the foramen jugulare posterius. In SMF Me3004, the basioccipital-exoccipital complex is overall well-preserved, with damage only affecting its most anterior, anterolateral, and dorsal aspects. The basioccipital-exoccipital complex forms the posterolateral wall and posteroventral floor of the braincase and the lateral and ventral margins of the foramen magnum (Figs 3F, 9A). The basioccipital-exoccipital complex contacts the parabasisphenoid anteriorly, the pterygoid anterolaterally and laterally, along the elongate tubercula basioccipitale, and the supraoccipital dorsally (visible in HLMD Me14997; Figs 2A, B, F, 3A, B, F). Additional contact with the opisthotic was likely present, but is not preserved. Posterolaterally, the basioccipital-exoccipital complex forms most of the elongate tubercula basioccipitale, the ventrolateral aspect of it being formed by the pterygoid (Figs 2A, B, 3A, B, 7, 9). Elongate tubercula basioccipitale are also present in *Allaeochelys meylani* (Rollot et al. 2025), *Allaeochelys libyca* (Havlik et al. 2014; Rollot et al. 2024a), and *Carettochelys insculpta* (Waite 1905; Walther 1922; Rollot et al. 2024b), which contrasts with the short tubercula seen in *Anosteira pulchra* (Joyce et al. 2018). The basioccipital-exoccipital complex of SMF Me3004 also forms the posterior wall of the recessus scalae tympani (Fig. 9A). In the posterolateral corner of the recess, the basioccipital-exoccipital complex forms a foramen that leads into a canal, which extends posterolaterally through the bone. The canal joins the external cranial surface via a relatively large foramen jugulare posterius just medial to the suture with the pterygoid (Fig. 9B). The foramina and canal are particularly well-preserved on the right side of SMF Me3004. Within the braincase, ventrally, the basioccipital-exoccipital complex forms two foramina for the hypoglossal nerve (CN XI), the anterior foramen being the smallest of the two (Fig. 9A). Each foramen leads into a separate canal that extends posteroventrolaterally. The anterior and smallest canal joins the posterior surface of the cranium by means of a posterior hypoglossal nerve foramen located just ventromedial to the foramen jugulare posterius (Fig. 9B). The posterior and largest canal also joins the posterior surface of the cranium, but its posterior hypoglossal nerve foramen is located more medially, closer to the occipital condyle (Fig. 9B). Some variation is apparent, as the two posterior hypoglossal nerve foramina are closer to one another on the left side of the specimen. Two posterior foramina for the hypoglossal nerve are also present in *Anosteira pulchra* (Joyce et al. 2018), *Allaeochelys libyca* (Rollot et al. 2024a), and *Carettochelys insculpta* (Walther 1922; Rollot et al. 2024b), contra the single foramen seen in *Anosteira maomingensis* (Danilov et al. 2017a) and *Allaeochelys meylani* (Rollot et al. 2025). In HLMD Me7592, the foramen and canalis oropharyngeale are preserved and the basioccipital-exoccipital complex forms the anterolateral margin of the canal. In SMF Me3004, on the posterior surface of the basioccipital-exoccipital complex, it forms a relatively low, but broad neurapophyseal ridge (Fig. 9B). The neurapophyseal ridge is visible just lateral to the foramen magnum, where it extends ventrolaterally for about half its preserved portion, then bends and extends laterally towards the anterior base of the tubercula basioccipitale, separating the foramen jugulare posterius from the posterolateral hypoglossal nerve foramen. The neurapophyseal ridge laterally ends at the most posterior level of the hypoglossal nerve foramina. The neurapophyseal ridge separates the posterior surface of the basioccipital-exoccipital complex into two distinct fossae, located ventromedial and dorsolateral from the ridge, as also seen in *Allaeochelys meylani* (Rollot et

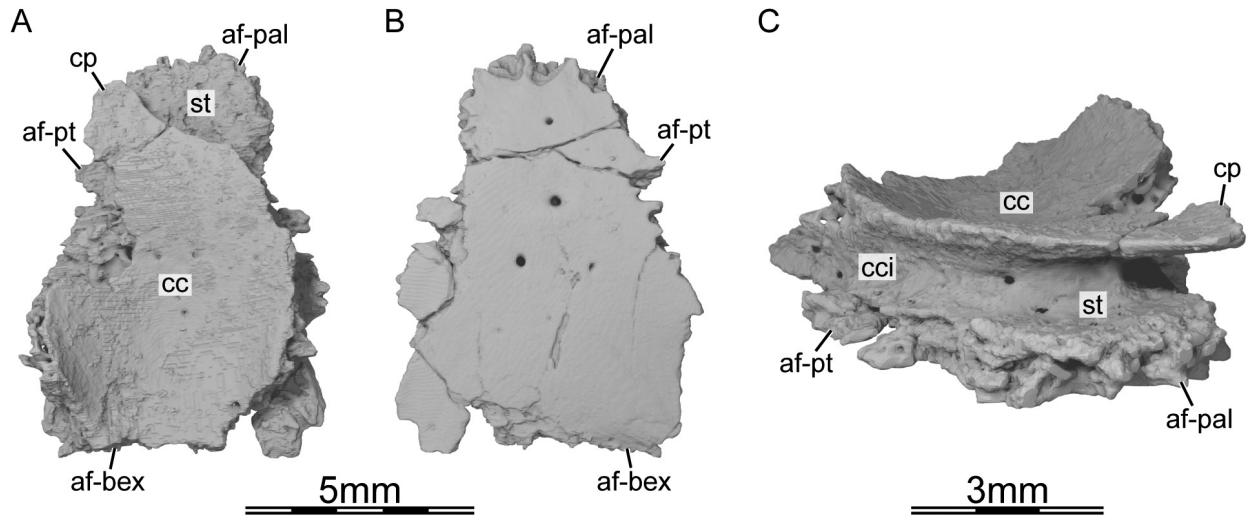


Figure 10. Three-dimensional renderings of the reconstructed parabasisphenoid of *Allaeochelys crassesculpta* (SMF Me3004). **A.** Dorsal view; **B.** Ventral view; **C.** Right anterolateral view. Abbreviations: af-bex, articulation facet for basioccipital-exoccipital complex; af-pal, articulation facet for palatine; af-pt, articulation facet for pterygoid; cc, cavum cranii; cci, canalis caroticus internus; cp, clinoid process; st, sella turcica.

al. 2025), *Allaeochelys libyca* (Rollot et al. 2024a), and *Carettochelys insculpta* (Rollot et al. 2024b). In SMF Me3004, the central part of the ventral surface of the basioccipital-exoccipital complex is flat (Figs 2B, 3B), contrasting with the morphology of this area in other carettochelyids, in which the basioccipital forms a semi-circular depression (Waite 1905; Havlik et al. 2014; Danilov et al. 2017a; Joyce et al. 2018; Rollot et al. 2024a, 2025).

Parabasisphenoid. The parabasisphenoid of SMF Me3004 is overall well-preserved with most of the damage affecting the rostrum basisphenoidale, the left anterolateral aspect, and the right clinoid process (Figs 2B, 3B, 10). Although the parabasisphenoid is nearly complete, we are not able to assess its dorsal contacts and contributions to anatomical structures as the central part of the cranium is completely crushed. The parabasisphenoid contacts the palatine anteriorly, the pterygoid laterally, and the basioccipital-exoccipital complex posteriorly (Figs 2B, 3B, 10). The anterior contact of the parabasisphenoid with the palatine prevents the pterygoid from contacting its counterpart medially (Figs 2B, 3B), as in all carettochelyids (Waite 1905; Walther 1922; Havlik et al. 2014; Danilov et al. 2017a; Joyce et al. 2018; Rollot et al. 2025). Laterally, the parabasisphenoid forms a tall, concave, and smooth surface. Given the position of the foramen posterius canalis carotici interni, which is located just lateral to the parabasisphenoid-pterygoid suture, we can confidently infer that this concave surface corresponds to the medial margin of the canalis caroticus internus and canalis caroticus basisphenoidalis (Fig. 10C). The path of the canalis caroticus internus is preserved in HLMD Me7592, in which it extends anteromedially along the pterygoid-parabasisphenoid suture. Just anterior to the foramen posterius canalis carotici interni, the canalis caroticus internus laterally connects to the canalis pro ramo nervi vidiani, which serves as a passage for the vidian nerve from the geniculate ganglion to the canalis caroticus internus. Slightly anterior to that point, a small canal seems to split from the canalis caroticus internus laterally. This split may correspond to the bifurcation between the canalis caroticus internus and canalis nervus vidianus, but the area is not sufficiently preserved to assess the identity of this canal with confidence. On the right side of HLMD Me3566, a similar arrangement of canals is present, with the possible canalis nervus vidianus bifurcating from the canalis caroticus internus along the pterygoid-parabasisphenoid suture, then laterally merging with an unidentified canal coming from the posterior and anteriorly extending through the pterygoid and, very likely, the palatine. Furthermore, in HLMD Me3566, still on the right side, no additional canal seems to split from the canalis caroticus internus nor extend anteriorly along the pterygoid-parabasisphenoid suture and we, therefore, postulate that the canalis caroticus lateralis is absent in *Allaeochelys crassesculpta*, as in *Allaeochelys libyca* (Rollot et al. 2024a) and *Carettochelys insculpta* (Rollot et al. 2021, 2024b). In HLMD Me7592, the canalis caroticus internus anteriorly becomes the canalis caroticus basisphenoidalis, which extends through the parabasisphenoid and joins the sella turcica by means of the foramen anterius canalis carotici basisphenoidalis. Some variation is apparent in HLMD Me7592, as the right internal carotid canal is about three to four times larger than its left counterpart. In SMF Me3004, the parabasisphenoid anteriorly forms the broad rostrum basisphenoidale, which is mostly missing. The rostrum basisphenoidale likely extended over the posterodorsal surface of the palatine, as the latter surface is developed as an articular facet, as seen in *Carettochelys insculpta* (Rollot et al. 2024b). Anterodorsally, the parabasisphenoid of SMF Me3004 forms a relatively thin dorsum sellae that projects anteriorly over the sella turcica (Fig. 10C). On the left side, the clinoid process appears to be completely preserved

and consists of a short process that extends anterolaterally (Fig. 10A, C), as in *Carettochelys insculpta* (Rollot et al. 2024b). In SMF Me3004, the dorsal surface of the parabasisphenoid is concave. The foramina and canals associated with the path of the abducens nerve (CN VI) are apparent in HLMD Me7592. In the latter specimen, the parabasisphenoid anteriorly forms the foramen posterius canalis nervi abducentis along its dorsal surface. The latter foramen leads into the canalis nervus abducentis, which extends anteriorly within the parabasisphenoid, and anteriorly exits the parabasisphenoid by means of the foramen anterius canalis nervi abducentis, which appears to be located somewhat ventral to the base of the clinoid process, as in *Carettochelys insculpta* (Rollot et al. 2024b). Based on the right side of the specimen, the foramen anterius canalis nervi abducentis seems to be exclusively formed by the parabasisphenoid, but as it is located immediately medial to the lateral articular facet of the parabasisphenoid, a minor contribution of the pterygoid and/or prootic may be present. In SMF Me3004, the posterior and posterolateral surfaces of the parabasisphenoid appear to be nearly intact and the shape of the parabasisphenoid is, therefore, likely very similar to that of other carettochelyids (Havlik et al. 2014; Rollot et al. 2024a, 2024b). This area may have had a similar morphology to that of *Carettochelys insculpta* (Rollot et al. 2024b), which exhibits a ventrally enlarged cavum labyrinthicum, but the lack of preservation of the surrounding bones hinders certainty regarding this observation.

Mandible

General comments. SMNK Pal45053 is a nearly complete mandible that is slightly crushed (Fig. 11). Most of the damage that affects the mandible is located around the fossa Meckelii. The mandibular bones are generally well-preserved, except for the prearticular and surangular, where the anterior half is damaged on both sides. The mandible generally closely resembles that of *Carettochelys insculpta* (Evers et al. 2022; Rollot et al. 2024b) and only minor differences can be identified (see below).

Dentary. The dentaries are fused in SMNK Pal45053 along a slightly expanded symphysis (Fig. 11A, B). The dentary contacts the coronoid posterodorsally, the surangular posteriorly, and the angular posteroventrally (Fig. 11). The dentary forms a low labial ridge, which is best visible along the anterior half of the element (Fig. 11G–J). The posterior half of the triturating surface of the dentary is slightly concave (Fig. 11D), forming a similar depression to that observed in *Carettochelys insculpta* (Rollot et al. 2024b). Some variation is apparent, as this depression is only formed by the dentary in SMNK Pal45053, but by the dentary and coronoid in adult *Carettochelys insculpta* (Rollot et al. 2024b). In *Anosteira maomingensis*, the morphology of the mandible is different, as the triturating surface is subdivided into a flattened posterior expanded region, which is anteromedially delimited by a low, longitudinal ridge (Tong et al. 2010). A lingual ridge is absent in SMNK Pal45053 (Fig. 11H, J). In lateral view, along its posterior half, the dentary forms a deep adductor fossa (Fig. 11G, I), which likely served as the insertion area for the *M. zygomaticomandibularis* as seen in *Carettochelys insculpta* (Werneburg 2011; Rollot et al. 2024b). In SMNK Pal45053, the adductor fossa is anterolaterally and ventrolaterally delineated by a lateral dentary ridge (*sensu* Evers et al. (2022)). Along the anterior margin of the fossa, the dentary forms the foramen dentofaciale majus. In medial view, the dentary forms a groove that extends anteroposteriorly for most of its length and which is the anterior continuation of the fossa Meckelii (Fig. 11H, J). Just dorsal to this groove and ventral to the suture between the dentary and coronoid, the dentary forms the foramen alveolare inferius.

Surangular. The surangular of SMNK Pal45053 forms most of the posterolateral aspect of the mandible (Fig. 11). The surangular contacts the dentary anteriorly and anteroventrally, the prearticular anteromedially, the articular medially and posteromedially, and the angular ventrally (Fig. 11). The anterodorsal process is almost completely missing and contact with the coronoid is, therefore, not preserved. Such a contact was nevertheless likely present given the arrangement of these two bones and by reference to *Carettochelys insculpta*, in which it is present (Evers et al. 2022; Rollot et al. 2024b). In lateral view, posterior to the adductor fossa and ventral to the anterior aspect of the ectocondylar flange, the surangular forms the foramen auriculotemporalis (Fig. 11G). Although the area of the fossa Meckelii is severely damaged, a small portion of the surangular remains preserved, showing that it formed the posterolateral wall of the fossa. Anterodorsomedially, the surangular forms a large dorsal surangular foramen (*sensu* Evers et al. (2022); Fig. 11A), which is located just lateral to the suture with the articular and appears to be larger than that of *Carettochelys insculpta* (Rollot et al. 2024b). Posterodorsally, the surangular forms a laterally expanded ectocondylar flange, which forms slightly more than half of the mandibular articular surface (Fig. 11C). Posterior to the mandibular articular surface, the surangular borders the retroarticular process of the articular laterally (Fig. 11C, F).

Coronoid. The two coronoids are almost completely preserved in SMNK Pal45053 (Fig. 11A–D, F–J). Only their most posteroventromedial aspect is slightly damaged. The coronoid contacts the dentary anteroventrally and the prearticular posteroventromedially (Fig. 11A–D, F–J). Contact with the surangular was likely present posteroventrolaterally, but damage to the latter bone prevents assessment (see Surangular above). The coronoid forms a process anteromedially that extends over the dentary medially and forms the posteromedial corner of the triturating surface (Fig. 11C, D, F). The coronoid also forms the most dorsal aspect of the adductor fossa (Fig. 11G, I). The coronoid process is tall and slightly recurved posteriorly (Fig. 11G–J), as in *Carettochelys insculpta* (Evers et al. 2022; Rollot et al. 2024b), but unlike *Anosteira maomingensis*, where the anterior margin of the coronoid is vertically oriented (Tong et al. 2010). A weak coronoid notch is present in SMNK Pal45053 (Fig. 11G–J), again as in *Carettochelys insculpta* (Evers et al. 2022; Rollot et

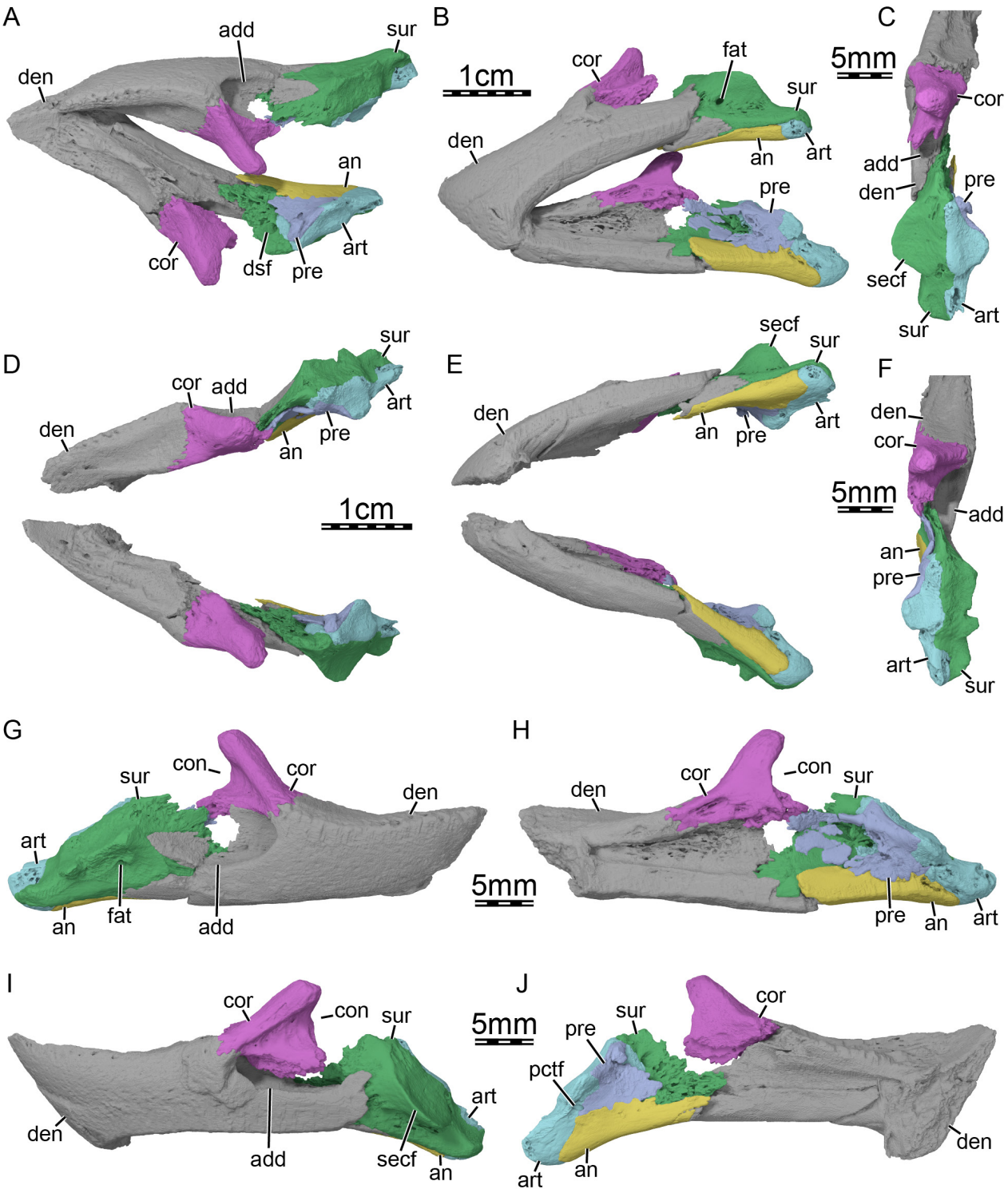


Figure 11. Three-dimensional renderings of the segmented mandible of *Allaeochelys crassesculpta* (SMNK Pal45053). **A.** Dorsolateral view; **B.** Ventrolateral view; **C.** Dorsal view of left ramus; **D.** Dorsal view of reconstructed mandible; **E.** Ventral view of reconstructed mandible; **F.** Dorsal view of right ramus; **G.** Lateral view of right ramus; **H.** Medial view of right ramus; **I.** Lateral view of left ramus; **J.** Medial view of left ramus. Abbreviations: add, adductor fossa; an, angular; art, articular; con, coronoid notch; cor, coronoid; den, dentary; dsf, dorsal surangular foramen; fat, foramen auriculotemporalis; pctf, posterior chorda tympani foramen; pre, prearticular; secf, ectocondylar flange of the surangular; sur, surangular.

al. 2024b). On its lateral surface, the coronoid of SMNK Pal45053 forms a shallow depression, similar to that of *Carettochelys insculpta* (Evers et al. 2022; Rollot et al. 2024b), albeit larger than in the latter as it expands on almost all the lateral surface of the element (Fig. 11G, I).

Prearticular. The prearticular is heavily damaged on both sides in SMNK Pal45053 (Fig. 11A–F, H, J). The preserved bony contacts of the prearticular are with the surangular anteroventrally, the angular ventrally, and the articular laterally (Fig. 11A–F, H, J). On the right side,

several small and thin pieces of bone were segmented and attributed to the prearticular, based on their morphology and position on the medial and posteromedial side of the mandible. The most anterodorsal of these plates slightly contacts the coronoid anterodorsally and likely represents the most anterior portion of the anterodorsal process of the prearticular (Fig. 11H), as seen in *Carettochelys insculpta* (Evers et al. 2022; Rollot et al. 2024b). The small plates of bone on the right side of SMNK Pal45053, identified as belonging to the prearticular, thus also form the medial wall of the fossa Meckelii and the medial margin of its dorsal foramen. A posterior chorda tympani foramen seems to be preserved on the left prearticular and is located just medial to the prearticular-articular suture and ventral to the anterior extent of the ectocondylar flange of the articular (Fig. 11J).

Angular. The angular is nearly completely preserved on both sides in SMNK Pal45053 (Fig. 11A, B, E, F, G–J). The angular is small and elongate and forms the posteroventromedial aspect of the mandible (Fig. 11E). The anterior half of the angular is developed as a mediolaterally thin sheet of bone, whereas the posterior half of the element is mediolaterally more expanded and almost as wide as tall. The angular contacts the dentary anteriorly and anterolaterally, the surangular laterally and posterolaterally, the prearticular dorsomedially, and the articular dorsally and posterodorsally (Fig. 11A, B, E, F, G–J).

Splenial. The splenials are absent in SMNK Pal45053, as in *Carettochelys insculpta* (Evers et al. 2022; Rollot et al. 2024b) and, likely, *Anosteira maomingensis* (Tong et al. 2010).

Articular. The articular is nicely preserved on both sides of SMNK Pal45053 and only shows minor signs of damage surficially along the retroarticular process (Fig. 11). The articular contacts the prearticular anteromedially, the angular ventrally and ventromedially, and the surangular laterally (Fig. 11). As the articular is dorsally expanded and tightly sutured to the surangular and prearticular along the entire height of the latter two bones, it forms a tall wall that structures the posterior margin of the fossa Meckelii, which is posteriorly completely enclosed by bone as in adult *Carettochelys insculpta* (Rollot et al. 2024b). The articular of SMNK Pal45053 also forms the medial portion of the mandibular articular surface, which represents slightly less than half of the entire surface, most of it being shaped by the surangular (Fig. 11C, F). Posteriorly, the articular forms the retroarticular process (Fig. 11C, F, H, J). Between the mandibular articular surface and distal part of the retroarticular process, the articular forms a smooth and slightly concave surface, which corresponds to the articular notch (Fig. 11H, J).

Shell

General comments. *Allaeochelys crassesculpta* is known from more than a hundred often complete and articulated specimens. As mentioned above (see Material and methods), we here focus on the material housed at HLMD and SMF, with the addition of one nicely preserved specimen from the SMNK.

As most specimens are flattened, carapacial bones are typically slightly displaced, often preventing accurate assessment of the exact contacts between bones, in particular between the costals and peripherals. A few specimens, however, at least partially preserve the original morphology of the shell and we explicitly refer to those in the following sections when needed. We otherwise describe the shell morphology of *Allaeochelys crassesculpta* without specific reference to individual specimens because of the great number of specimens studied herein (Figs 12–29). Likewise, concerning intraspecific variation, reference to single specimens is only made when such variation can confidently be identified among our sample.

The shell of *Allaeochelys crassesculpta* is covered by the typical surface ornamentation of carettochelyids consisting of thick ridges separated by equally-sized grooves. As in all carettochelyids, the carapace has a midline keel, a nuchal, ten peripherals, a single suprapygal, and a pygal (Waite 1905; Walther 1922; Havlik et al. 2014; Joyce 2014). The plastron of *Allaeochelys crassesculpta* resembles that of other carettochelyids by having a triangular entoplastron, large epiplastra, and plastral kinesis (Havlik et al. 2014; Joyce 2014). The carapace of *Allaeochelys crassesculpta* notably differs from that of *Kizylkumemys* spp. and *Anosteira* spp. by lacking carapacial scutes (Leidy 1873; Clark 1932; Zangerl 1947; Chow and Liu 1955; Nessov 1977; Tong et al. 2005) and from that of *Carettochelys insculpta* by having an uninterrupted neural series (Walther 1922; Joyce 2014). The plastron of *Allaeochelys crassesculpta* differs from the earliest branching representatives *Kizylkumemys schultzi* and *Anosteira* spp. by having a larger posterior plastral lobe (Leidy 1873; Gilmore 1931; Clark 1932; Zangerl 1947; Chow and Liu 1955; Nessov 1977), which is similar in width to that of other *Allaeochelys* species (Broin 1977; Carbot-Chanona et al. 2020; Rollot et al. 2025), but narrower than that of *Carettochelys insculpta* (Waite 1905; Walther 1922; Joyce 2014). The plastron of *Allaeochelys crassesculpta* also differs from *Kizylkumemys schultzi* by lacking plastral scutes (Nessov 1977), a similar condition to that observed in other carettochelyids (Leidy 1873; Gilmore 1931; Clark 1932; Zangerl 1947; Chow and Liu 1955; Young and Chow 1962; Broin 1977; Hutchison et al. 2004; Carbot-Chanona et al. 2020; Rollot et al. 2025).

Nuchal. The nuchal forms the anterior margin of the shell. The shape of the anterior margin shows minor variation and is either completely straight (HLMD Me1461, Fig. 14; HLMD Me13721, Fig. 18; SMF Me611, Fig. 21; SMF Me1794, Fig. 22; SMNK Pal986, Fig. 29) or slightly concave (HLMD Be158, Fig. 12; HLMD Be159, Fig. 13; SMF Me3783, Fig. 27), but this may be a taphonomic artefact. A straight anterior carapace margin is also observed in *Kizylkumemys schultzi* (Nessov 1977), *Kizylkumemys khoratensis* (Tong et al. 2005), and *Carettochelys insculpta* (Waite 1905; Walther 1922), but differs from *Anosteira mongoliensis* (Gilmore 1931), *Anosteira ornata* (Leidy 1873) and, perhaps, *Anosteira pulchra* (Clark 1932), where a pronounced anterior emargination can be observed. The nuchal of *Allaeochelys crassesculpta* is wider than long and contacts peripheral I laterally, costal I posterolaterally, and neural I posteriorly.

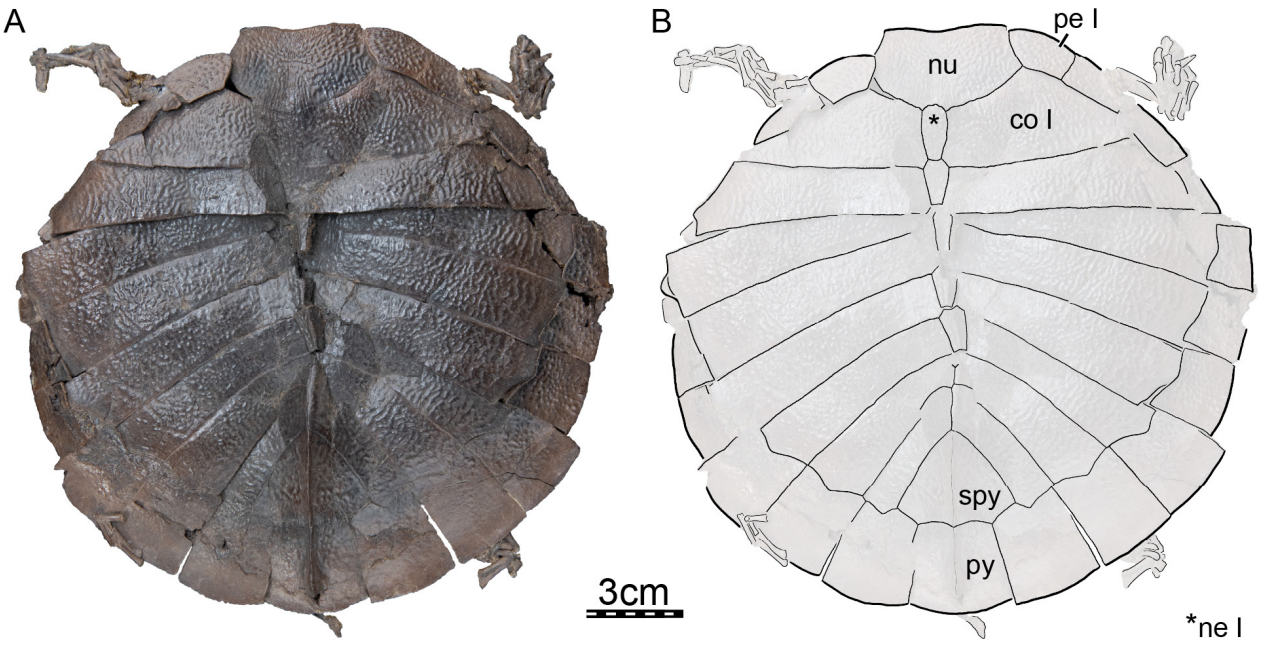


Figure 12. HLMD Be158, a nearly complete skeleton of *Allaeochelys crassesculpta*. **A.** Photograph in dorsal view; **B.** Interpretive line drawing in dorsal view. Abbreviations: co I, costal I; ne I, neural I; nu, nuchal; pe I, peripheral I; py, pygal; spy, suprapygal.

On its ventral surface, the nuchal forms paired nuchal processes, which are particularly visible in specimen SMF Me2449 (Fig. 23).

Neurals. Among our sample of *Allaeochelys crassesculpta*, the neural series is usually damaged, incomplete, or hidden from view in many specimens, but a few individuals preserve the entire intact series (HLMD Be159, Fig. 13; HLMD Me1461, Fig. 14; HLMD Me7429, Fig. 17; SMF Me611, Fig. 21; and SMF Me11418, Fig. 28), showing that *Allaeochelys crassesculpta* has an uninterrupted series of seven neurals. An uninterrupted series of neurals is observed in all carettochelyids (Leidy 1873; Clark 1932; Zangerl 1947; Broin 1977), except *Carettochelys insculpta*, in which the neural series is interrupted by midline contacts between pairs of costals (Waite 1905; Walther 1922; Joyce 2014). In *Allaeochelys crassesculpta*, the first neural is four-sided, whereas neurals II to VI are hexagonal, with short anterolateral and long posterolateral sides. Neural VII is hexagonal, too, albeit much smaller than the other neurals and about as wide as long. Neurals I to III are elongate and much longer than wide. Neural V and perhaps sometimes neural IV (e.g., HLMD Be158, Fig. 12; and SMNK Pal986, Fig. 29) appear to be somewhat slightly wider than neurals I–III. It is nevertheless clear that a progressive decrease in length of the neurals can be observed from neural V to VII. Neural I contacts the nuchal anteriorly, costal I laterally, and neural II posteriorly. Neurals II to VII each contact two pairs of costals: costals I–II, II–III, III–IV, IV–V, V–VI, and VI–VII, respectively. The outlines and contacts of the neurals appear to be nearly identical in most carettochelyids (Leidy 1873; Zangerl 1947; Broin 1977; Nessov 1977; Tong et al. 2005), but three deviations to the common neural arrangement can be observed. In *Anosteira pulchra*, neurals II and III are four-sided and only contact one pair of costals, costals II and III, respectively (Clark 1932). In *Allaeochelys liliae*, neural VII is a fairly robust element that is relatively larger than in other carettochelyids and also much longer than wide (Carbot-Chanona et al. 2020). Finally, in *Carettochelys insculpta*, the neural series is interrupted by midline contacts of several pairs of costals (Waite 1905; Walther 1922; Joyce 2014). The carapace of *Allaeochelys crassesculpta* forms a midline keel to which several neurals may contribute. There appears to be variation to the neural on which the keel anteriorly commences, but caution is required when interpreting this feature, as the shells studied herein show different amounts of crushing and because the keel of carettochelyids generally forms gradually. In our sample of *Allaeochelys crassesculpta*, the keel seems to commence anteriorly at either neural II (HLMD Me1461, Fig. 14; HLMD Me7593, Suppl. material 1: fig. S1.8), neural III (HLMD Me4282, Fig. 15), neural IV (SMF Me3783, Fig. 27; SMNK Pal986, Fig. 29), neural V (HLMD Me7429, Fig. 17; HLMD Me15012, Fig. 19; SMF Me11418, Fig. 28), or even more posteriorly along costal pair VII or VIII (SMF Me611, Fig. 21; SMF Me1794, Fig. 22).

Costals. Eight pairs of costals are present in the carapace of *Allaeochelys crassesculpta*. Costals I and II are recurved towards the anterior, costal III is nearly straight, and costals IV to VIII are recurved towards the posterior, with the degree of curvature progressively increasing from costal IV to VIII. The mediolateral width of costals IV to VIII also progressively decreases towards the back of the carapace, with costal IV being the widest element and costal VIII the narrowest. Costal I is the largest costal and contacts the nuchal anteromedially, peripheral I anterolaterally, peripheral II laterally, peripheral III posterolaterally, neural I medially, neural II posteromedially, and costal II posteriorly. Costals II to VI each contact two pairs of neurals: neurals II–III, III–IV, IV–V, V–VI, and VI–VII, respectively. Costal VII contacts neural VII

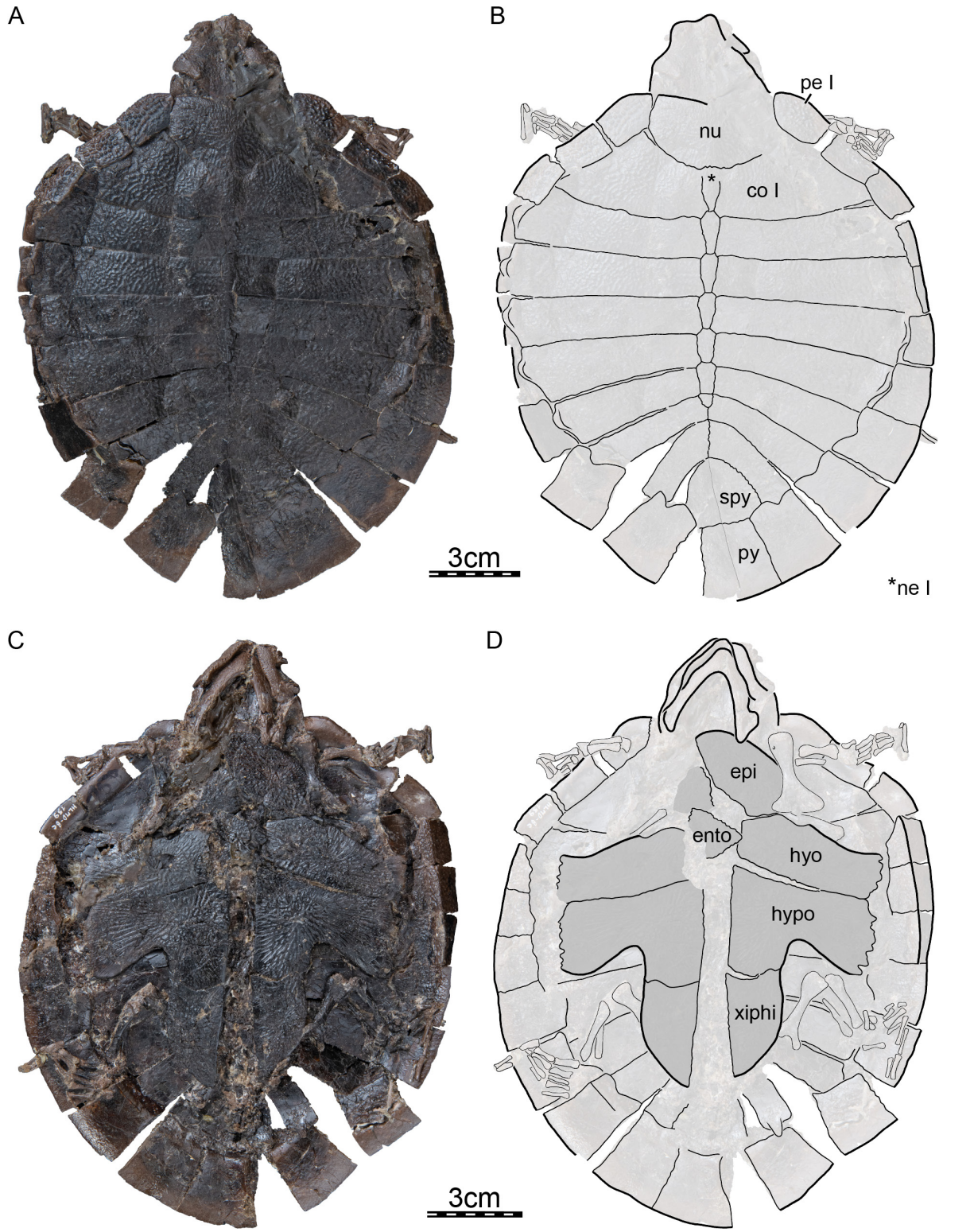


Figure 13. HLMD Be159, a nearly complete skeleton of *Allaeochelys crassesculpta*. **A.** Photograph in dorsal view; **B.** Interpretive line drawing in dorsal view; **C.** Photograph in ventral view; **D.** Interpretive line drawing in ventral view. Abbreviations: co I, costal I; ento, entoplastron; epi, epiplastron; hyo, hyoplastron; hypo, hypoplastron; ne I, neural I; nu, nuchal; pe I, peripheral I; py, pygal; spy, suprapygal; xiphi, xiphiplastron.

anteromedially and its counterpart medially, while costal VIII medially only contacts its counterpart. Laterally, the contacts of the costals with the peripherals are difficult to assess due to crushing and flattening of most specimens that slightly displaced most carapacial bones. This prevents us from unequivocally determining morphological variation, as apparent differences in contacts might be the result of crushing, not intraspecific variation. We nevertheless tentatively identify the most likely contacts between costals and peripherals by reference to

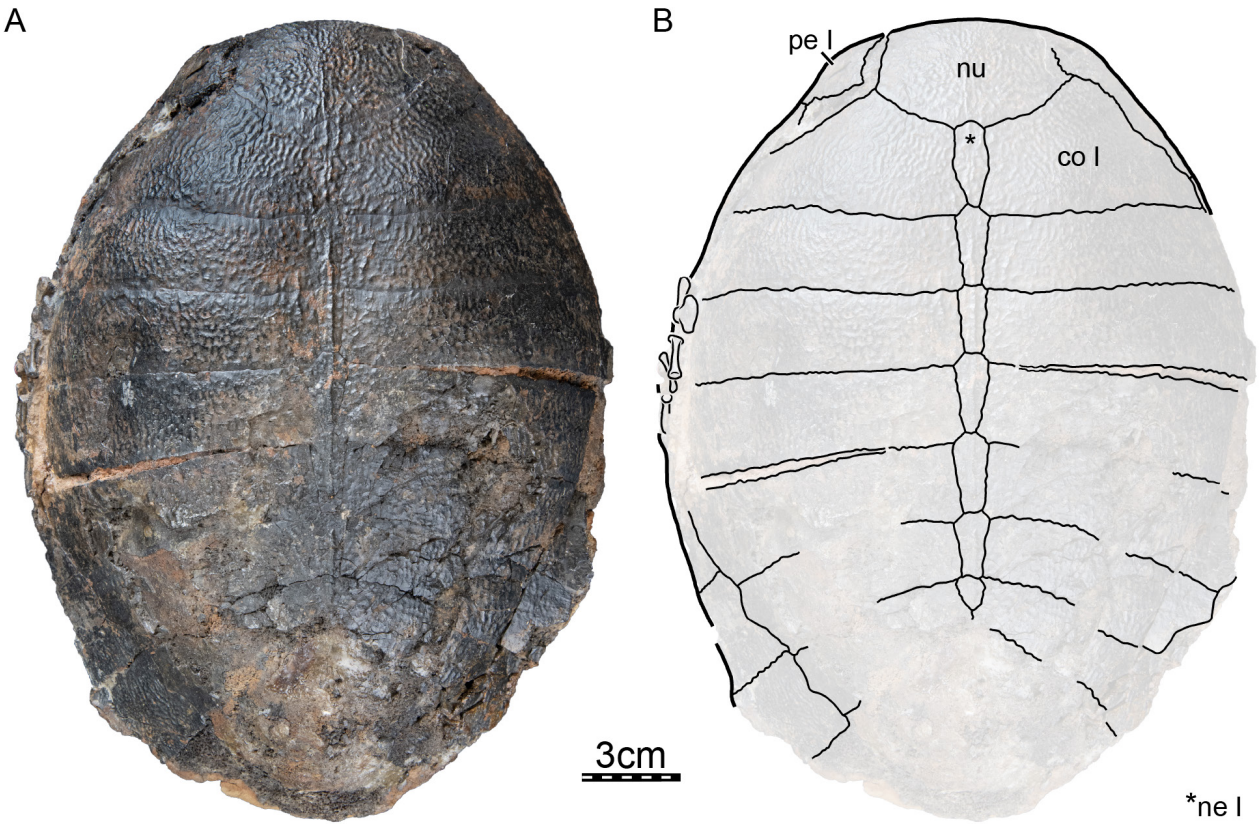


Figure 14. HLMD Me1461, one of three syntypes, a nearly complete shell of *Allaeochelys crassesculpta*. **A.** Photograph in dorsal view; **B.** Interpretive line drawing in dorsal view. Abbreviations: co I, costal I; ne I, neural I; nu, nuchal; pe I, peripheral I.

single specimens (sometimes even on one side only) that show the least crushing and displacement in the areas of interest. The lateral aspect of costal II is best preserved on the left side of SMF Me3018, where it contacts peripherals III and IV (Fig. 24). For costal III, genuine lateral contacts are preserved in SMF Me3018 and SMF Me11418, in which it contacts peripheral V for most of its length and peripheral VI posterolaterally for a very short distance (Figs 24, 28). A brief contact with peripheral IV might have occurred anterolaterally, but remains hypothetical because of crushing. For costal IV, contacts are best preserved in SMF Me1794 and SMF Me3018, which show an elongate suture of this bone joining with peripheral VI laterally and, perhaps, a short contact with peripheral VII posterolaterally (Figs 22, 24). HLMD Me7429 and SMF Me1794 best preserve the lateral aspect of costal V, which mostly contacts peripheral VII laterally and, likely, also peripheral VIII posterolaterally (Figs 17, 22). The morphology of costal VI is particularly well-preserved in numerous specimens, including HLMD Be158 (Fig. 12), HLMD Me7429 (Fig. 17), SMF Me1794 (Fig. 22), SMF Me3783 (Fig. 27), and SMF Me11418 (Fig. 28), in which the bone mostly contacts peripheral VIII and also has a short contact posterolaterally with peripheral IX. For costal VII, contacts are best visible in HLMD Be158 (Fig. 12), HLMD Me1461 (Fig. 14), HLMD Me7429 (Fig. 17), HLMD Me14920 (Suppl. material 1: fig. S1.21), and HLMD Me15012 (Fig. 19), in which costal VII only contacts peripheral IX. However, in SMF Me1794, an additional contact with peripheral X is visible posterolaterally on both sides, which appears to reflect the actual bony arrangement in the area rather than being the result of crushing, highlighting possible intraspecific variation for this feature (Fig. 22). Although many specimens seem to nicely preserve costal VIII, a close look reveals that minor damage or displacement prevents us from being certain of the lateral contacts of costal VIII. In specimens HLMD Me7428 (Fig. 16), HLMD Me7429 (Fig. 17), and HLMD Me14920 (Suppl. material 1: fig. S1.21), costal VIII mostly contacts peripheral X, but also has an extremely short contact with peripheral IX posterolaterally.

Peripherals. Ten pairs of peripherals contribute to the carapacial rim in *Allaeochelys crassesculpta*. As the contacts between the peripherals and costals are difficult to identify and were discussed in detail above (see Costals), we here only list the most certain contacts of each peripheral with the neighboring costals. According to our observations, the peripherals have the following contacts: peripheral I with the nuchal medially, costal I posteriorly, and peripheral II posterolaterally; peripheral II with peripheral I anteromedially, costal I posteromedially, and peripheral III posterolaterally; peripheral III with peripheral II anteriorly, costal I anteromedially, costal II posteromedially, and peripheral IV posteriorly; peripheral IV with peripheral III anteriorly, costal II medially, and with peripheral V posteriorly; peripheral V with peripheral IV anteriorly, costal III medially, and peripheral VI posteriorly; peripheral VI with peripheral V anteriorly, costal III anteromedially, costal IV

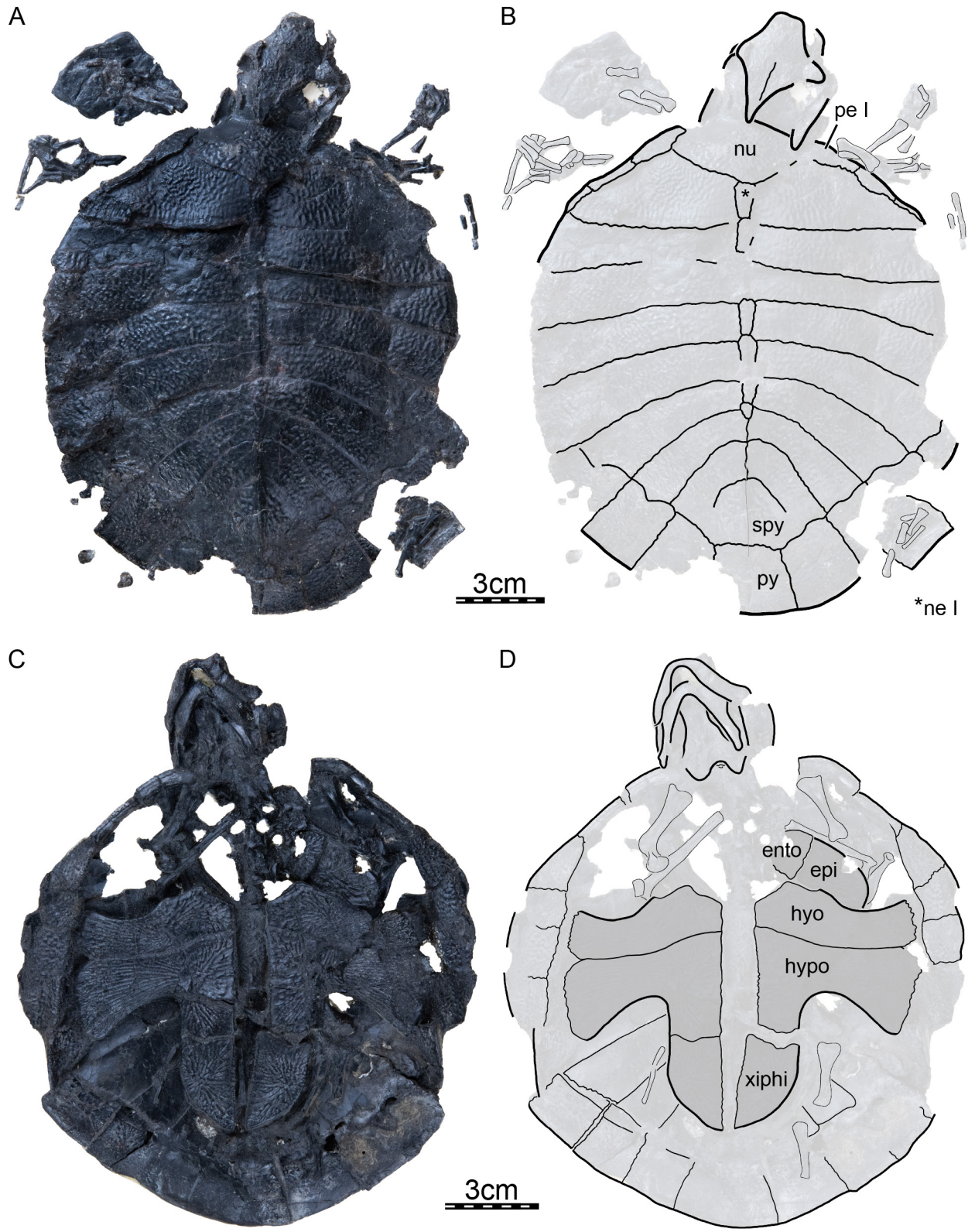


Figure 15. HLMD Me4282, a nearly complete skeleton of *Allaeochelys crassesculpta*. **A.** Photograph in dorsal view; **B.** Interpretive line drawing in dorsal view; **C.** Photograph in ventral view; **D.** Interpretive line drawing in ventral view. Abbreviations: co I, costal I; ento, entoplastron; epi, epiplastron; hyo, hyoplastron; hypo, hypoplastron; ne I, neural I; nu, nuchal; pe I, peripheral I; py, pygal; spy, suprapygal; xiphi, xiphiplastron.

medially, and peripheral VII posteriorly; peripheral VII with peripheral VI anteriorly, costal V medially, and peripheral VIII posteromedially; peripheral VIII with peripheral VII anteriorly, costal VI medially, and peripheral IX posteromedially; peripheral IX with peripheral VIII anterolaterally, costal VI anteromedially, costal VII medially, and peripheral X posteromedially; peripheral X with peripheral IX anterolaterally, costal

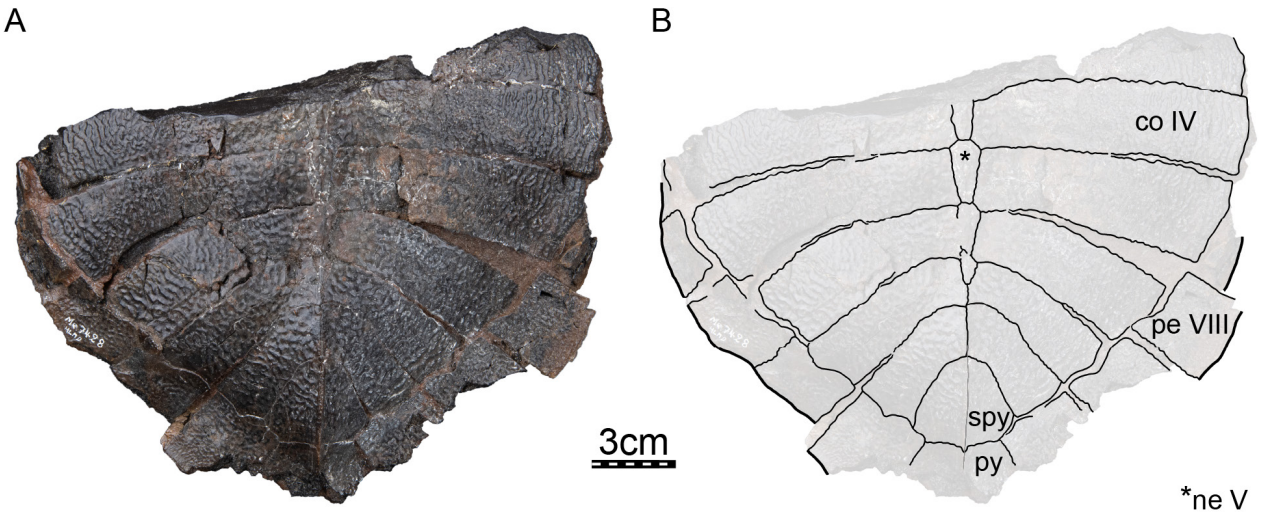


Figure 16. HLMD Me7428, posterior half of a carapace of *Allaeochelys crassesculpta*. **A.** Photograph in dorsal view; **B.** Interpretive line drawing in dorsal view. Abbreviations: co IV, costal IV; ne V, neural V; pe VIII, peripheral VIII; py, pygal; spy, suprapygal.

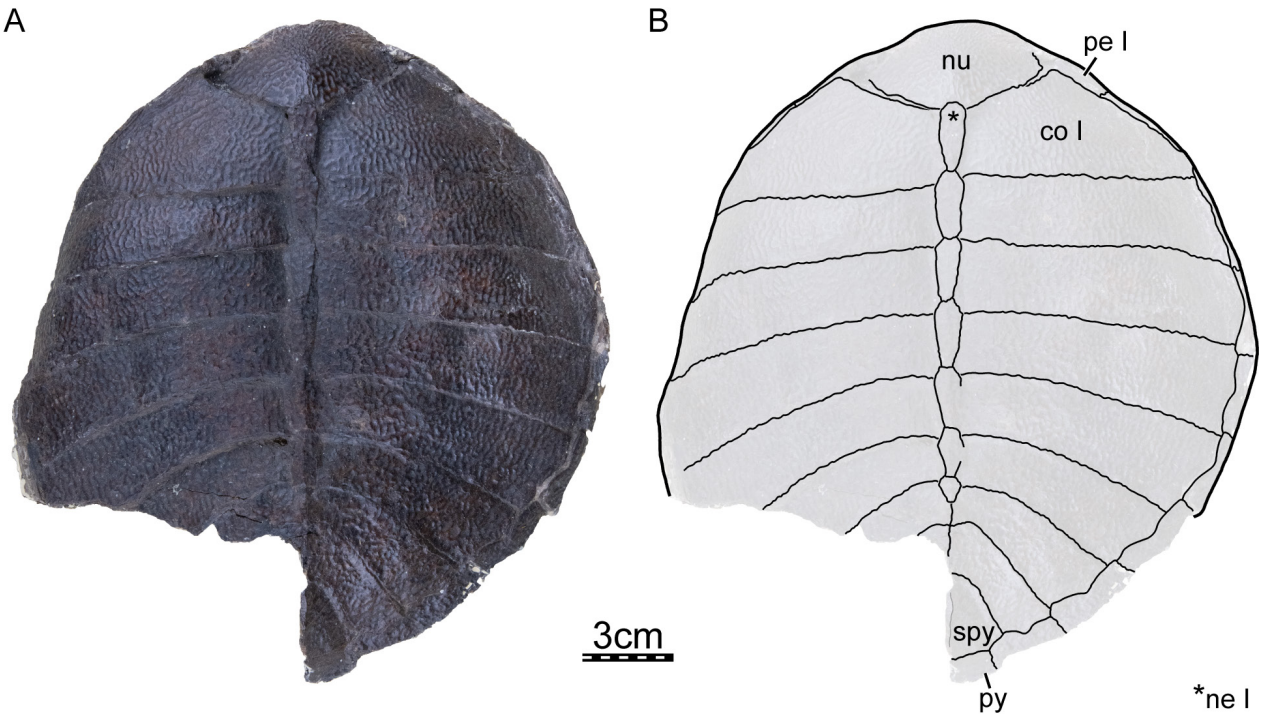


Figure 17. HLMD Me7429, a nearly complete carapace of *Allaeochelys crassesculpta*. **A.** Photograph in dorsal view; **B.** Interpretive line drawing in dorsal view. Abbreviations: co I, costal I; ne I, neural I; nu, nuchal; pe I, peripheral I; py, pygal; spy, suprapygal.

VIII anteromedially, the suprapygal medially, and the pygal posteromedially. Peripherals IV to VII contribute to the formation of the bridge, which is particularly well-preserved in specimens HLMD Me7593 (Suppl. material 1: fig. S1.8), HLMD Me9722 (Suppl. material 1: fig. S1.12), HLMD Me13484 (Suppl. material 1: fig. S1.19), HLMD Me15012 (Fig. 19), HLMD Me15956 (Fig. 20), SMF Me1794 (Fig. 22), SMF Me3018 (Fig. 24) and SMF Me3566 (Fig. 25). Peripherals IV to VII are V-shaped in cross-section and their ventromedial edge forms a series of sockets for articulation with the hyo- and hypoplastron. The bridge anteriorly starts at about one third to half of the anteroposterior length of peripheral IV and posteriorly ends along the anterior aspect of peripheral VII, which only contributes its anterior third. The extent of the bridge in juveniles seems to be similar (see below). The posterior peripheral elements (i.e. peripherals VII to X and the pygal) form a continuous lip along their visceral side, as in other carettochelyids (Leidy 1873; Dollo 1886; Nessov 1977; Joyce 2014; Rollot et al. 2025).

Suprapygal. A single suprapygal is present in *Allaeochelys crassesculpta*, as in other carettochelyids (Leidy 1873; Dollo 1886; Waite 1905; Walther 1922; Chow and Liu 1955; Broin 1977; Nessov 1977; Carbot-Chanona et al. 2020; Rollot et al. 2025). The suprapygal is pentagonal with short posterolateral sides, making it mostly triangular. The suprapygal is about

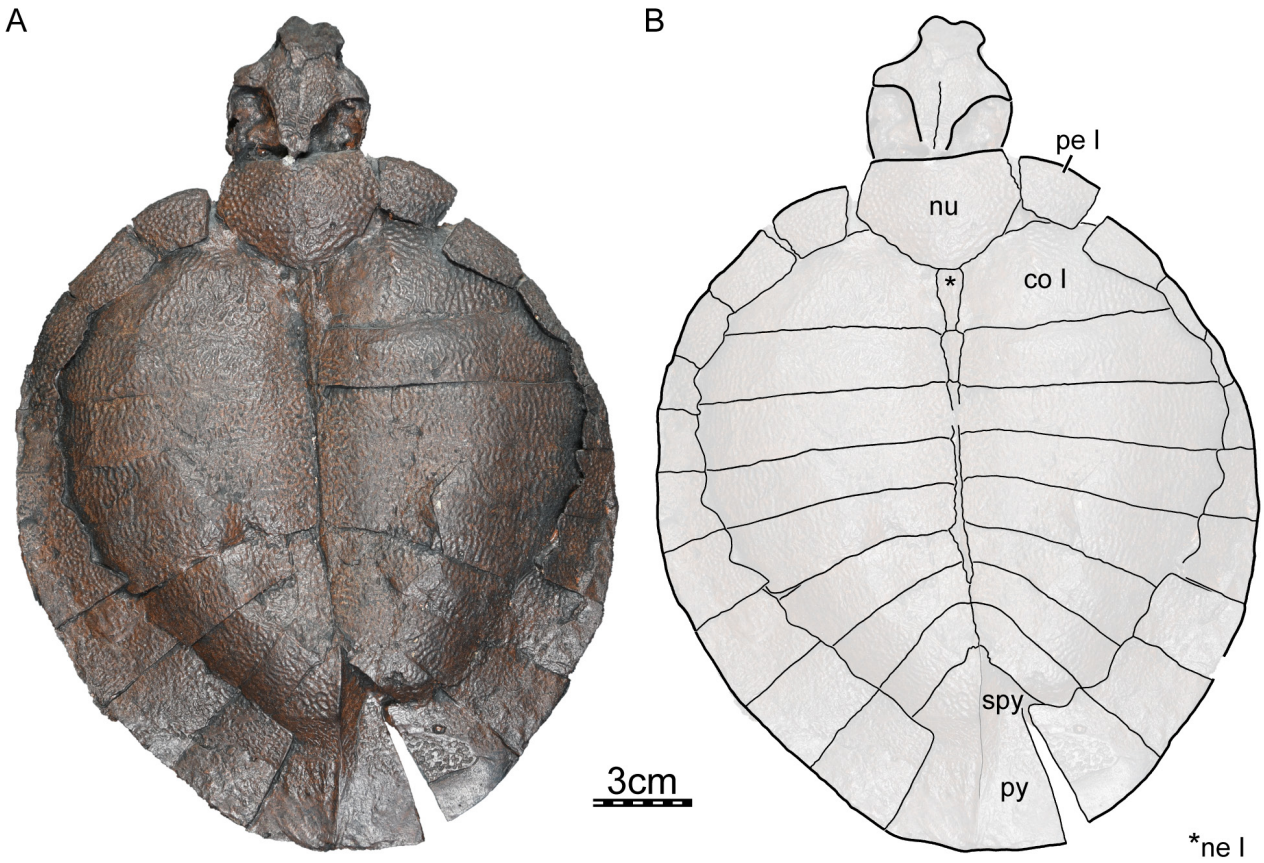


Figure 18. HLMD Me13721, a nearly complete skeleton of *Allaeochelys crassesculpta*. **A.** Photograph in dorsal view; **B.** Interpretive line drawing in dorsal view. Abbreviations: co I, costal I; ne I, neural I; nu, nuchal; pe I, peripheral I; py, pygal; spy, suprapygal.

as wide as long, as in *Kizylkumemys schultzi* (Nessov 1977), *Allaeochelys delheidi* (Dollo 1886), *Allaeochelys parayrei* (Broin 1977), *Allaeochelys liliae* (Carbot-Chanona et al. 2020), and *Allaeochelys meylani* (Rollot et al. 2025), which likely contrasts with *Allaeochelys magnifica* (Hutchison et al. 2004), where the suprapygal is slightly longer than wide. The suprapygal contacts costal VIII anteriorly and laterally, peripheral X posterolaterally, and the pygal posteriorly. A sutural articulation to the pygal only occurs along the dorsal half of the latter, as its ventral part forms a continuous lip with peripherals VII to X. The midline keel crosses the full length of the suprapygal, which is also visible in the juveniles.

Pygal. The pygal is a single element that forms the posterior margin of the carapace. It is slightly longer than wide and contacts the suprapygal anteriorly and peripheral X laterally. The pygal forms a relatively thick lip on its visceral side that is continuous with peripherals VII to X, as in other carettochelyids (Leidy 1873; Dollo 1886; Nessov 1977; Joyce 2014; Rollot et al. 2025). The keel that extends anteroposteriorly along the midline of the carapace ends on the pygal, very close to the posterior margin of the carapace, in both adult and juvenile individuals.

Epiplastron. The epiplastron of *Allaeochelys crassesculpta* is a relatively large element, that, along with its counterpart, forms most of the anterior plastral lobe and the anterior and anterolateral margin of the plastron. The anterior plastral lobe is similar to that of *Allaeochelys parayrei* (Broin 1977), broader than that of *Kizylkumemys schultzi* (Nessov 1977), and slightly narrower than that of *Carettochelys insculpta* (Waite 1905; Walther 1922; Joyce 2014). The epiplastron is notably broad as in *Allaeochelys parayrei* (Broin 1977) and similar to that of *Carettochelys insculpta* (Waite 1905; Walther 1922; Joyce 2014), but broader than in *Kizylkumemys schultzi* (Nessov 1977) and *Anosteira manchuriana* (Zangerl 1947). The epiplastron of *Allaeochelys crassesculpta* contacts its counterpart anteromedially, the entoplastron posteromedially, and the hyoplastron posteriorly. The midline suture of the epiplastron that is shared with its counterpart is about as long as or slightly longer than the length of the entoplastron, as in *Carettochelys insculpta* (Waite 1905; Walther 1922; Joyce 2014). This differs from *Kizylkumemys schultzi* (Nessov 1977) and *Anosteira manchuriana* (Zangerl 1947), in which the midline suture between the epiplastra is clearly shorter than the length of the entoplastron. As in other carettochelyids, the epiplastra form a unit with the entoplastron that is ligamentously connected to the remainder of the plastron along a sinuous contact that allows for some kinesis. For this reason, these two bones are usually found disarticulated.

Entoplastron. The entoplastron of *Allaeochelys crassesculpta* forms the central part of the anterior plastral lobe. The shape of the entoplastron is that of a nearly perfect equilateral triangle, with straight anterolateral sides and a subtly convex posterior side. The shape and

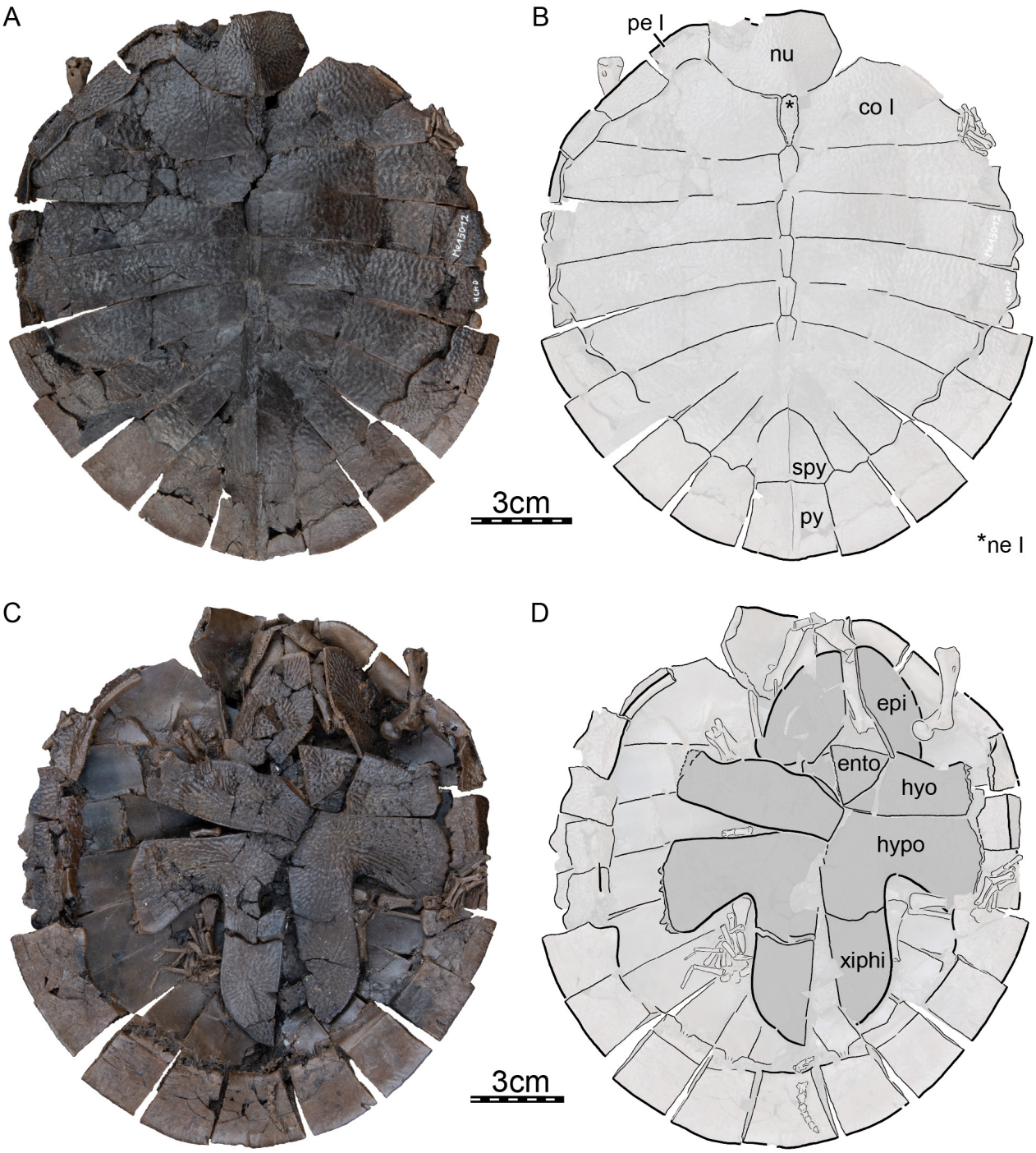


Figure 19. HLMD Me15012, a nearly complete skeleton of *Allaeochelys crassesculpta*. **A.** Photograph in dorsal view; **B.** Interpretive line drawing in dorsal view; **C.** Photograph in ventral view; **D.** Interpretive line drawing in ventral view. Abbreviations: co I, costal I; ento, entoplastron; epi, epiplastron; hyo, hyoplastron; hypo, hypoplastron; ne I, neural I; nu, nuchal; pe I, peripheral I; py, pygal; spy, suprapygal; xiphi, xiphiplastron.

dimensions of the entoplastron are very similar to that of *Allaeochelys parayrei* (Broin 1977) and *Carettochelys insculpta* (Waite 1905; Walther 1922; Joyce 2014), but clearly different from that of *Kizylkumemys schultzi* (Nessov 1977) and *Anosteira manchuriana* (Zangerl 1947), in which the entoplastron is an elongate element with clearly longer anterolateral sides. The entoplastron of *Allaeochelys crassesculpta* contacts the epiplastron anteriorly and laterally and the hyoplastron posteriorly.

Hyoplastron. The hyoplastron is relatively short anteroposteriorly and forms the anterior aspect of the plastral bridge. The medial third of the anterior margin of the hyoplastron forms a dorsoventrally expanded surface that serves as an articular facet for kinetic contact with the epiplastron anteriorly and entoplastron anteromedially. This surface is slightly convex and laterally ends in a well-defined notch. The morphology of the hyoplastron is similar to that of *Allaeochelys lingnanica* (Young

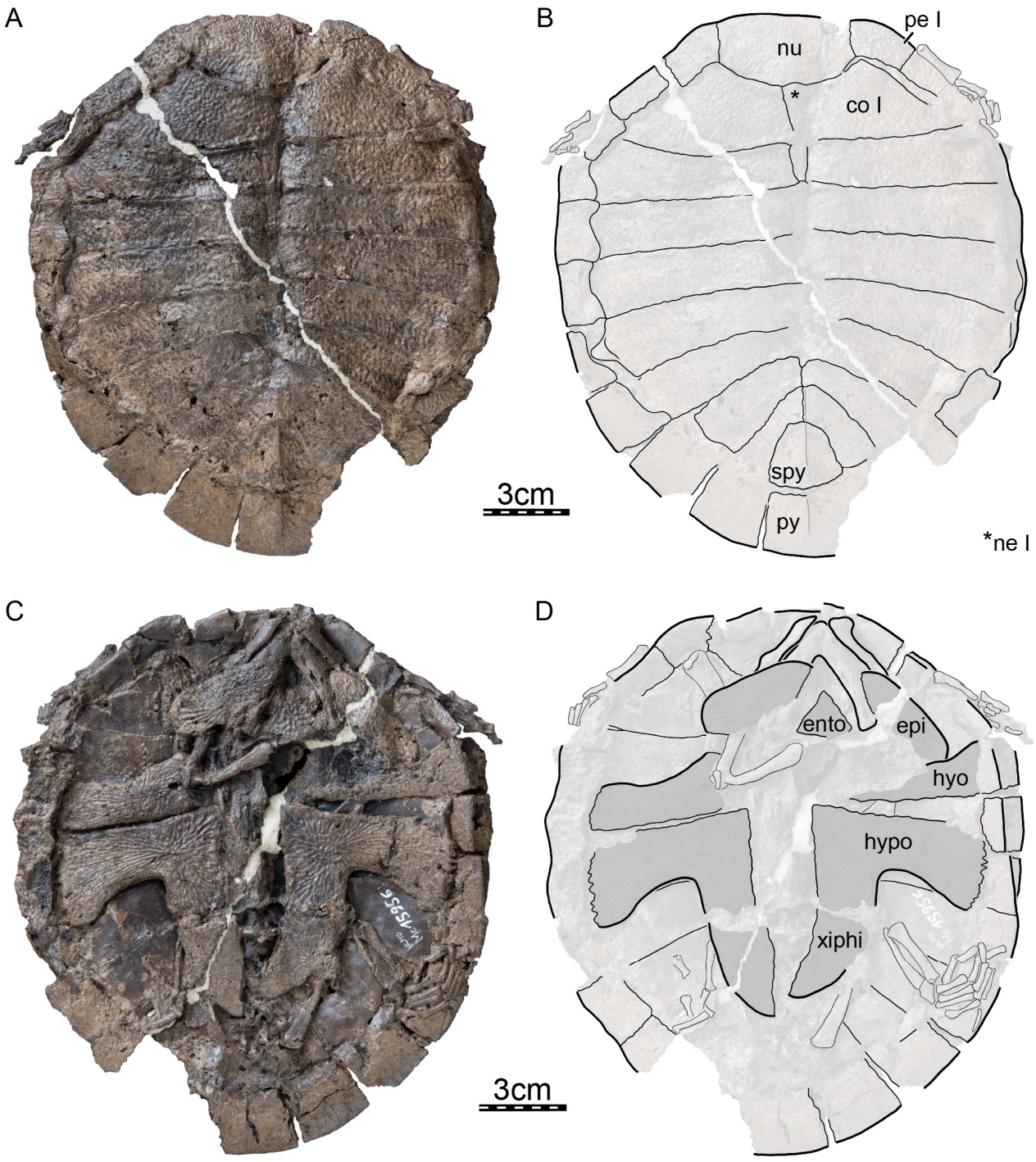


Figure 20. HLMD Me15956, a nearly complete skeleton of *Allaeochelys crassesculpta*. **A.** Photograph in dorsal view; **B.** Interpretive line drawing in dorsal view; **C.** Photograph in ventral view; **D.** Interpretive line drawing in ventral view. Abbreviations: co I, costal I; ento, entoplastron; epi, epiplastron; hyo, hyoplastron; hypo, hypoplastron; ne I, neural I; nu, nuchal; pe I, peripheral I; py, pygal; spy, suprapygal; xiphi, xiphiplastron.

and Chow 1962) and *Allaeochelys parayrei* (Broin 1977), but it is more robust and more anteroposteriorly expanded than that of *Kizylkumemys schultzi* (Nessov 1977), *Anosteira manchuriana* (Zangerl 1947), *Anosteira maomingensis* (Chow and Liu 1955), *Anosteira mongoliensis* (Gilmore 1931), *Anosteira ornata* (Leidy 1873) and *Anosteira pulchra* (Clark 1932), but less so than in *Carettochelys insculpta* (Waite 1905; Walther 1922; Joyce 2014). Laterally, the hyoplastron of *Allaeochelys crassesculpta* forms a series of short processes that articulate with the carapace, inserting into the sockets formed by peripherals IV and V. The hyoplastron also contacts its counterpart medially and the hypoplastron posteriorly.

Hypoplastron. The hypoplastron is the largest element of the plastron and forms the posterior part of the plastral bridge and the anterior half of the posterior plastral lobe.

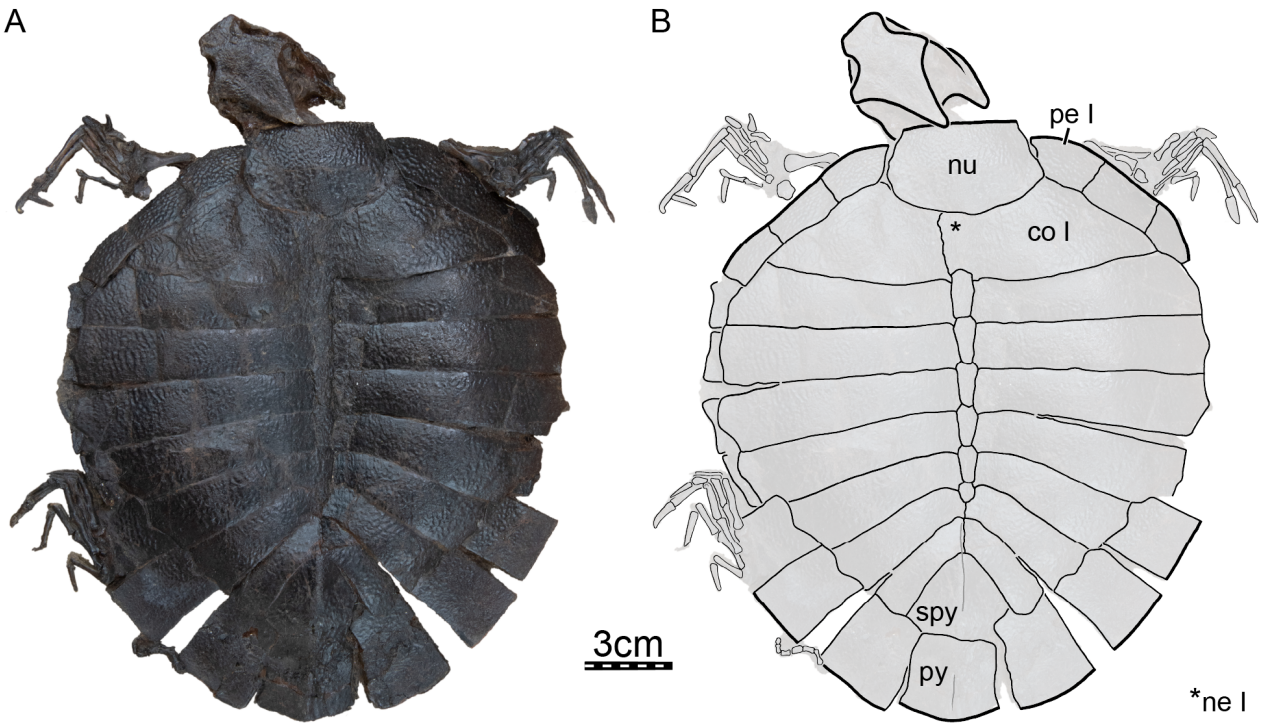


Figure 21. SMF Me611, a nearly complete skeleton of *Allaeochelys crassesculpta*. **A.** Photograph in dorsal view; **B.** Interpretive line drawing in dorsal view. Abbreviations: co I, costal I; ne I, neural I; nu, nuchal; pe I, peripheral I; py, pygal; spy, suprapygal.

Laterally, the hypoplastron forms short processes that articulate with the carapace and insert into sockets formed by peripherals V, VI, and VII. The hypoplastron otherwise contacts the hyoplastron anteriorly, the xiphiplastron posteriorly, and its counterpart medially. The shape of the suture between the hypo- and xiphiplastron varies in *Allaeochelys crassesculpta* and can be either straight or wavy. This difference was already noted by Joyce et al. (2012) and interpreted as sexual dimorphism, with males having the akinetic, wavy suture and females the straight suture, which likely allowed for limited kinesis during oviposition (Fig. 26). In addition, females are about 20% larger than males and have proportionally shorter tails.

Xiphiplastron. The xiphiplastron forms the most posterior extent of the plastron and the posterior half of the posterior plastral lobe. The posterior plastral lobe is relatively large and notable differences can be observed with other carettochelyids, based on the morphology of the xiphiplastron. In *Allaeochelys crassesculpta*, the xiphiplastron is moderately large and has straight, anteroposteriorly oriented margins for at least half of its length, similar to that of *Allaeochelys parayrei* (Broin 1977) and *Allaeochelys liliae* (Carbot-Chanona et al. 2020). This morphology contrasts with that of *Kizylkumemys schultzi* (Nessov 1977), in which the posterior plastral lobe and xiphiplastron are extremely narrow and that of *Anosteira manchuriana* (Zangerl 1947), *Anosteira maomingensis* (Chow and Liu 1955), and *Anosteira mongoliensis* (Gilmore 1931), where the posterior plastral lobe and xiphiplastron are slightly narrower and the lateral margin of the xiphiplastron is inclined posteromedially for most of its length. The morphology observed in *Allaeochelys crassesculpta* also differs from that of *Carettochelys insculpta*, which has a much broader posterior plastral lobe and xiphiplastron than any other carettochelyid (Waite 1905; Walther 1922; Joyce 2014). The xiphiplastron contacts the hypoplastron anteriorly, along a suture that can be either straight (females) or wavy (males) as described above (see Hypoplastron and Joyce et al. (2012)).

Appendicular skeleton

General comments. The left fore- and hindlimb of SMF Me611 were segmented and reconstructed and, therefore, serve as a primary base for the description of the limbs of *Allaeochelys crassesculpta*, unless stated otherwise by explicit reference to other specimens. The left forelimb is complete and although some damage and displacement may affect the bones individually, the general anatomy of most elements is apparent (Fig. 30). The left hindlimb, however, is incomplete, as the femur is not preserved and the tibia and fibula are damaged. Preliminary descriptions of the femur, tibia and fibula are nevertheless provided to the extent possible, with the addition of supplementary insights, based on other specimens included in our study that preserve these bones.

Humerus. The left humerus of SMF Me611 is slightly damaged and lacks most of its medial process and a substantial part of its distal end, with the capitellum and radial epicondyle mostly missing (Fig. 31A–F). Overall, the humerus of *Allaeochelys crassesculpta* is similar to that of *Carettochelys insculpta* (Walther 1922; Hermanson et al. 2024). The proximal end of the humerus of *Allaeochelys crassesculpta* consists of a large humeral head, which seems proportionally larger than that of *Carettochelys insculpta* (Hermanson et al. 2024), and a greatly reduced lateral process. Although the medial process is broken near its base

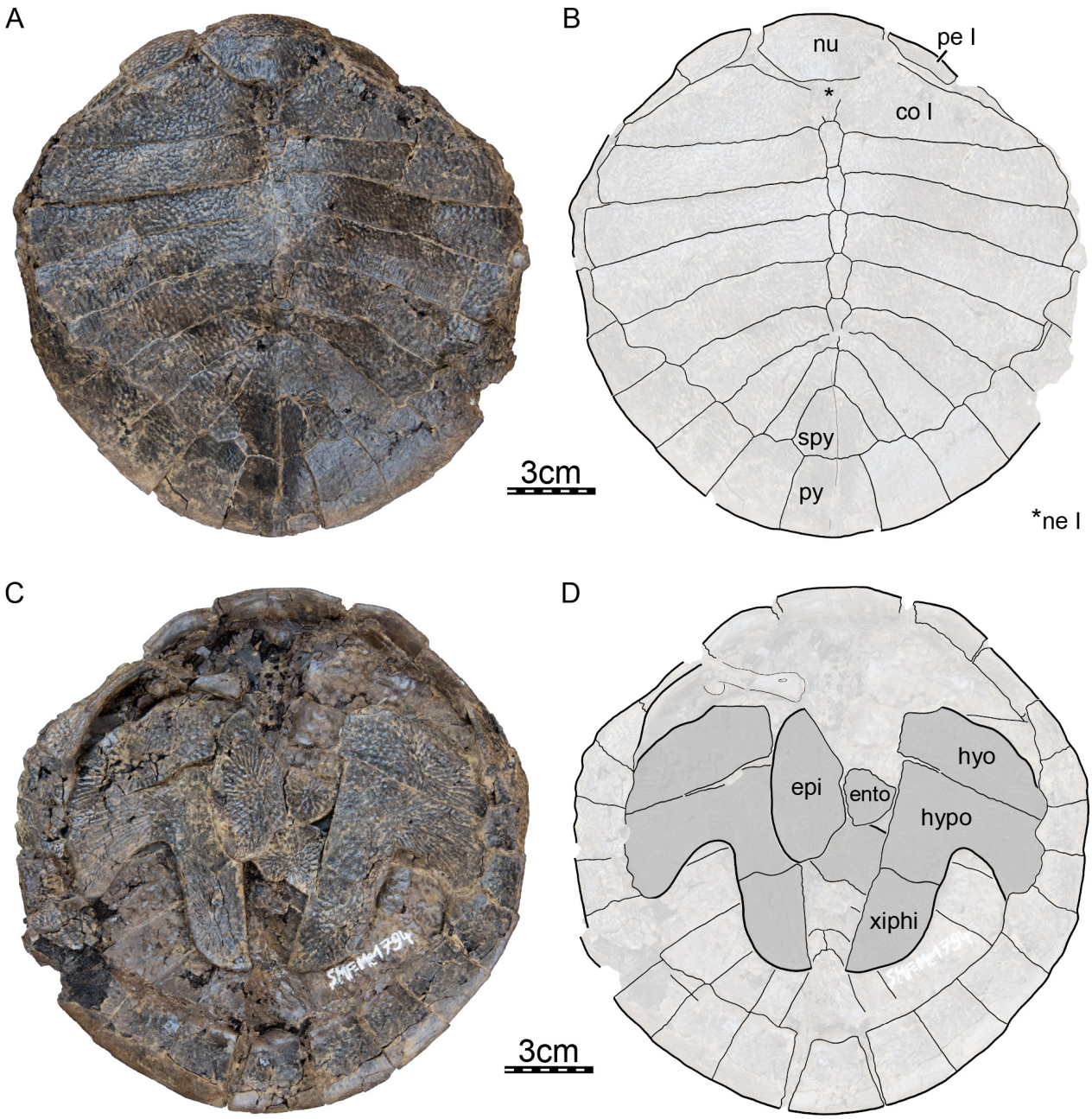


Figure 22. SMF Me1794, a nearly complete shell of *Allaeochelys crassesculpta*. **A.** Photograph in dorsal view; **B.** Interpretive line drawing in dorsal view; **C.** Photograph in ventral view; **D.** Interpretive line drawing in ventral view. Abbreviations: co I, costal I; ento, entoplastron; epi, epiplastron; hyo, hyoplastron; hypo, hypoplastron; ne I, neural I; nu, nuchal; pe I, peripheral I; py, pygal; spy, suprapygal; xiphi, xiphiplastron.

in SMF Me611 (Fig. 31B, D), it is perfectly preserved in HLMD Be159 (Fig. 13C, D) and SMF Me3566 (Fig. 25A, B), showing that it is well-developed in *Allaeochelys crassesculpta*, similar to that of *Carettochelys insculpta* (Hermanson et al. 2024). In *Allaeochelys crassesculpta*, on the radial side of the humeral head, the humerus forms a reduced shoulder (Fig. 31B). The shoulder seems slightly better developed in *Allaeochelys crassesculpta* than in adult *Carettochelys insculpta* (Hermanson et al. 2024), as the area between the shoulder and humeral head is slightly more concave and the shoulder forms a low ridge on the capitular side of the humerus, which extends proximally for a short distance towards the humeral head, albeit not joining it. As in *Carettochelys insculpta* (Hermanson et al. 2024), the proximal limit of the lateral process is positioned much more distally than the proximal border of the humeral head (Fig. 31C). In *Allaeochelys crassesculpta*, the medial and lateral processes are separated from one another by a shallow intertubercular fossa (Fig. 31D). Just next to the lateral process, immediately distal and radial to the intertubercular fossa, the humerus forms a small, narrow, but well-defined and oval-shaped pit, which is also present in *Carettochelys insculpta*, where it has been interpreted as a possible secondary intertubercular fossa

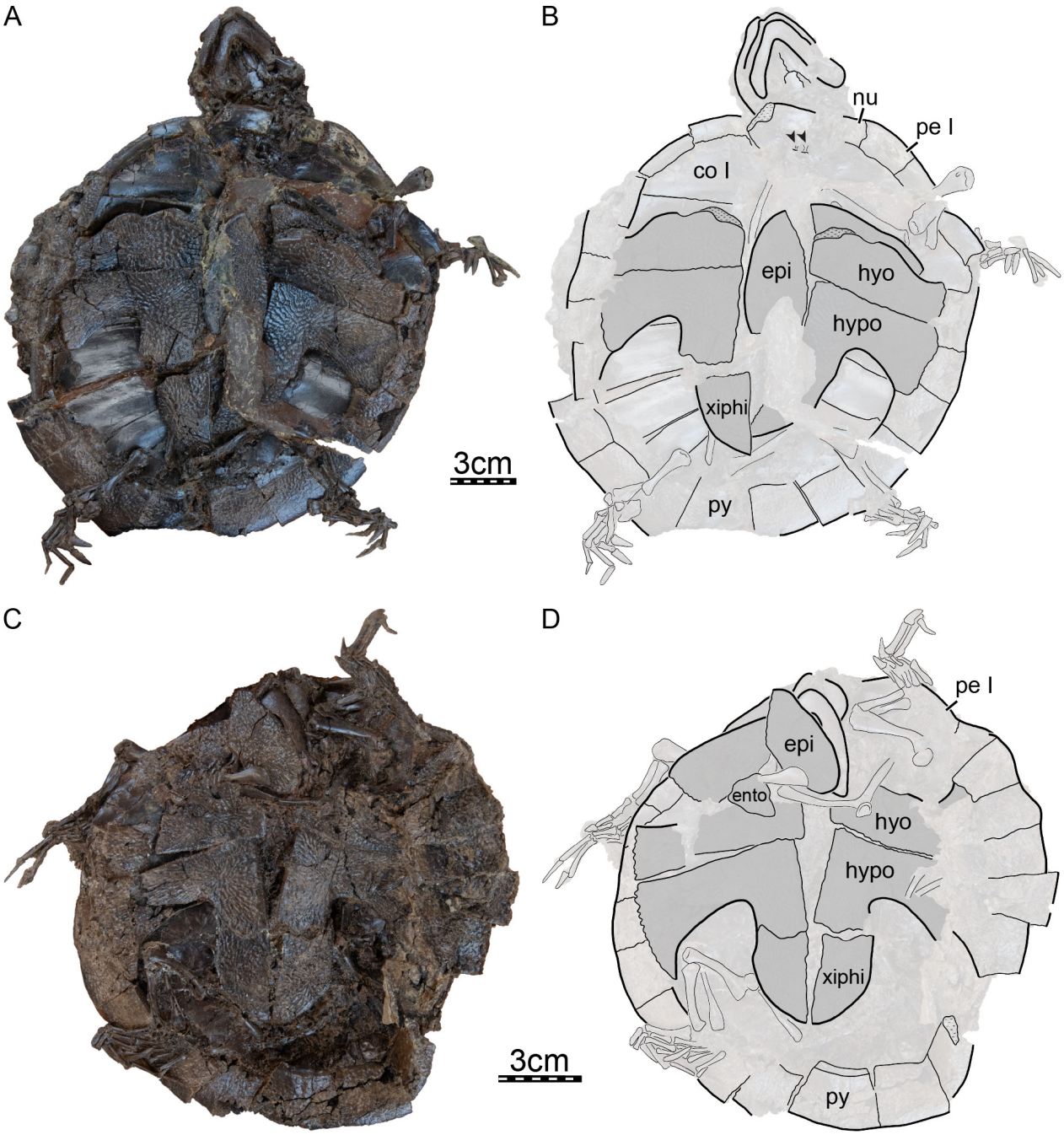


Figure 23. SMF Me2449, a nearly complete pair of skeletons of *Allaeochelys crassesculpta* preserved in vicinity to each other. **A.** Photograph in ventral view of female; **B.** Interpretive line drawing in ventral view of female; **C.** Photograph in ventral view of male; **D.** Interpretive line drawing in ventral view of male. Abbreviations: co I, costal I; ento, entoplastron; epi, epiplastron; hyo, hyoplastron; hypo, hypoplastron; nu, nuchal; pe I, peripheral I; py, pygal; xiphi, xiphiplastron. Black arrowheads indicate the paired nuchal processes.

(Hermanson et al. 2024). A subcapitular fossa is present in *Allaeochelys crassesculpta* and visible on the capitular side of the humerus, within the proximal third of the element (Fig. 31B). The distal expansion of the humerus starts more proximally along the length of the element and distal ulnar-radial width is not greatly expanded relative to shaft, as in *Carettochelys insculpta* (Hermanson et al. 2024). The humerus of *Allaeochelys crassesculpta* exhibits minimal shaft curvature and is essentially straight (Fig. 31A, C), again as in *Carettochelys insculpta* (Hermanson et al. 2024). In *Allaeochelys crassesculpta*, the distal end of the humerus of SMF Me611 is damaged (Fig. 31B–D, F). The ulnar epicondyle and trochlea are almost completely preserved, but the capitellum is heavily damaged and the radial epicondyle is almost completely missing (Fig. 31B, D, F). It is nevertheless clear that the

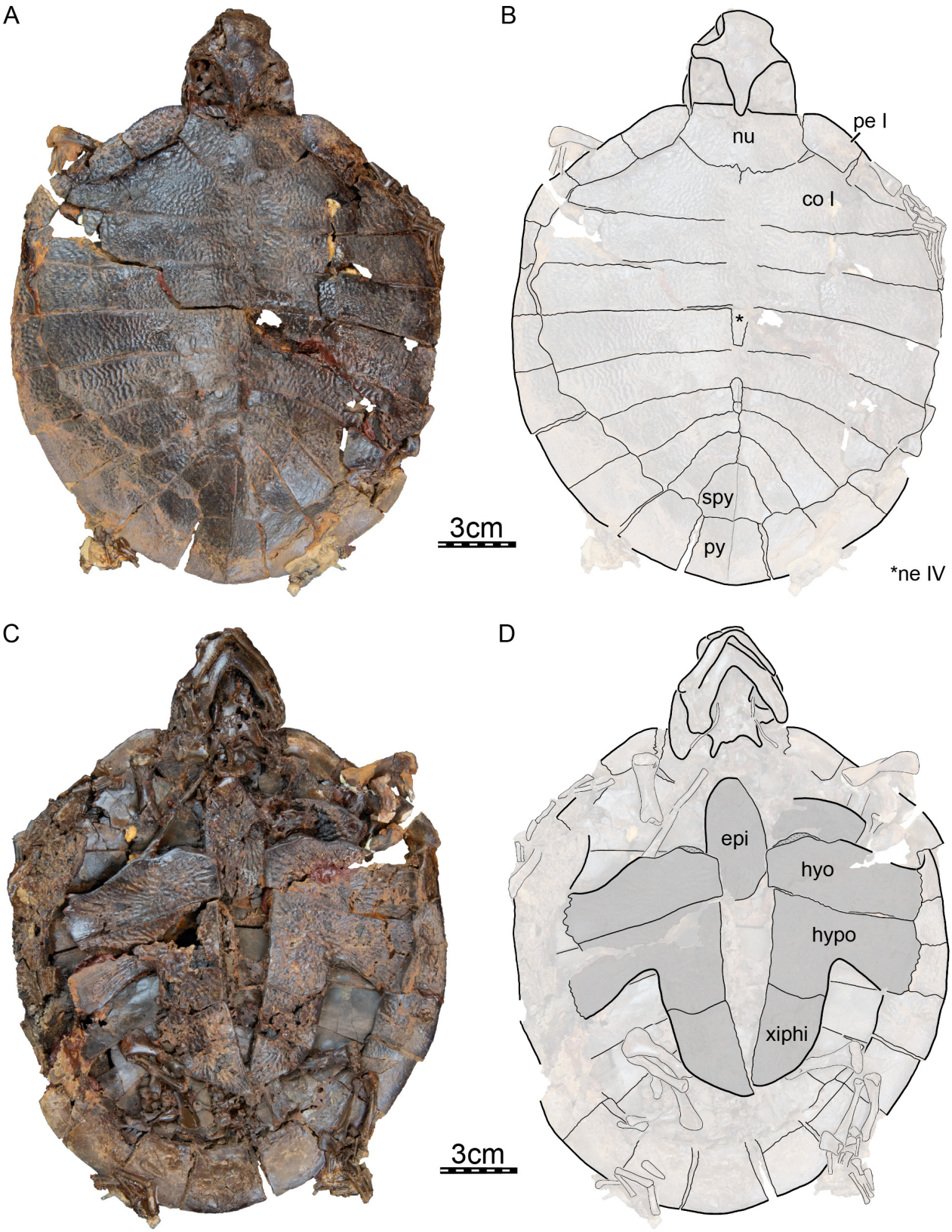


Figure 24. SMF Me3018, a nearly complete skeleton of *Allaeochelys crassesculpta*. **A.** Photograph in dorsal view; **B.** Interpretive line drawing in dorsal view; **C.** Photograph in ventral view; **D.** Interpretive line drawing in ventral view. Abbreviations: co I, costal I; epi, epiplastron; hyo, hyoplastron; hypo, hypoplastron; ne IV, neural IV; nu, nuchal; pe I, peripheral I; py, pygal; spy, suprapygal; xiphi, xiphiplastron.



Figure 25. SMF Me3566, a nearly complete pair of skeletons of *Allaeochelys crassesculpta* preserved in vicinity to each other. **A.** Photograph in ventral view of female; **B.** Interpretive line drawing in ventral view of female; **C.** Photograph in ventral view of male; **D.** Interpretive line drawing in ventral view of male. Abbreviations: ento, entoplastron; epi, epiplastron; hyo, hyoplastron; hypo, hypoplastron; nu, nuchal; pe I, peripheral I; py, pygal; xiphi, xiphiplastron.

trochlea is located more proximally than the capitellum (Fig. 31D), as in *Carettochelys insculpta* and unlike most turtles (Walther 1922; Hermanson et al. 2024), and that an intercondylar groove is present that separates the trochlea from the capitellum (Fig. 31D, F). Despite damage in the area, it seems that a shallow fossa or depression is present between the distal end of the ulnar epicondyle and ulnar side of the trochlea, which contrasts with the morphology of the humerus in *Carettochelys insculpta*, where this area is straight (Hermanson et al. 2024). The ectepicondylar

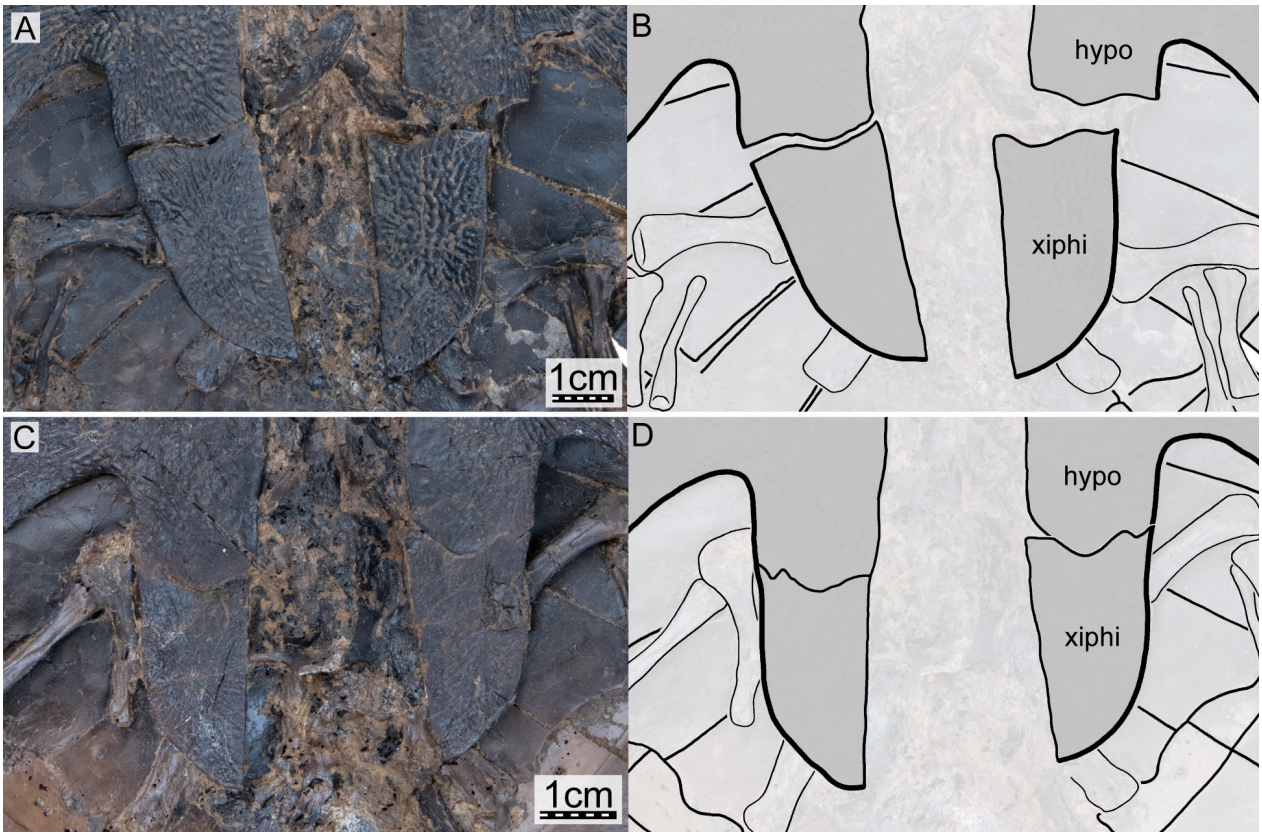


Figure 26. Close-up on the posterior plastral lobe of SMF Me3566. **A.** Photograph in ventral view of female; **B.** Interpretive line drawing in ventral view of female; **C.** Photograph in ventral view of male; **D.** Interpretive line drawing in ventral view of male. Abbreviations: hypo, hypoplastron; xiphi, xiphiplastron.

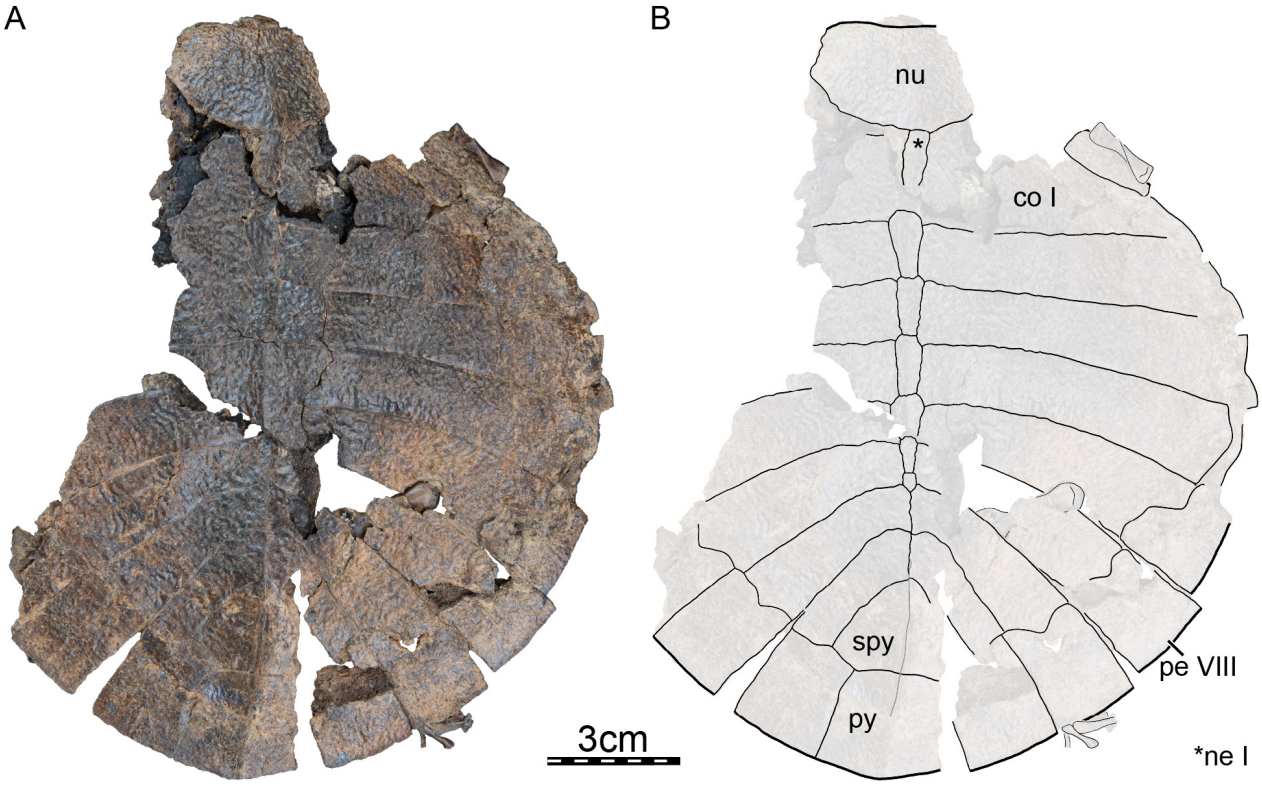


Figure 27. SMF Me3783, a partial skeleton of *Allaeochelys crassesculpta*. **A.** Photograph in dorsal view; **B.** Interpretive line drawing in dorsal view. Abbreviations: co I, costal I; ne I, neural I; nu, nuchal; pe VIII, peripheral VIII; py, pygal; spy, suprapygal.

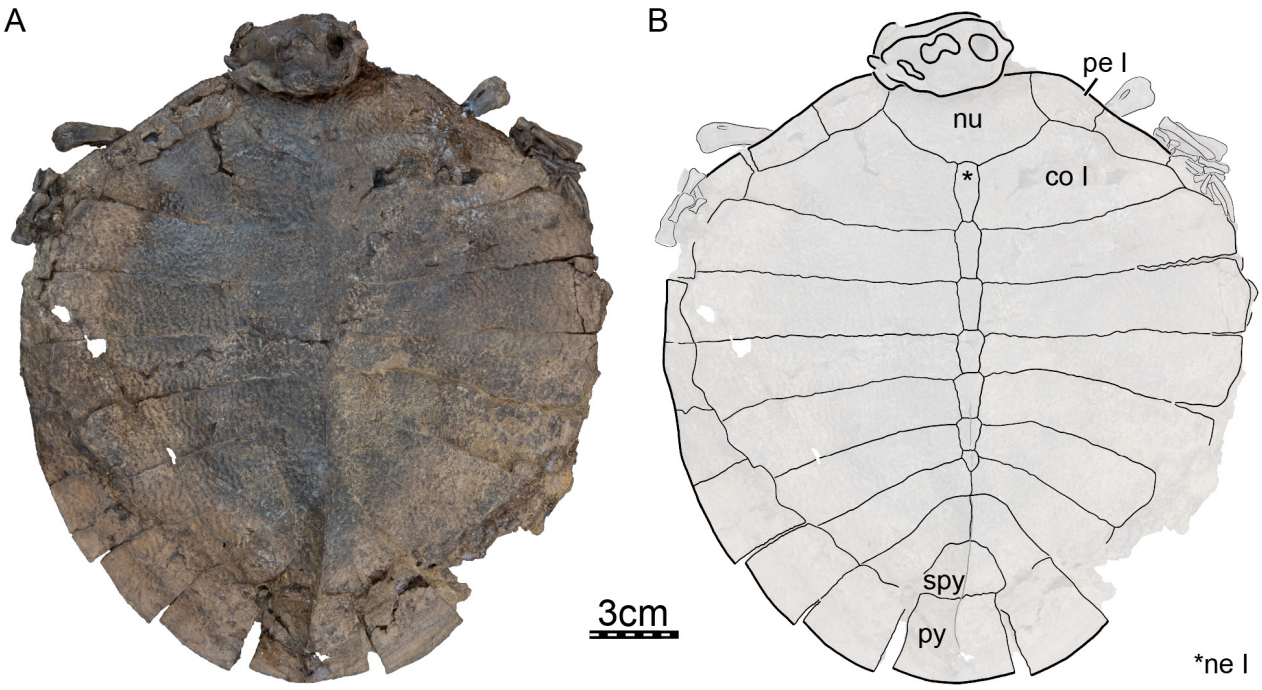


Figure 28. SMF Me11418, a nearly complete skeleton of *Allaeochelys crassesculpta*. **A.** Photograph in dorsal view; **B.** Interpretive line drawing in dorsal view. Abbreviations: co I, costal I; ne I, neural I; nu, nuchal; pe I, peripheral I; py, pygal; spy, suprapygal.

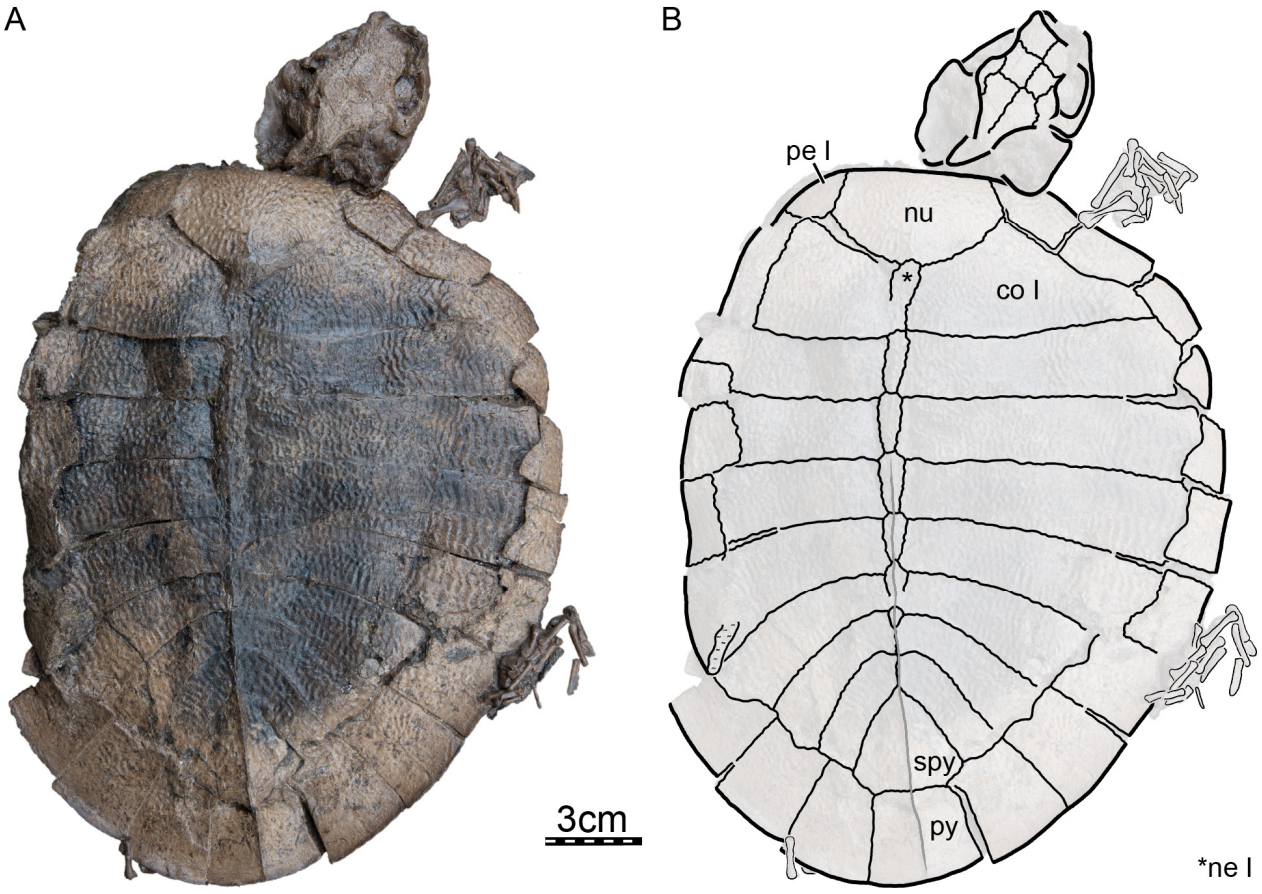


Figure 29. SMNK Pal986, a nearly complete skeleton of *Allaeochelys crassesculpta*. **A.** Photograph in dorsal view; **B.** Interpretive line drawing in dorsal view. Abbreviations: co I, costal I; ne I, neural I; nu, nuchal; pe I, peripheral I; py, pygal; spy, suprapygal.

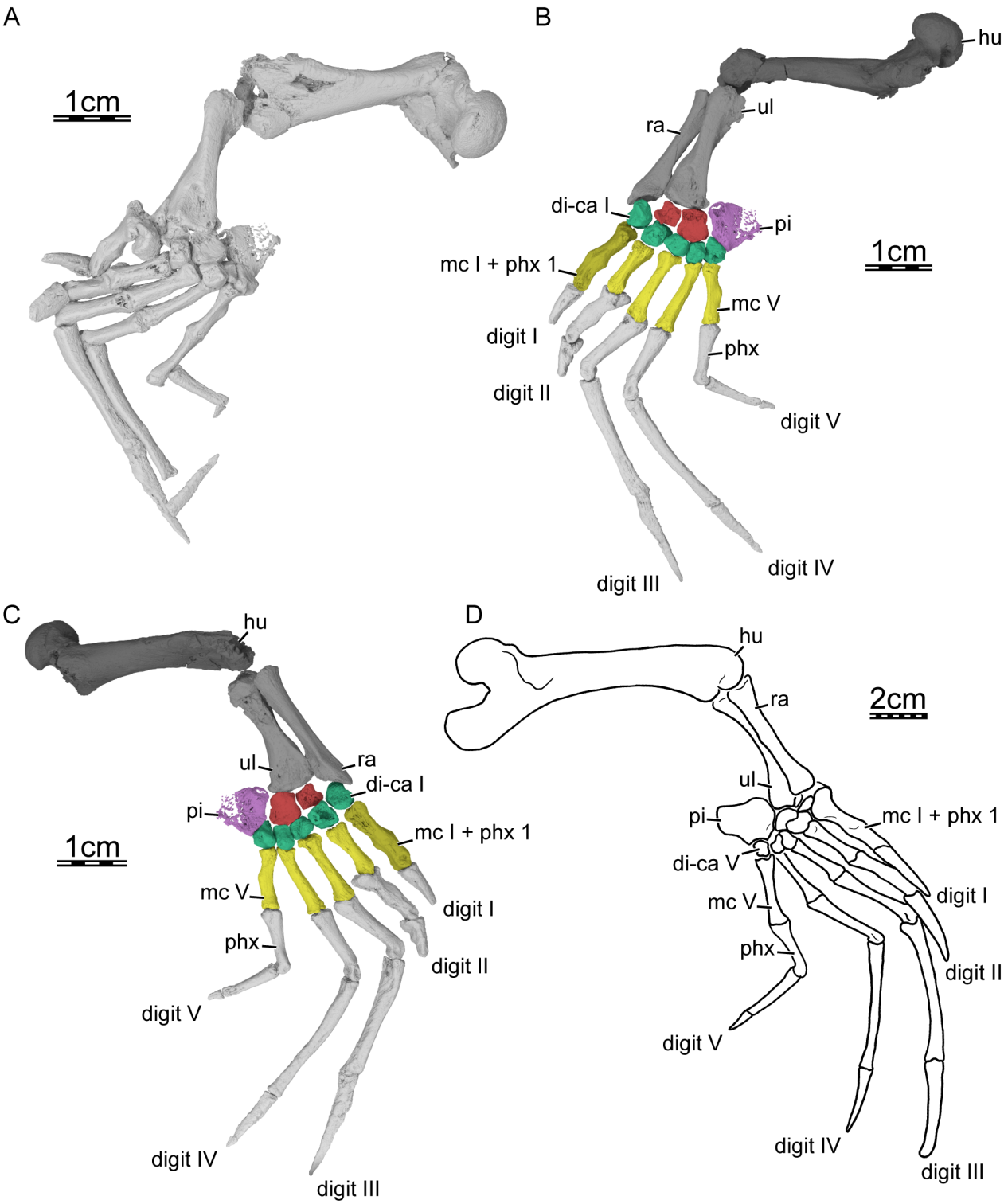


Figure 30. Three-dimensional renderings of a segmented left forelimb of *Allaeochelys crassesculpta* (SMF Me611). **A.** Dorsal view; **B.** Reconstructed dorsal view; **C.** Reconstructed ventral view; **D.** Interpretive line drawing of the left forelimb of *Carettochelys insculpta* in ventral view (redrawn from Walther (1922): pl. XXII, fig. 19). Abbreviations: di-ca I, distal carpal I; di-ca V, distal carpal V; hu, humerus; mc I + phx 1, fused metacarpal I and first phalanx of digit I; mc V, metacarpal V; phx, phalanx; pi, pisiform; ra, radius; ul, ulna. The red bones are the intermedium and ulnare, the ulnare being the larger of the two and in contact with the pisiform and ulna.

foramen is not preserved in SMF Me611 of *Allaeochelys crassesculpta*, but undoubtedly visible in HLMD Me15012 (Fig. 19C, D) and SMF Me1794 (Fig. 22C, D), in which it appears to be in a similar position as that of *Carettochelys insculpta* (Hermanson et al. 2024), although it is perhaps slightly smaller. The humerus of *Allaeochelys crassesculpta* also appears to form a very shallow supraepicondylar fossa, which is visible on the intertubercular fossa proximal to the trochlea.

Radius. The proximal end of the radius is subcircular with a slightly oval outline (Fig. 31M). It is only slightly larger mediolaterally than it is at midshaft, but is expanded to a greater degree dorsoventrally. The proximal articulation surface is oval and concave, serving for articulation with the capitellum of the humerus. Ventrolateral and just distal to the proximal end, the radius forms a tuberosity that expands distally, nearly reaching the midshaft. (Fig. 31K, L), which might correspond to the attachment site of the superior radio-ulnar ligament (Haines 1946; Gaffney 1990). In *Carettochelys insculpta* (specimen MAGNT R35037), the radius also forms a low ridge along its medial side, just distal to the proximal end, which extends for about one third of the length of the radius. Such a ridge is not visible in the radius of *Allaeochelys crassesculpta* specimen SMF Me611, but this could also be a preservation artefact. Likewise, dorsolaterally at about mid-shaft, the radius of *Carettochelys insculpta* forms a very low and short ridge that is not visible in specimen SMF Me611 of *Allaeochelys crassesculpta*. The ventral aspect of the distal half of the radius is developed as a relatively low, but broad ridge (Fig. 31K, L), on which two low bumps can be identified. The most proximal bump is located at about the level of midshaft, while the most distal one is visible just proximal to the distal end of the radius. In *Carettochelys insculpta* (specimen MAGNT R35037), no bumps are visible and the ventral aspect of the radius is more ventrally expanded and forms a mediolaterally flattened shelf that extends distally to the sigmoid process. The distal part of the radius of *Allaeochelys crassesculpta* broadens mediolaterally, but remains only weakly expanded dorsoventrally (Fig. 31K, L, N). The medial edge is nearly straight, whereas the lateral edge forms a process with a lateral surface that is developed as a triangular tuberosity, which seems to be slightly larger in *Carettochelys insculpta* (specimen MAGNT R35037) than in *Allaeochelys crassesculpta*. Distomedially, the styloid process of the radius of *Allaeochelys crassesculpta* is well-developed and expanded distally (Fig. 31K). The distal articulation surface is elongate and oval, forming a shallow depression, but the articulation facets are not completely preserved (Fig. 31N). Light damage and erosion of the bony surface prevent the facets from being clearly observed or distinguished from one another. Nevertheless, we infer that two facets were present by reference to other turtles (Gaffney (1990); Sterli et al. (2007); Joyce et al. (2014); Szczygielski and Piechowski (2023)), with the most proximolateral facet corresponding to the intermedium and the most distomedial one associated with the first distal carpal.

Ulna. The proximal end of the ulna is about twice as large as the midshaft and about as broad as tall (Fig. 31G, H). The olecranon is likely located on the proximodorsal side of the proximal end, by reference to *Carettochelys insculpta* (specimen MAGNT R35037), but the area is damaged in *Allaeochelys crassesculpta* specimen SMF Me611 (Fig. 31I). The proximal articulation surface (i.e., the sigmoid notch) is subdivided into two parts: one nearly flat ventromedial facet, which is dorsoventrally elongate and forms slightly more than one third of the entire articulation surface, and one ventrolateral facet, which forms nearly two thirds of the sigmoid notch (Fig. 31I). In *Carettochelys insculpta* (MAGNT R35037), similar facets are present and the ventrolateral facet is gently concave. Despite damage to the ulna of *Allaeochelys crassesculpta* specimen SMF Me611, the preserved portion shows that the morphology of the proximal end was likely similar to that of *Carettochelys insculpta*. In *Allaeochelys crassesculpta*, the ulnar midshaft is not flattened and is approximately as broad as tall. The shape of the midshaft in cross-section is diamond-shaped, with four well-defined sides (Fig. 31G, H). The edges between sides are quite abrupt, which slightly differs from *Carettochelys insculpta* (MAGNT R35037), in which the midshaft is slightly more circular and the limits between faces are smoother. In *Allaeochelys crassesculpta*, the distal end of the ulna is mediolaterally expanded, about twice as broad as the midshaft, flattened, and has a distal margin that is sinusoidal in shape in dorsal view (Fig. 31G, H, J). In distal view, the distal articulation surface is about twice as broad as tall and has a semilunar, curved shape (Fig. 31J). The distal articulation surface was originally preserved as slightly compressed against the intermedium, ulnare, and radius, resulting in minor surface damage that obscures the articular facets and prevents their accurate description. However, the general morphology of the distal end of the ulna greatly resembles that of *Carettochelys insculpta* (MAGNT R35037) and we, therefore, base most anatomical insights on the latter. In *Carettochelys insculpta*, the distal articulation surface is subdivided into two facets. The ventromedial facet is the smallest, forming about one third of the entire articulation surface; it is circular, gently concave, and articulates with the intermedium (Fig. 31J). The lateral facet is the largest, forming about two thirds of the entire articular surface; it is triangular, approximately twice as broad as tall, with the dorsal and ventral margins being the longest, and it articulates with the ulnare (Fig. 31J). The surface of the lateral facet is quite complex. The most dorsomedial portion forms a shallow depression, while the most lateral and ventrolateral part is nearly flat and the area between the two is slightly domed. Dorsomedially, between the ventromedial and lateral facets, the ulna forms a short, blunt process that separates the two facets along their dorsal half and likely inserted between the intermedium and ulnare. It is unclear if such a process is present in *Allaeochelys crassesculpta* as the area

is damaged in SMF Me611. In *Carettochelys insculpta*, the lateral side of the distal process forms a moderately deep notch, which is also visible in *Allaeochelys crassesculpta*, albeit slightly less deep than in the latter (Fig. 31G, H). In *Carettochelys insculpta*, the area distolateral to the notch is slightly expanded and, on the lateral side, forms another facet between the lateral notch and distal articulation surface. In lateral view, this facet has a straight distoventral margin, but is otherwise rounded and as broad as tall, articulating with the pisiform. In *Allaeochelys crassesculpta*, the morphology of the ulna suggests that a similar facet was also likely present, as the distolateral aspect of the ulna is slightly expanded just distal to the notch (Fig. 31G, H). In *Carettochelys insculpta*, the ventromedial aspect of the ulna, immediately proximoventral to the distal articular surface, forms an elongate, rough surface that is about three times longer than tall, likely corresponding to a tuberosity.

Carpus and manus. The carpus of *Allaeochelys crassesculpta* has a reduced number of elements, as in *Carettochelys insculpta* (Harrassowitz 1922; Walther 1922), which are the intermedium, ulnare, pisiform, and distal carpals I–V (Fig. 30A–C). Proximodistal compression of the forelimb has produced minor damage and localized surface erosion on several elements, introducing some uncertainty in the reconstruction and orientation of the distal carpals.

The intermedium is a small bone that is nearly square, except for its distomedial edge, which is developed as a short but stout process (Fig. 30B, C). The distal surface of the process forms a round and very gently concave articular surface, which likely joins with distal carpal I. The lateral half of the distal side is straight and flat and contacts distal carpal II. A point contact with the radius might have been present proximomedially, as in *Carettochelys insculpta* (Walther 1922), but remains hypothetical in *Allaeochelys crassesculpta* because of the deformation of the forelimb. The proximal side of the intermedium forms a gently concave articular surface for the ulna. The lateral side of the intermedium is subdivided into two parts: one flat distal surface that is oriented proximodistally and one flat proximal surface that is slightly inclined proximomedially. Both surfaces contact the ulnare.

The ulnare is an octagonal bone that is slightly larger than the intermedium (Fig. 30B, C). The distal half of the element is flat, albeit slightly dorsoventrally expanded along its distal end, whereas the proximal half is clearly thickened. The proximal half of the ulnare is cone-shaped in lateral view and its proximal surface forms a large, circular, and very gently concave surface that serves for the articulation with the ulna. The lateral side of the ulnare is subdivided into two surfaces: the proximal surface, which constitutes about half of the lateral side, is gently concave and oriented proximodistally, whereas the distal surface is gently convex and slightly oriented distalomedially. Both surfaces contact the medial side of the intermedium. Distally, the ulnare is also subdivided into two surfaces that are equally sized, gently concave and positioned 130° from one another. The medial surface contacts distal carpal III, while the lateral surface contacts distal carpal IV. A contact of the ulnare with distal carpal II was reported in *Carettochelys insculpta* (Walther 1922), but is not evident in *Allaeochelys crassesculpta*. The distolateral edge of the ulnare forms a small, flat surface that is almost circular. According to our reconstruction of the forelimb, this surface might represent an articular surface for distal carpal V, but there is no such contact in *Carettochelys insculpta* (Walther 1922). Alternatively, this surface could form a short contact laterally with the pisiform. The lateral side of the ulnare of *Allaeochelys crassesculpta* is much less expanded dorsoventrally than the medial side. It is developed as a curved, smooth and very gently concave surface, but does not resemble an articular surface. Point contacts with the pisiform were perhaps present proximally and/or distally, but an expanded contact — such as the broad articulation between the ulnare and distal carpals III–IV — was likely absent, as in *Carettochelys insculpta* (Walther 1922). This is also supported by the morphology of the pisiform, as its medial surface, which faces the ulnare, is concave.

The pisiform of *Allaeochelys crassesculpta* is the largest element of the carpus (Fig. 30B, C). The lateral half of the element is heavily damaged, but nevertheless shows that the pisiform is laterally greatly expanded, forming a flat and thin process, as in *Carettochelys insculpta* (Walther 1922). In *Allaeochelys crassesculpta*, only the most medial aspect of the pisiform is moderately thickened. The medial side of the pisiform forms a curved, smooth and concave surface that faces the ulnare. The distomedial edge of the pisiform forms a broad and oval-shaped articulation surface, which is about two times broader than tall and contacts distal carpal V. The most distomedial aspect of this surface might have contacted the ulnare, but such a contact remains hypothetical (see ulnare section above). The proximomedial edge of the pisiform forms a circular and very gently concave surface that serves for articulation with the ulna. This articular surface is slightly inclined distoventrolaterally. The most medial aspect of the articulation surface perhaps contacted the most proximolateral part of the ulnare, but remains hypothetical (see ulnare section above).

Five distal carpals are preserved in the carpus of *Allaeochelys crassesculpta* (Fig. 30B, C). The taphonomic compression of the forelimb was relatively minimal, but all distal carpals were nevertheless displaced and damaged, which complicated their identification and reconstruction. Although we provide detailed descriptions in the following section, our insights into the identification and anatomy of the distal carpals should be taken with caution because of this displacement and damage. Distal carpal I is a relatively large element, which is slightly taller than wide. Its general shape is quite irregular and each side forms surfaces that are either convex or concave. As preserved and reconstructed, distal carpal I contacts the radius proximomedially, the fused metacarpal and first phalanx of digit I distally, distal carpal II laterally and, perhaps, the intermedium proximolaterally. Distal carpal

II is a relatively large and columnar element, of which a substantial portion of its ventral part is damaged and missing. The dorsal half of the element is more elongate proximodistally, whereas the ventral half is more elongate mediolaterally. The dorsal surface of distal carpal II is eroded. The proximal and lateral sides form concave surfaces, which serve for articulation with the intermedium and distal carpal III, respectively. The medial and distal sides seem to have more complex morphologies, but are also affected by damage, which hinders detailed descriptions. The distal side is perhaps subdivided into two facets, with a centrally located fossa separating the two, while the medial side might be subdivided into two nearly equally-sized facets, facing mediodorsally and medioventrally. Distal carpal III is a small element, of which we estimate about half is missing. As reconstructed and oriented, we are able to identify four sides of distal carpal III: dorsal, proximal, lateral, and distal. The dorsal side is concave and laterally and medially bordered by low ridges, which gives this 'fossa' a gutter-like morphology with a proximodistal orientation. This side could also, perhaps, correspond to an articular surface for contact with metacarpal III, in which case the element would be falsely oriented in our reconstruction by 90° towards the ulnare. The distal side is incomplete, but appears to have been largely flat, except for its lateralmost portion, which curves to merge with the lateral surface and forms the articulation with metacarpal III. The lateral side is incomplete too and forms a convex surface that articulates with distal carpal IV. The proximal side likely preserves only its dorsal half, which is flat and contacts the ulnare. Distal carpal IV is a columnar element, of which all sides appear to be damaged. As currently oriented, only parts of the proximal, medial and ventral surfaces seem to be preserved. The proximal surface is flat and contacts the ulnare, the medial side is flat and contacts distal carpal III, and the ventral surface is convex and smooth and faces ventrally. Distal carpal V is incomplete and was rotated laterally by about 45° to fit in our reconstruction of the forelimb. The proximal side forms a concave surface that seems to fit for articulation with metacarpal V. The most distal aspect of the medial side forms a flat surface that contacts distal carpal IV. The lateral side appears to be mostly preserved, forming a very gently concave surface that serves for articulation with the pisiform.

The manus of *Allaeochelys crassesculpta* has a digital formula of 2-3-3-3-3 (Fig. 30B, C), as *Carettochelys insculpta* (Walther 1922; Delfino et al. 2010). The first digit of *Allaeochelys crassesculpta* is the shortest, followed by digit II and digit V. Digits III and IV are the longest, about twice the length of digits I and II. The length of the digits relative to one another is very similar to that of *Carettochelys insculpta* (Walther 1922). Phalanges 2 and 3 of digits III and IV of *Allaeochelys crassesculpta* are notably elongate. Metacarpal I is fused to the first phalanx of digit I, again as in *Carettochelys insculpta* (Walther 1922). The metacarpal portion of the fused element is slightly longer than the phalangeal one. Metacarpal I is the shortest, but thickest among the metacarpals, forming a robust rod that proximally articulates with distal carpal I. Metacarpal II of *Allaeochelys crassesculpta* is slightly longer and more slender than metacarpal I and its proximal end is more expanded than the distal one. Metacarpal II articulates with distal carpal II proximally and the fused phalanges 1 and 2 distally. Harrassowitz (1922) noted that metacarpal II was fused with phalanges 1 and 2 of the second digit in HLMD Me1461 (his 'Exemplar 6'; see Harrassowitz (1922), pl. 4.3), but we are not able to confirm the identification of the bones made by Harrassowitz (1922) nor establish if fusion exists between the bones of interest. In SMF Me611, it is unambiguous that only the first two phalanges are fused and that metacarpal II remains an isolated element. The same observation can be made in the two individuals preserved in SMF Me3566 (Fig. 25). However, variation in this feature seems to occur in *Carettochelys insculpta* and might, therefore, also be present in *Allaeochelys crassesculpta*. Indeed, Walther (1922) described metacarpal II of *Carettochelys insculpta* as being fused to the phalanges 1 and 2, although remnants of the articulation between metacarpal II and the first phalanx remain visible. Radiographs provided by Delfino et al. (2010) likely show a partial fusion between phalanges 1 and 2 of digit II and also possibly the beginning of fusion with metacarpal II, as the articulation of the latter with the first phalanx is faint in the image, which contrasts with other articulations in the manus. Finally, personal observations of KU H158563 (juvenile) show a complete fusion between metacarpal II and phalanges 1 and 2. It is, therefore, possible that similar variation occurs in *Allaeochelys crassesculpta*. Metacarpal III of *Allaeochelys crassesculpta* is longer and more slender than metacarpal II and appears, along with metacarpal IV, to be the longest. Metacarpal III articulates with distal carpal III proximally and the first phalanx of digit III distally. Metacarpal IV has a very similar morphology to that of metacarpal III and is as long as the latter. The proximal and distal ends of metacarpal IV are perhaps slightly less expanded than those of metacarpal III, but that could be the result of damage. They articulate with distal carpal IV and the first phalanx of digit IV, respectively. Metacarpal V is shorter than metacarpal III and IV, slightly more robust than the latter, and about the same length as metacarpal II. Metacarpal V is distinctly curved, with the concave surface facing medially. On its lateral side at mid-length, metacarpal V forms a low, but distinct swelling that expands for nearly one third of the proximodistal length of the element.

Digit I consists of two phalanges, of which the first one is tightly fused to metacarpal I. Phalanx 1 was the smallest bone of the first digit and is slightly shorter than phalanx 2, which is claw-like. Digit II consists of three phalanges, of which the first and second are fused. Phalanges 1 and 2 were likely equally sized, but the former was more robust. Phalanx 3 is claw-like and about as long as phalanges 2 and 3. Digit III is elongate and

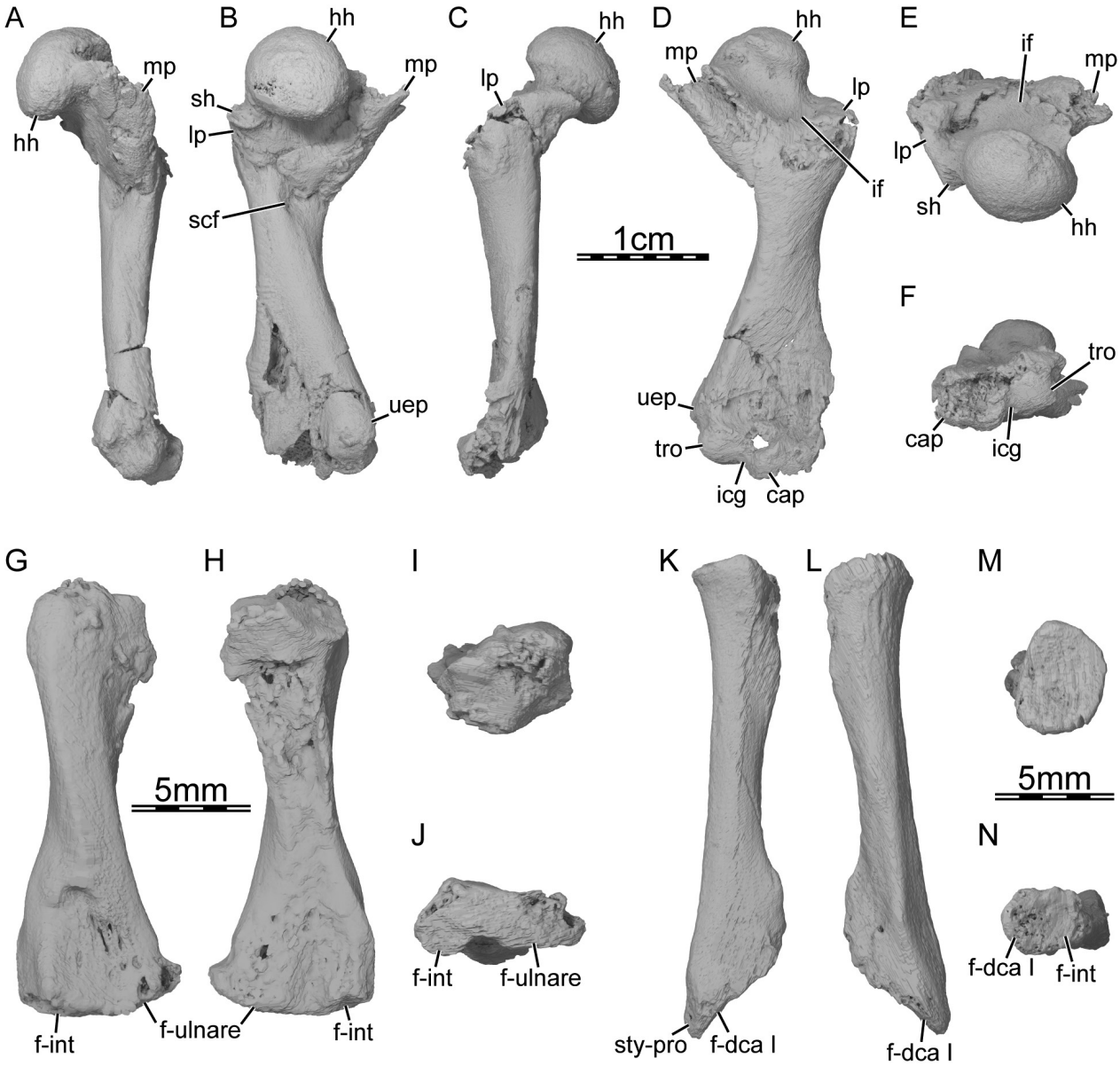


Figure 31. Three-dimensional renderings of a left humerus, ulna, and radius of *Allaeochelys crassesculpta* (SMF Me611). **A.** Humerus in ulnar view; **B.** Humerus in capitular view; **C.** Humerus in radial view; **D.** Humerus in intertubercular view; **E.** Humerus in proximal view; **F.** Humerus in distal view; **G.** Ulna in dorsal view; **H.** Ulna in ventral view; **I.** Ulna in proximal view; **J.** Ulna in distal view; **K.** Radius in dorsal view; **L.** Radius in ventral view; **M.** Radius in proximal view; **N.** Radius in distal view. Abbreviations: cap, capitellum; f-dca I, facet for articulation with distal carpal I; f-int, facet for articulation with intermedium; f-ulnare, facet for articulation with ulnare; hh, humeral head; icg, intercondylar groove; if, intertubercular fossa; lp, lateral process; mp, medial process; scf, subcapitular fossa; sh, shoulder; sty-pro, styloid process; tro, trochlea; uep, ulnar epicondyle.

much longer than digits I and II. The three phalanges are clearly elongate. The longest phalanx is the second, which is slightly longer than the entire digit II. Phalanges 2 and 3 are similar in length and each is slightly longer than the fused phalanges 1 and 2 of digit II. Digit IV is elongate and as long as digit III, although the proportions of the phalanges differ from those of digit III. The first phalanx of digit IV is slightly shorter than that of digit III, whereas the second phalanx is clearly longer than that of digit III. Phalanx 3 is the shortest of the three, albeit only slightly shorter than phalanx 1 and clearly shorter than phalanx 3 of digit III. Digit V is the third longest digit and slightly longer than digit II, but clearly shorter than digits III and IV. The first phalanx of digit V is as long as metacarpal V and only slightly shorter than phalanx 2. Phalanx 2 is the longest, whereas phalanx 3 is greatly reduced and the smallest phalanx of the manus.

Femur. The left femur is not preserved in SMF Me611 (Fig. 32). Other specimens, which were not scanned, preserve femora and allow us to provide some preliminary albeit limited anatomical insights on its anatomy. A femur is preserved in HLMD Be159 (left side; Fig. 13C, D), exposing its ventral side, in SMF Me2449 (right side of male; Fig. 23C, D), where it shows its anterior side, in SMF

Me3018 (Fig. 24C, D), where it shows its dorsal side on the right and its ventral side on the left, and in SMF Me3566 (Fig. 25), in which the femur is preserved on both sides in both specimens, revealing either its anterior or ventral side. The proximal portion of the femur forms the trochanter major, the trochanter minor, and the femoral head. The femoral head is not clearly visible in any specimen. It can be recognized as such on the right side of SMF Me2449, but is greatly eroded (Fig. 23C, D). The trochanter major is visible in HLMD Be159 (Fig. 13C, D), in which its proximal aspect seems damaged, and in SMF Me3566 (Fig. 25), in which it seems complete. The trochanter major is well-developed and proximally extends far beyond the proximal level of the femoral head, similar to that of *Carettochelys insculpta* (MAGNT R35037), but different from other turtles (Zug 1971; Walker 1973; Gaffney 1990; Sterli et al. 2007; Marzola 2019; Szczygielski and Piechowski 2023). The trochanter minor is visible in SMF Me2449 (Fig. 23C, D), in which its proximal extent is greatly reduced to the trochanter major and just reaches about mid-height of the femoral head, as in *Carettochelys insculpta* (MAGNT R35037). The anteroproximal edge of the trochanter minor seems to be smooth and curved, whereas that of *Carettochelys insculpta* (MAGNT R35037) forms a somewhat ovoid and flat platform. In ventral view, the intertrochanteric fossa is broad and C-shaped. The shaft is likely nearly straight for most of its length, as is the case in *Carettochelys insculpta* (MAGNT R35037), which contrasts with that of other turtles, in which it bends more strongly ventrodistally (Zug 1971; Walker 1973; Gaffney 1990; Sterli et al. 2007; Marzola 2019; Szczygielski and Piechowski 2023). The distal end of the femur is anteroposteriorly expanded. On its anterior side, the distal end forms a low and proximodistally elongate protuberance, which is visible in SMF Me2449 (Fig. 23C, D) and in *Carettochelys insculpta* specimen MAGNT R35037 where it likely corresponds to an anterior epicondyle. The fibular and tibial condyle can hardly be differentiated from one another because of damage, but the popliteal fossa appears to be shallow.

Tibia. Most of the left tibia is preserved in SMF Me611 but damaged (Fig. 32A–C). The proximal articulation surface is eroded and damage locally affects the more distal aspect of the proximal end on all sides. The tibia is also broken at about two thirds of its proximodistal length, where some of the bone is missing. The proximal end of the tibia is greatly expanded, and its mediolateral width is at least twice that of the shaft. The proximal articular surface is mostly eroded, which prevents assessment of its general shape, but some margins remain preserved nearly intact. The dorsal and lateral margins appear to be straight and are oriented nearly perpendicular to one another. The most medial aspect of the dorsal margin is slightly convex. The dorsomedial part of the articular surface is slightly projected proximally and forms the highest point of the tibia. The ventromedial portion of the articulation is inclined medially. Dorsally, the tibia forms a low cnemial crest that extends proximodistally from slightly distal to the proximal articular surface to beyond the midshaft. Damage to the distal part of the tibia prevents assessing the exact distal end of the cnemial crest and we are not able to identify it dorsally along the distal end of the tibia. On the ventral surface of the tibia, along its proximal end, the tibia seems to form a low and blunt, but relatively broad ridge that separates the ventral surface into two gently concave areas. The distal articulation surface is well-preserved. The central part of the surface has the shape of a shallow gutter that is oriented dorsoventrally. The lateral portion of the surface is slightly raised relative to the gutter and is also gently convex. The medial edge of the articular surface is projected distally, forming a short but relatively broad process and is greatly convex in medial view. Ventrally, along the distal aspect of the distal end, the tibia forms a ridge that extends proximodistally. This ridge subdivides the ventral surface of the tibia into two very gently concave areas and distally joins the edge of the articular surface, separating the latter into two distinct edges. The ventromedial edge of the articular surface is rounded and gently concave and slightly upturned, forming a low lip that is particularly visible in ventral view. The ventrolateral edge is slightly rounded and convex.

Fibula. Only the distal part of the fibula is preserved in SMF Me611, though it is slightly damaged (Fig. 32A–C). The distal part is triangular in shape, with nearly equally-expanded sides. The medial edge of the fibula is notably flattened. The dorsomedial and ventromedial sides of the fibula are gently concave, whereas the lateral side is flat. The distal articular surface is convex, but it is not possible to determine how many facets were present. The lateral side is almost completely straight except along its most dorsal and ventral aspects, which are gently convex. The dorsomedial edge is straight and the ventromedial edge is concave. The three sides are approximately equal in length, but a small piece of the articular surface is missing ventrolaterally and the lateral edge was perhaps the longest.

Tarsus and pes. The tarsus is not complete in SMF Me611, but likely consists of at least five elements: the astragalocalcaneum, which is not preserved, and distal tarsals I–IV, which are preserved (Fig. 32A–C). The astragalocalcaneum seems to be preserved in HLMD Me15956 (Fig. 20C, D) and SMF Me3566 (left side of female; Fig. 25A, B), but is badly crushed, precluding anatomical description. As was the case for the carpus, most elements were slightly displaced and some of them are, therefore, damaged and eroded. Thus, some uncertainty also remains here regarding the reconstruction and orientation of the distal tarsals. Harrassowitz (1922) identified only two tarsals in *Allaeochelys crassesculpta*, but our reconstruction of the hindlimb of SMF Me-611 shows that four distal tarsals are present, as in *Carettochelys insculpta* (TMM M18053). In specimen SMF Me611 of *Allaeochelys crassesculpta*, distal tarsal I is damaged, but appears to be a relatively broad element, clearly wider than long with a concave anterior surface that articulates with metatarsal I. The morphology of distal tarsal II is uncertain because of damage, which is quite substantial along its distal, medial,

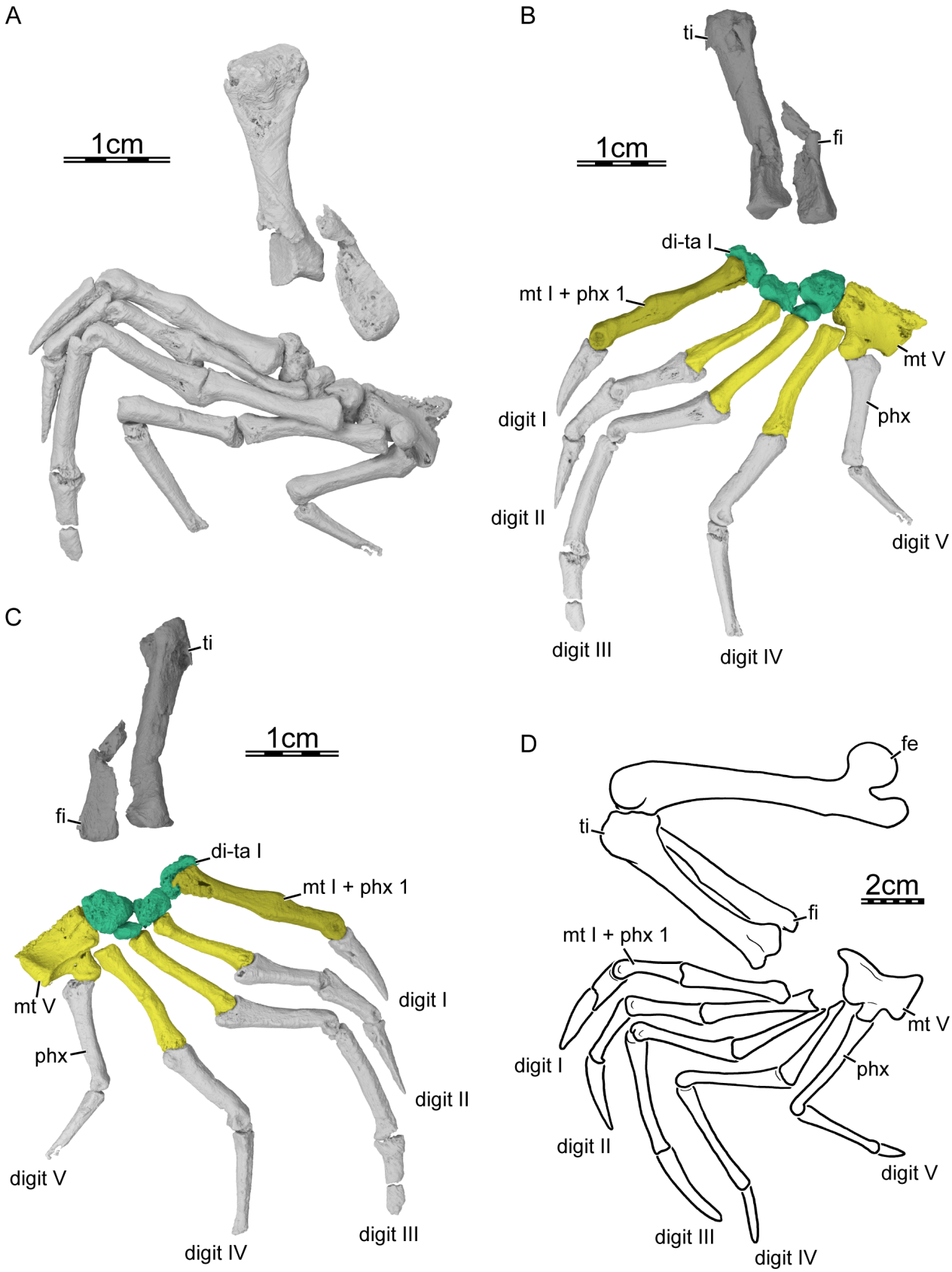


Figure 32. Three-dimensional renderings of a segmented left hindlimb of *Allaeochelys crassesculpta* (SMF Me611). **A.** Dorsal view; **B.** Reconstructed dorsal view; **C.** Reconstructed ventral view; **D.** Interpretive line drawing of left hindlimb of *Carettochelys insculpta* (redrawn from Walther (1922): pl. XXIII, fig. 24). Abbreviations: di-ta I, distal tarsal I; fe, femur; fi, fibula; mt I + phx 1, fused metatarsal I and fist phalanx of digit I; mt V, metatarsal V; phx, phalanx; ti, tibia.

and ventral sides as currently oriented. The proximal side of distal tarsal II is deeply concave. The medial side is clearly convex, forming a bump that is punctured by a fossa distodorsally. Distal tarsal III is the smallest bone of the tarsus. Distal tarsal III is dorsoventrally quite elongate, moderately broad, but proximodistally reduced. It is medially, medioventrally and ventrally damaged. The dorsal side of distal tarsal III is convex, whereas the preserved portions of its proximal and distal sides are flat. Distal tarsal IV is the largest of the four distal tarsals, but its morphology is also uncertain as several parts of the element are eroded. Distal tarsal IV appears to be as tall as broad as long, with convex medial and lateral sides. The dorsal part of its distal side forms a triangular fossa that, perhaps, serves as a contact or articulation facet with distal tarsal III.

The pes of *Allaeochelys crassesculpta* consists of five metatarsals and five digits (Fig. 32B, C). The pes of SMF Me611 only preserves phalanges 1 and 2 for digits IV and V, but three phalanges are present in those digits in specimens SMF Me-2449 (female) and SMF Me-3566 (female). Thus, the digital formula is 2-3-3-3-3, as in the manus and as in the pes of *Carettochelys insculpta* (Walther 1922). However, it seems that all digits of the pes of *Allaeochelys crassesculpta* are slightly shorter than those of *Carettochelys insculpta* (Walther 1922). The first pes digit of *Allaeochelys crassesculpta* is perhaps the smallest, but the incompleteness of digit V prevents certainty regarding which of the two is smallest. Digit II is the third smallest digit and digits III and IV are the longest, but determining which is the longest is not possible as the third phalanx is missing in digit IV. Metatarsal I is fused to the first phalanx, which also occurs in *Carettochelys insculpta* (Walther 1922). In *Allaeochelys crassesculpta*, the metatarsal portion of the fused element is slightly longer than the phalangeal one and appears to be slightly thicker than metatarsals II–IV and it contacts distal tarsal I. Metatarsal II is as long as metatarsal I, albeit slightly more slender, and it articulates with distal tarsal II proximally and the first phalanx distally. Metatarsal III is slightly longer than metatarsal II and is the longest along with metatarsal IV. Metatarsal III articulates with distal carpal III proximally and phalanx 1 distally. Metatarsal IV is as long as metatarsal III and slightly curved, with its concave surface facing laterally, and it contacts distal carpal III proximomedially and metatarsal V proximolaterally. Metatarsal V is slightly damaged and its most proximal aspect is missing. Metatarsal V has a peculiar morphology as it is not elongate as the other metatarsals, but rather rectangular and blocky, bearing a distinct and rounded process distodorsally. Metatarsal V is dorsoventrally curved with a dorsal convex surface and a ventral concave surface. The lateral side of metatarsal V is dorsoventrally expanded and nearly as tall as wide, forming a gently concave surface that contacts distal tarsal IV. The medial side of metatarsal V is relatively thick, albeit clearly less expanded than the lateral surface, and forms a slightly convex surface that represents the distomedial limit of the pes. The distal side of metatarsal V is gently concave and topped by a large process that protrudes distodorsally. The distal end of this process forms a rounded surface that articulates with phalanx 1 of digit V distomedially and metatarsal IV distolaterally. Digit I consists of two phalanges and the first is fused to metatarsal I. Phalanx 1 is likely the smallest bone of the first digit as it appears slightly shorter than phalanx 2, which is claw-like. Digit II consists of three phalanges which are nearly equally long, with phalanx 2 being slightly shorter than the other two and phalanx 1 likely slightly longer than phalanx 3. Phalanx 3 is claw-like. Digit III is elongate and much longer than digits I and II. The three phalanges are clearly elongate and longer than the respective phalanges on digits I and II. The longest phalanx is the second. Although the distal end of phalanx 3 is missing, most of the element seems to be preserved and it was likely slightly shorter than phalanx 1. Digit IV is elongate, but phalanx 3 is not preserved. The first phalanx appears identical in shape and size to that of digit III, whereas the second phalanx is slightly more slender than that of digit III, which is notably visible at about mid-length and perhaps also slightly shorter. Digit V is also incompletely preserved, as phalanx 3 is completely missing and the distal end of phalanx 2 is damaged. The first phalanx of digit V is as long as that of digit IV, but is slightly thinner. The preserved portion of phalanx 2 appears to be slightly more gracile than phalanx 2 of digit IV and it was, therefore, at least slightly shorter than the latter.

Insights into the anatomy of juveniles of *Allaeochelys crassesculpta*

In addition to a large sample of skeletally mature specimens, Messel Pit has also yielded numerous juvenile turtles (Smith et al. 2018), of which some can be assigned to *Allaeochelys crassesculpta*. While the identification of various hard-shelled species known from Messel is difficult since the available juveniles insufficiently document the shell characters used for their identification, diagnosing juvenile *Allaeochelys crassesculpta* is surprisingly simple, as they clearly display the morphology of adults in miniature. The most notable characteristics include the shell ornamentation typical of carettochelyids, the presence of a pygal and peripherals (absent in the trionychid "*Trionyx*" *messeliana* [Reinach 1900; Cadena 2016]), a notably short tail that barely extends beyond the carapacial margin (long tail present in the common geoemydid *Palaeoemys messeliana* [Cadena et al. 2018]), and the absence of plastral buttresses (present in *Palaeoemys messeliana* [Cadena et al. 2018] and the podocnemidid *Neochelys franzeni* [Schleich 1993; Cadena 2015]). Using these features, we were able to identify five specimens as juvenile *Allaeochelys crassesculpta* (HLMD Be169, IRSNB MeR007, IRSNB MeR015, SMF Me11381, and FHM 46; Fig. 33, Suppl. material 1: fig. S1.39). We also



Figure 33. Juvenile specimens of *Allaeochelys crassesculpta*. **A.** HLMD Be169, dorsal view; **B.** SMF Me11381, ventral view; **C.** IRSNB MeR007, dorsal view; **D.** IRSNB MeR007, ventral view; **E.** IRSNB MeR015, dorsal view; **F.** IRSNB MeR015, ventral view. Scale bars are 1 cm. The coin in C and D is a one Euro coin with a diameter of 23.25 mm.

measured the carapace length of a selection of juveniles and adults to generate a rough estimate of juvenile body size relative to that of adults. The carapace length and length ratio relative to that of adults could be estimated in HLMD Be169, IRSNB MeR007 and FHM 46 and the results are shown in Table 4.

Only minimal insights can be obtained regarding the craniomandibular anatomy of the juveniles, as all skulls are flattened. It nevertheless appears from HLMD Be169 and FHM 46 that the general shape of the cranium resembles that of the adults, the orbits are laterally oriented, and the upper temporal emargination is deep (Fig. 33A; Suppl. material 1: fig. S1.39). Scute sulci are not discernible in any juvenile specimen, as is the case in the adults.

Table 4. Measurements of carapace length in juveniles and length ratios relative to carapace length of adults. Measurements were taken along the midline of the carapace, i.e. from the anterior margin of the nuchal to the posterior margin of the pygal, in specimens that fully preserve this area. Carapace length of adults was measured in specimens HLMD Be158, HLMD Be159, HLMD Me4282, HLMD Me13721, HLMD Me15012, HLMDMe15956, SMF Me611, SMF Me1794, SMF Me2449, SMF Me3018, SMF Me3566 (male and female), SMF Me3783, SMF Me11418, and SMNK Pal986. The ratio of carapace length in juveniles relative to that of adults was calculated by using the mean value of all measurements obtained from the adults, which is 18.67 cm.

Specimen	Carapace length (cm)	Ratio relative to carapace length of adults
HLMD Be169	4	21.4%
IRSNB MeR007	5	26.8%
FHM 46	7.5	40.2%

The carapace consists of a nuchal, 10 peripherals, 8 costals, a suprapygal, and a pygal, as in the adults (Fig. 33A, C, E). The number of neurals cannot be ascertained. The nuchal forms the anterior margin of the carapace and forms a nuchal notch (Fig. 33E; Suppl. material 1: fig. S1.39), which appears to be absent in the adults (see Nuchal section above). All juveniles show the presence of a midline keel that seems to extend from the anterior portion of the carapace, likely from neural I or II, to the posterior quarter of the pygal (Fig. 33A, C, E). The peripherals have a wavy medial margin, with the central aspect of the margin forming a distinct notch (Fig. 33E). This contrasts with the morphology observed in adults, where the anterior peripherals have a straight medial margin. Carapacial fontanelles seem to be absent in all juvenile specimens.

The plastron is particularly well-preserved in IRSNB MeR015, which serves as the basis for our descriptive insights about the anatomy of juveniles (Fig. 33F). The plastron consists of a pair of epiplastra, a single entoplastron, and paired hyo-, hypo-, and xiphiplastra (Fig. 33F). The entoplastron is triangular with equilateral sides, as in the adults. The most anterior socket that serves for the articulation of the hyoplastron with the carapace is located at mid-length of the peripheral IV, which differs from adults, where it is generally located along the anterior third of peripheral IV (although intraspecific variation occurs among adults; Fig. 33F). The most posterior socket that serves to articulate the hypoplastron with the carapace is located along the anterior third of peripheral VII, as in adults (Fig. 33F). The posterior plastral lobe is relatively broad, but might be slightly narrower than in adults (Fig. 33F). The hypo-xiphiplastral suture is well-preserved in IRSNB MeR015 and distinctly sinuous, suggesting this individual was a male by reference to the morphology of this area as documented in adult individuals (Joyce et al. 2012).

Some insights can be provided about the forelimb anatomy of juveniles, which are at least partially preserved in HLMD Be169, IRSNB MeR007, IRSNB MeR015, and FHM 46. The hindlimbs cannot be studied in any specimen. A nearly complete humerus is preserved on the left side of IRSNB MeR007 in intertubercular view (Fig. 33D). The humerus forms a large and tall medial process, like that of adults. Parts of the manus are preserved in HLMD Be169, IRSNB MeR007, and FHM 46 (Fig. 33A, C; Suppl. material 1: fig. S1.39). Although damage prevents precisely assessing the relative size and proportion of the manus relative to the rest of the body, the preserved phalanges in IRSNB MeR007 and FHM 46 show that the phalanges were clearly elongate (Fig. 33C; Suppl. material 1: fig. S1.39). Comparison of the manus of IRSNB MeR007 with the humerus from that same specimen also suggests that the manus is longer than the humerus, providing evidence that the forelimb was likely developed as a flipper in juveniles of *Allaeochelys crassesculpta*, as is the case in juveniles of *Carettochelys insculpta* (Heaphy 1990).

Discussion

Alpha-taxonomy

The fossil record of carettochelyids is moderately rich, with 21 species known from the Early Cretaceous to the Middle Miocene. One of the major difficulties with this record is the overall scarcity or incompleteness of the remains that were reported until present. Most taxa considered valid are either known by incomplete specimens, relatively complete but single shells, or collections of fragmentary material, which prevents assessing their anatomy in detail and hinders a detailed reconstruction of the evolutionary history of the group. A few taxa, however, are known from more complete material that provides key insights into some general evolutionary trends among the group, such as the progressive loss of plastral and carapacial scutes during its evolutionary history and the likely origin of the group in Asia during the Late Jurassic (Joyce 2014; Thomson et al. 2021; Kim et al. 2025). *Allaeochelys crassesculpta*

stands out among the fossil record of carettochelyids by being known by more than a hundred specimens, most of which are nearly complete, articulated, though flattened skeletons. However, *Allaeochelys crassesculpta* only benefited from brief descriptive insights provided more than a hundred years ago by Harrassowitz (1922), who identified two carettochelyid taxa from the middle Eocene Messel Pit of Germany, namely *Anosteira crassesculpta* and *Anosteira gracilis*. *Anosteira gracilis* was synonymized later with *Anosteira crassesculpta* (Gramann 1956), before this single taxon was referred to *Allaeochelys* (Nessov 1976). Of the available material, only some were collected while the oil shales were mined at Messel (1859–1971), including those serving as the basis for the study of Harrassowitz (1922). These specimens are often preserved somewhat three dimensionally as they originate from concretions. The majority of specimens now available for study were collected after mining had ceased and after methods had been developed that allow preserving the fragile skeletons found in the actual oil shales using synthetic polymers (Smith et al. 2018). As the present contribution is the first detailed description and review of known material from the main collections that house *Allaeochelys crassesculpta* specimens, we provide detailed comparisons with all carettochelyid taxa we consider valid in the sections below.

Byeoljubuchelys yeosuensis is known by a nearly complete shell and some elements of the appendicular skeleton from the Early Cretaceous of South Korea (Kim et al. 2025), which provide comparative insights with the shell and limbs of *Allaeochelys crassesculpta*. The shell of *Allaeochelys crassesculpta* resembles that of *Byeoljubuchelys yeosuensis* (following Kim et al. (2025)) in the absence of scute sulci on the plastron. *Allaeochelys crassesculpta* differs from *Byeoljubuchelys yeosuensis* in its much greater size, the presence of paired nuchal processes, neural reversal on neural I (neural II in *Byeoljubuchelys yeosuensis*), a midline keel that extends onto the neurals (restricted to the suprapygal in *Byeoljubuchelys yeosuensis*), absence on scutes sulci on the carapace (present on costals IV–VII in *Byeoljubuchelys yeosuensis*), location of the most anterior socket for articulation of the hyoplastron with peripheral IV on the anterior third of peripheral IV (at the middle third of peripheral IV in *Byeoljubuchelys yeosuensis*), location of the most posterior socket for articulation of the hyoplastron with peripheral VII on the anterior third of peripheral VII (at mid-length of peripheral VII in *Byeoljubuchelys yeosuensis*), an equilateral entoplastron (lateral sides longer than posterior side in *Byeoljubuchelys yeosuensis*), a wider posterior lobe of the plastron, a medial process of the humerus that extends far over the humeral head, a moderate twisting of the proximal end of the humerus (reduced twisting in *Byeoljubuchelys yeosuensis*), and a more extended and prominent lateral process of the humerus that is slightly separated distally from the humeral head.

Only little comparative insights can be provided for *Kizylkumemys khoratensis* as it is only known by a partial carapace that includes the nuchal, neurals I–IV, and the medial aspects of peripherals I and costals I–V, and a handful of isolated and damaged shell elements from the Early Cretaceous of Thailand (Tong et al. 2005). Following Tong et al. (2005), *Allaeochelys crassesculpta* shares with *Kizylkumemys khoratensis* a neural reversal at neural I, but differs from the latter by the absence of carapacial scute sulci, a midline keel that extends onto the neurals (likely only on the suprapygal in *Kizylkumemys khoratensis*), an equilateral entoplastron (lateral sides longer than posterior side in *Kizylkumemys khoratensis*), and a wider posterior plastral lobe.

The Late Cretaceous *Kizylkumemys schultzi* is mostly known by isolated shell elements, although a partial cranium and partial mandible were also reported by Nessov from Uzbekistan (Nessov 1977, 1986, 1987). Despite the fragmentary nature of the known fossils, dozens of elements were reported by Nessov (1977, 1986, 1987) that allow extensive comparisons with *Allaeochelys crassesculpta*. *Allaeochelys crassesculpta* resembles *Kizylkumemys schultzi* by the presence of an anterior margin of the cavum tympani formed by the quadratojugal, presence of a large antrum postoticum, absence of a ventral enfolded ridge of the pterygoid, a foramen posterius canalis carotici interni located near midlevel of the parabasisphenoid, a small quadrate fossa, a deep adductor fossa, and presence of paired nuchal processes. *Allaeochelys crassesculpta* differs from *Kizylkumemys schultzi* by having an anteroposteriorly continuous mandibular triturating surface, a midline keel on the carapace not developed as a dorsal shark-like fin, a most anterior socket for articulation of the hyoplastron with the carapace located on the anterior third of peripheral IV (middle third of peripheral IV in *Kizylkumemys schultzi*), absence of carapacial and plastral scute sulci, and a much wider posterior plastral lobe.

Anosteira ornata is known by a nearly complete shell and many isolated shell elements from the early to middle Eocene (Bridgerian) of Wyoming, USA (Leidy 1873; Hay 1906, 1908), which allows comparisons with the shell of *Allaeochelys crassesculpta*. *Allaeochelys crassesculpta* resembles *Anosteira ornata* by a midline keel that likely extends onto the neurals and absence of plastral scute sulci. *Allaeochelys crassesculpta* differs from *Anosteira ornata* by a straight anterior margin of the carapace (carapace margin forms a slight emargination in *Anosteira ornata*), absence of carapacial scute sulci, an equilateral entoplastron (lateral sides longer than posterior side in *Anosteira ornata*), a more anteroposteriorly expanded hyoplastron, and a wider posterior plastral lobe.

The middle Eocene (Uintan) *Anosteira pulchra* from Utah, USA is known by a nearly complete, albeit crushed cranium and several partial shells (Clark 1932; Joyce et al. 2018; Adrian et al. 2020), allowing extensive comparisons to be made with *Allaeochelys crassesculpta*. *Allaeochelys crassesculpta* resembles *Anosteira*

pulchra by having a longer than wide rectangular dorsal plate of the prefrontal, a large contribution of the frontal to the orbit margin, presence of an ophthalmic slit, an anteroposteriorly short postorbital, a contribution of the quadratojugal to the margin of the cavum tympani, a large antrum postoticum, a straight labial margin on the maxilla, a foramen posterius canalis carotici interni located at midlevel of the parabasisphenoid, absence of an enfolded ridge that ventrally covers the pterygoid fossa, a moderately deep quadrate fossa, two foramina nervi hypoglossi, and absence of plastral scute sulci. *Allaeochelys crassesculpta* differs from *Anosteira pulchra* by lacking a contact between the parietal and opisthotic, presence of a maxilla-quadratojugal contact that also prevents the jugal from contributing to the ventral margin of the cranium, absence of a contact between the quadratojugal and squamosal, absence of a contribution of the squamosal to the margin of the cavum tympani, a deeper pterygoid fossa, a smaller exposure of the parabasisphenoid on the ventral surface of the cranium, elongate tubercula basioccipitale (short tubercula in *Anosteira pulchra*), a flat ventral surface of the basioccipital (slightly concave in *Anosteira pulchra*), a straight anterior margin of the carapace (slightly emarginated in *Anosteira pulchra*), a midline keel not developed as a dorsal shark-like fin, absence of carapacial scute sulci, a more anteroposteriorly expanded hyoplastron, and a wider posterior plastral lobe.

Anosteira crowcreekensis from the late Eocene of Arkansas, USA is known by three isolated bones: a neural IV, a left peripheral VII, and a partial costal (Hutchison and Westgate 2024). Comparisons with *Allaeochelys crassesculpta* are, therefore, extremely limited, but *Allaeochelys crassesculpta* clearly differs from *Anosteira crowcreekensis* by lacking a midline keel of the carapace that is developed as a shark-like dorsal fin and absence of carapacial scutes.

Little information is available for *Anosteira manchuriana*, which is known only by a single partial shell from the late Eocene of Liaoning, China that comprises a partial nuchal, neurals I–VII, incomplete portions of the costals, and a complete, albeit dislocated plastron (Zangerl 1947). *Allaeochelys crassesculpta* resembles *Anosteira manchuriana* by a midline keel that extends onto the neurals and the absence of plastral scute sulci. *Allaeochelys crassesculpta* differs from *Anosteira manchuriana* by lacking carapacial scute sulci, an equilateral entoplastron (lateral sides longer than posterior side in *Anosteira manchuriana*), a more anteroposteriorly expanded hyoplastron, and a wider posterior plastral lobe.

The fossil record of *Anosteira maomingensis* from the late Eocene of Guangdong, China is quite rich compared to other carettochelyids as it consists of a nearly complete cranium (Danilov et al. 2017a), a complete mandible (Tong et al. 2010), and several partial shells (Chow and Liu 1955; Tong et al. 2010). *Allaeochelys crassesculpta* shares with *Anosteira maomingensis* a large contribution of the frontal to the orbit, a contribution of the quadratojugal to the anterior margin of the cavum tympani, a straight labial margin of the maxilla, a deep pterygoid fossa, absence of an enfolded ridge that ventrally covers the pterygoid fossa, a moderately deep quadrate fossa, a deep adductor fossa, a midline keel that extends onto the neurals, and absence of plastral scute sulci. *Allaeochelys crassesculpta* differs from *Anosteira maomingensis* by the absence of a contact between the parietal and opisthotic, an anteroposteriorly short postorbital, a smaller jugal, presence of a contact between the quadratojugal and maxilla that prevents the jugal from contributing to the ventral margin of the cranium, a shallow cheek emargination in the form of a small notch (large and deep emargination in *Anosteira maomingensis*), a posterior half of the triturating surface that is only slightly expanded (strongly expanded in *Anosteira maomingensis*), a more elongate contact between the quadratojugal and postorbital, absence of contact between the quadratojugal and squamosal, a larger antrum postoticum, absence of a squamosal contribution to the cavum tympani, a foramen posterius canalis carotici interni located at midlevel of the parabasisphenoid (located more posteriorly along the posterior end of the parabasisphenoid in *Anosteira maomingensis*), a flat ventral surface of the basioccipital (slightly concave in *Anosteira maomingensis*), two foramina nervi hypoglossi (single foramen in *Anosteira maomingensis*), lack of a posterior subdivision of the triturating surface of the mandible, a coronoid anterior margin oriented posteriorly (vertically oriented in *Anosteira maomingensis*), presence of a posterior process of the dentary that slightly overhangs the foramen auriculotemporalis, absence of carapacial scute sulci, an equilateral entoplastron (lateral sides longer than posterior side in *Anosteira maomingensis*), a slightly more anteroposteriorly expanded hyoplastron, and a slightly wider posterior plastral lobe.

Anosteira mongoliensis is only known by a partial shell and a few isolated elements from the late Eocene of Inner Mongolia, China (Gilmore 1931), which greatly limits comparisons with *Allaeochelys crassesculpta*. *Allaeochelys crassesculpta* seems to resemble *Anosteira mongoliensis* by the absence of plastral scute sulci, but differs from the latter by its greater size, a most anterior socket for articulation of the hyoplastron and carapace located at the anterior third of peripheral IV (located at anterior third of peripheral V in *Anosteira mongoliensis*), a more anteroposteriorly expanded hyoplastron, and a wider posterior plastral lobe.

Similar to the case mentioned above for *Anosteira mongoliensis*, very few anatomical insights are available for *Anosteira shantungensis* from Shandong, China, as the latter is only known by two highly fragmentary and incomplete specimens (Cheng 1961). *Allaeochelys crassesculpta* resembles *Anosteira shantungensis* by having a midline keel that extends onto the neurals, but differs from the latter by the absence of carapacial scute sulci and a reversal of neural I (reversed neural II in *Anosteira shantungensis*).

The Paleocene *Allaeochelys lingnanica* from Guangdong, China (Young and Chow 1962) is only known

by a single, partial shell that consists of an incomplete anterior half of the carapace and the left bridge area, including the most lateral aspect of the left hyo- and hypoplastron. It appears that *Allaeochelys crassesculpta* may share a lack of carapacial and plastral scutes with *Allaeochelys lingnanica*, although we are not able to assess this feature with confidence. However, *Allaeochelys crassesculpta* clearly differs from the latter by the location of the most anterior socket for articulation of the hyoplastron with the carapace on the anterior third of peripheral IV (located in the middle of peripheral IV in *Allaeochelys lingnanica*) and the location of the most posterior socket for articulation of the hypoplastron with the carapace on the anterior third of peripheral VII (located at mid-length of peripheral VII in *Allaeochelys lingnanica*).

Allaeochelys rouzilhacensis is known by a nearly complete, albeit crushed cranium and a few isolated shell fragments from the middle Eocene (MP10–11) of France (Godinot et al. 2018). While the shell material is too fragmentary to compare with *Allaeochelys crassesculpta*, we are able to provide some comparisons with the cranial material reported by Godinot et al. (2018). The cranium of *Allaeochelys crassesculpta* resembles that of *Allaeochelys rouzilhacensis* by having a large contribution of the frontal to the orbit margin, an elongate suture between the postorbital and quadratojugal, a straight labial margin of the maxilla and, perhaps, the absence of an anterior fossa on the triturating surface, a posterior half of the triturating surface of the maxilla only lightly expanded, presence of an ophthalmic slit, and a deep antrum postoticum. The only difference that can be identified between *Allaeochelys crassesculpta* and *Allaeochelys rouzilhacensis* is the size of the quadrate fossa, which Godinot et al. (2018) described as being larger in *Allaeochelys rouzilhacensis*. As these coeval taxa originate from the same landmass north of the Alps and because our phylogenetic analysis recovers them as closely related (nearly identical in their character scores; see below), we suggest revising *Allaeochelys rouzilhacensis* in light of a possible synonymy with *Allaeochelys crassesculpta*.

Eulalichelys labarrerei is known by a single, nearly complete, uncrushed cranium and two isolated carapace fragments of the carapace from the early Eocene (MP8–9) of France (Godinot et al. 2018). Only the cranium is sufficiently complete to allow comparisons with *Allaeochelys crassesculpta*. *Allaeochelys crassesculpta* resembles *Eulalichelys labarrerei* by the presence of a contact between the maxilla and quadratojugal that prevents the jugal from contributing to the ventral margin of the cranium and the presence of an ophthalmic slit. *Allaeochelys crassesculpta* differs from *Eulalichelys labarrerei* by having a posterior surface of the triturating surface of the maxilla that is only lightly expanded (greatly expanded in *Eulalichelys labarrerei*), the presence of a light cheek emargination in the form of a small notch (cheek emargination likely completely absent in *Eulalichelys labarrerei*), a foramen posterius canalis carotici interni located at midlevel of the parabasisphenoid (likely located more posteriorly in *Eulalichelys labarrerei*), a low quadrate below the cavum tympani (tall in *Eulalichelys labarrerei*) and absence of a squamosal contribution to the cavum tympani.

Allaeochelys delheidi is based on a posterior half of a carapace reported by Dollo (1886) from the early Eocene of Belgium, but Joyce (2014) expanded the hypodigm to include early Eocene material from France, Spain, and the UK, reported by Lydekker (1889), Jiménez Fuentes (1971, 1992), Broin (1977), Alonso Santiago and Alonso Andrés (2005) and Alonso Santiago et al. (2008), including fairly complete shells and skulls. Most of this material still awaits detailed revision and descriptions, but we here provide some comparisons, based on the illustrations available in the aforementioned studies. *Allaeochelys crassesculpta* resembles *Allaeochelys delheidi* by having a large contribution of the frontal to the orbit margin, a posterior surface of the triturating surface of the maxilla that is lightly expanded, the absence of carapacial scute sulci, a neural reversal located on neural I, an equilateral entoplastron, and a wide posterior plastral lobe. *Allaeochelys crassesculpta* differs from *Allaeochelys delheidi* by its smaller size, a thin margin of the external nares (the external nares are greatly thickened in *Allaeochelys delheidi*), an anteroposteriorly short postorbital, and a midline keel that extends onto the neurals (only extends on to the pygal and suprapygal in *Allaeochelys delheidi*).

Allaeochelys parayrei is only known by a few incomplete shells from the late Eocene of France (Noulet 1867; de Stefano 1902; Bergounioux 1931; Broin 1977). The shell of *Allaeochelys crassesculpta* greatly resembles that of *Allaeochelys parayrei* in its proportions, the absence of carapacial and plastral scutes, a reversal of neural I, an equilateral entoplastron, an anteroposteriorly expanded hyoplastron, and a wide posterior plastral lobe. The only notable difference we are able to identify is the extent of the midline keel, which is extended onto the neurals in *Allaeochelys crassesculpta*, whereas it only reaches the pygal and suprapygal (and, perhaps, costals VII and VIII) in *Allaeochelys parayrei*.

Allaeochelys magnifica is known by an assemblage of isolated shell fragments from the late middle Eocene of Myanmar (Hutchison et al. 2004). Although those elements only document a limited portion of the shell anatomy of this taxon, they notably highlight its large size, perhaps the greatest among known carettochelyid species. The fragmentary nature of the remains allows only minimal additional comparative insights with *Allaeochelys crassesculpta*. *Allaeochelys crassesculpta* might share with *Allaeochelys magnifica* a wide posterior plastral lobe, but differs from the latter by the proportions of the suprapygal, which is more anteroposteriorly elongate in *Allaeochelys magnifica*.

Carettochelys niahensis is only known by its holotype, which consists of a partial cranium from the Late Oligocene of Malaysia (White et al. 2023). *Allaeochelys crassesculpta* resembles *Carettochelys niahensis* by its

thin margin of the external nares, a large contribution of the frontal to the orbit, a large sulcus olfactorius, a slightly expanded posterior half of the triturating surface of the maxilla, a large contribution of the jugal to the orbit margin, and a contact between of the maxilla and quadratojugal that prevents the jugal from contributing to the ventral margin of the cranium. The cranium of *Allaeochelys crassesculpta* differs from that of *Carettochelys niahensis* by the presence of an ophthalmic slit (presence of an ophthalmic foramen in *Carettochelys niahensis*), a straight labial margin (wavy in *Carettochelys niahensis*) and, perhaps, an anteroposteriorly shorter postorbital.

Allaeochelys liliae is known by a single specimen from the Early Miocene of Mexico that consists of the posterior part of a shell (Carbot-Chanona et al. 2020), which greatly limits the comparisons that can be made with *Allaeochelys crassesculpta*. *Allaeochelys crassesculpta* is nevertheless similar to *Allaeochelys liliae* by the absence of carapacial and plastral scutes, an anteroposteriorly expanded hyoplastron and a wide posterior plastral lobe, but differs from the latter by a midline keel that extends onto the neurals (limited to the pygal and suprapygal in *Allaeochelys liliae*) and its likely smaller size.

The Early Miocene *Allaeochelys meylani* from Egypt is based on a partial cranium and a collection of shell elements is also referred, allowing the partial documentation of its shell anatomy (Rollot et al. 2025). *Allaeochelys crassesculpta* shares with *Allaeochelys meylani* the presence of a contact between the maxilla and quadratojugal that prevents the jugal from contributing to the ventral margin of the cranium, the absence of contact between the quadratojugal and squamosal above the cavum tympani, a lightly expanded posterior half of the triturating surface of the maxilla, a deep pterygoid fossa, the presence of a precolumellar fossa in the cavum tympani, a shallow dorsal embayment of the common crus, the absence of carapacial and plastral scutes, and a wide posterior plastral lobe. *Allaeochelys crassesculpta* differs from *Allaeochelys meylani* by a thin margin of the external nares, a larger contribution of the frontal to the orbit margin, the presence of an ophthalmic slit (presence of an ophthalmic foramen in *Allaeochelys meylani*), a larger contribution of the jugal to the orbit margin, a larger sulcus olfactorius, a straight labial margin of the maxilla (wavy in *Allaeochelys meylani*), an anteroposteriorly shorter postorbital, a more elongate suture between the postorbital and quadratojugal, a shallow cheek emargination (emargination absent in *Allaeochelys meylani*), a low quadrate height below the cavum tympani (tall quadrate in *Allaeochelys meylani*), the absence of a contribution of the squamosal to the cavum tympani, the absence of an additional fossa on the anterior portion of the triturating surface (present and large in *Allaeochelys meylani*), the absence of an enfolded ridge of the pterygoid, a foramen posterius canalis carotici interni located at mid-level of the parabasisphenoid (located posterior to the posterior border of the parabasisphenoid in *Allaeochelys meylani*), a contribution of the quadratojugal to the margin of the cavum tympani, a deep antrum postoticum (absent in *Allaeochelys meylani*), a small quadrate fossa (large fossa in *Allaeochelys meylani*), the absence of an accessory ridge on the posterior surface of the quadrate, a foramen oropharyngeale formed by the opisthotic (formed by the opisthotic and pterygoid in *Allaeochelys meylani*), a flat ventral surface of the basioccipital (concave in *Allaeochelys meylani*), two foramina nervi hypoglossi (one in *Allaeochelys meylani*), and the absence of a medial process of peripheral II.

Allaeochelys libyca is known by a partial cranium and a few, isolated fragments from the Middle Miocene of Libya that represent two partial hypoplastra, three peripherals and an incomplete supraoccipital (Havlik et al. 2014). Our comparisons with *Allaeochelys crassesculpta*, therefore, only pertain to the cranial anatomy, although the preserved hypoplastra suggest that *Allaeochelys crassesculpta* and *Allaeochelys libyca* share the absence of at least plastral scute sulci. The cranium of *Allaeochelys crassesculpta* is similar to that of *Allaeochelys libyca* by having a broad sulcus olfactorius, the absence of a contact between the parietal and opisthotic, a contribution of the quadratojugal to the margin of the cavum tympani, the absence of a contact between the quadratojugal and squamosal, the absence of a contribution of the squamosal to the margin of the cavum tympani, a deep pterygoid fossa, elongate tubercula basioccipitale, a wide sulcus that separates the two facets of the mandibular condyle, and two foramina nervi hypoglossi. The cranium of *Allaeochelys crassesculpta* differs from that of *Allaeochelys libyca* by a longer than wide dorsal plate of the prefrontal, a larger contribution of the frontal to the orbit margin, the presence of an ophthalmic slit (presence of an ophthalmic foramen in *Allaeochelys libyca*), an anteroposteriorly more elongate postorbital, a large antrum postoticum (small in *Allaeochelys libyca*), the absence of an enfolded ridge on the ventral surface of the pterygoid, a flat ventral surface of the basioccipital (concave in *Allaeochelys libyca*), a foramen oropharyngeale formed by the opisthotic (formed by the opisthotic and pterygoid in *Allaeochelys libyca*), the presence of precolumellar fossa, and a moderately deep quadrate fossa (deep in *Allaeochelys libyca*).

Allaeochelys crassesculpta resembles the extant *Carettochelys insculpta* (following Joyce (2014); Rollot et al. (2024b)) by a longer than wide dorsal plate of the prefrontal, the presence of an ophthalmic slit, a broad sulcus olfactorius, contact between the maxilla and quadratojugal that prevents the jugal from contributing to the ventral margin of the cranium, a thin margin of the external nares, a large contribution of the jugal to the orbit margin, a contribution of the quadratojugal to the anterior margin of the cavum tympani, a shallow cheek emargination in the form of a small notch, the absence of a contact between the quadratojugal and squamosal, a

low quadrate below the cavum tympani, the absence of a contribution of the squamosal to the margin of the cavum tympani, a deep pterygoid fossa, elongate tubercula basioccipitale, a foramen oropharyngeale formed by the opisthotic, two foramina nervi hypoglossi, an anteroposteriorly continuous triturating surface of the mandible, a posteriorly inclined anterior margin of the coronoid, the absence of carapacial and plastral scute sulci, an equilateral entoplastron, a broad posterior plastral lobe (albeit broader in *Carettochelys insculpta* than in any other carettochelyid), a straight shaft of the humerus, a well-developed medial process of the humerus, a moderate twisting of the proximal end of the humerus relative to its distal end, a lateral process slightly distally separated from the humeral head, and a more proximally located trochlea of the humerus relative to the capitellum. *Allaeochelys crassesculpta* differs from the extant *Carettochelys insculpta* by a larger contribution of the frontal to the orbit margin, an anteroposteriorly shorter postorbital, a deep antrum postoticum (absent in adult *Carettochelys insculpta*), a straight labial margin of the maxilla (wavy in *Carettochelys insculpta*), the absence of an additional fossa on the anterior part of the triturating surface of the maxilla, absence of an enfolded ridge on the ventral surface of the pterygoid, location of the foramen posterius canalis carotici interni at midlevel of the parabasisphenoid (located posterior to the posterior end of the parabasisphenoid in *Carettochelys insculpta*), the presence of a precolumellar fossa, a moderately deep quadrate fossa (deep in *Carettochelys insculpta*), a wider sulcus separating the two facets of the mandibular condyle, a shallow dorsal embayment of the common crus (deep in *Carettochelys insculpta*), the presence of a posterior ramus of the dentary that slightly overhangs the foramen auriculotemporalis, the absence of a posterolateral accessory coronoid ridge, a continuous neural series (disrupted by mid-line contacts between pairs of costals in *Carettochelys insculpta*), a most posterior socket for articulation with the hypoplastron located at the anterior third of peripheral VII (located at midlength of peripheral VII in *Carettochelys insculpta*), a slightly less anteroposteriorly expanded hyoplastron, and a somewhat better developed shoulder of the humerus.

Paleoecology and locomotor mode

Carettochelys insculpta is unique among extant freshwater turtles as the only species to have its limbs developed into flippers, similar to those of sea turtles (Walther 1922). The convergence with sea turtles also applies to the kinematics of the fore flipper during swimming, as the motion of the two forelimbs is synchronous while swimming (Rivera et al. 2013; Krahl 2021; Krahl and Werneburg 2023). Detailed studies have shown, however, that the forelimb kinematics of *Carettochelys insculpta* are more similar to those of rowing freshwater turtles, such as *Apalone ferox*, than to the flapping of sea turtles, though closest to the flapping of sea turtles amongst all freshwater turtles studied (Rivera et al. 2013). Major differences in forelimb kinematics pertain to the movement of the humerus, as *Carettochelys insculpta* exhibits significantly more anteroposterior humeral motion and protraction and significantly less dorsoventral humeral motion and depression than sea turtles (Rivera et al. 2013). Rivera et al. (2013), therefore, suggested *Carettochelys insculpta* should be termed a 'synchronous rower' or 'hybrid rower-flapper.' Krahl and Werneburg (2023) identified a series of similarities in the osteology of the limbs between sea turtles and *Carettochelys insculpta*. In *Carettochelys insculpta*, the humerus closely resembles that of sea turtles: it is broader and straighter than in most other turtles, the long axis of the humeral head is less oblique relative to the shaft, the medial process is enlarged and extends proximally beyond the humeral head, and the lateral process is displaced distally. Further similarities with sea turtles also include a similarly angled lower arm and an enlarged pisiform. In addition to these osteological features, differences in forelimb proportions (i.e. length of the humerus vs. ulna vs. manus) are known to reflect the ecology of turtles, with sea turtles and *Carettochelys insculpta* possessing particularly elongate hands relative to the rest of the forelimb (Joyce and Gauthier 2004).

Kim et al. (2025) recently pointed out several differences in the morphology of the humerus of *Byeoljubuchelys yeosuensis*, the earliest branching carettochelyid, relative to that of *Carettochelys insculpta* and *Allaeochelys crassesculpta*, suggesting that the peculiar locomotor mode of *Carettochelys insculpta* is not shared by all carettochelyids and that 'synchronous rowing' evolved at a later time in carettochelyid evolution. While the kinematics of the forelimb can obviously not be studied in *Allaeochelys crassesculpta*, the morphology of the forelimb and of the humerus can be studied in detail as several specimens among our sample nicely preserve these body parts. In the following section, we provide several lines of evidence that support the inference that *Allaeochelys crassesculpta* likely swam like *Carettochelys insculpta*.

The shape and proportions of the left forelimb of SMF Me611 resemble the fore flipper of *Carettochelys insculpta* (Walther 1922), as previously noted (Harrassowitz 1922; Joyce 2014). The manus represents more than 50% of the entire length of the forelimb (see Table 2), similar to that of *Carettochelys insculpta* and chelonioids, suggesting that this taxon lived in open bodies of water (Joyce and Gauthier 2004; Fig. 34).

The morphology of the humerus of *Allaeochelys crassesculpta* is close to that of *Carettochelys insculpta* and suggests adaptation to a similar style of swimming. The humerus of *Allaeochelys crassesculpta* shares with *Carettochelys insculpta* and sea turtles a flattening of the shaft, which is generally seen in secondarily aquatic-adapted amniote groups (Evers et al. 2019; Motani and Vermeij 2021; Hermanson et al. 2024). The humerus of *Allaeochelys crassesculpta*

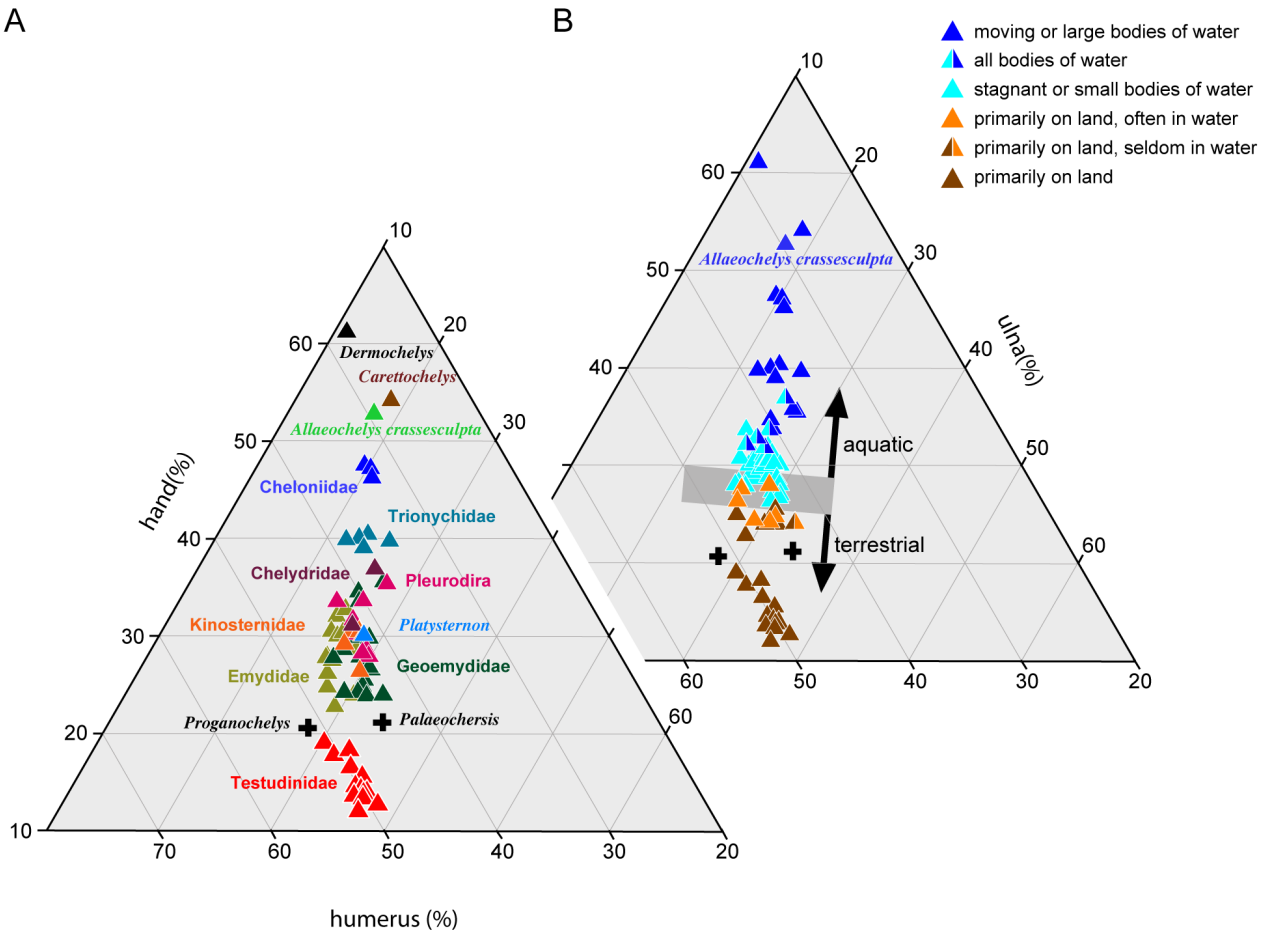


Figure 34. Ternary plot of turtle forelimb measurements. **A.** Data point color coded for taxa; **B.** Data point color coded for habitat preferences. The assemblage of turtles in the intermediate grey field drawn in figure subpanel B is from both terrestrial and aquatic settings. Full percentage range of each side of the triangles is not depicted.

also exhibits a distally displaced lateral process and a large, columnar medial process that extends far above the humeral head. These are features observed in both *Carettochelys insculpta* and sea turtles that anchor hypertrophied muscles involved in swimming (Walker 1973; Hendrickson 1980; Krahl et al. 2020; Hermanson et al. 2024).

Another striking feature of *Allaeochelys crassesculpta* that suggests a high degree of adaptation to an aquatic lifestyle is present in the cranium. The µCT datasets that we used for the present study reveal that the cranium of *Allaeochelys crassesculpta* is highly porous, which is similar to the condition observed in cranial bones of sea turtles (see Scheyer et al. (2014) for other turtle body parts). This extreme bone porosity is clearly apparent in SMF Me3004, the cranium we fully reconstructed, particularly in the frontal, parietal, opisthotic, pterygoid, squamosal and basioccipital-exoccipital complex (Fig. 35).

The morphological, anatomical, and morphometric features presented above provide strong evidence that *Allaeochelys crassesculpta* was well-adapted to aquatic environments and to active swimming, likely similar to that seen in *Carettochelys insculpta*. As such an adaptation to swimming appears to be absent in the Early Cretaceous carettochelyid *Byeoljubuchelys yeosuensis*, the synchronous rowing of extant carettochelyids may have evolved somewhere between the Late Cretaceous and Paleocene.

The likely capability for "synchronous rowing" in *Allaeochelys crassesculpta* suggests that this turtle lived in the surface waters of the lake at Messel, searching its surface for edible morsels. It is also near the surface of the lake that this turtle may have encountered mates, which have been preserved during copulation when sinking into deeper strata poisoned by volcanic gases (Joyce et al. 2012). The rare occurrence of juveniles of varying size, however, suggests that Messel was not a systematic death trap for mating pairs, but rather supported a viable population.

The preference of *Allaeochelys crassesculpta* for a lacustrine habitat is likely the reason why this turtle dominates the Messel fauna. Although sampling is certainly not random, *Allaeochelys crassesculpta* is the most common turtle at Messel, followed by the aquatic geoemydid *Palaeoemys messeliana* (Hervet 2004; Claude and Tong 2004; Cadena et al. 2018; Ascarrunz et al. 2021), the trionychid "*Trionyx*" *messeliana* (Reinach 1900; Cadena 2016), the podocnemidid *Neochelys franzeni* (Schleich 1993; Cadena 2015) and an unnamed ptychogasterid known from a single plastral fragment (Ascarrunz and Joyce 2024). This stands in stark contrast to the roughly coeval turtle fauna of nearby

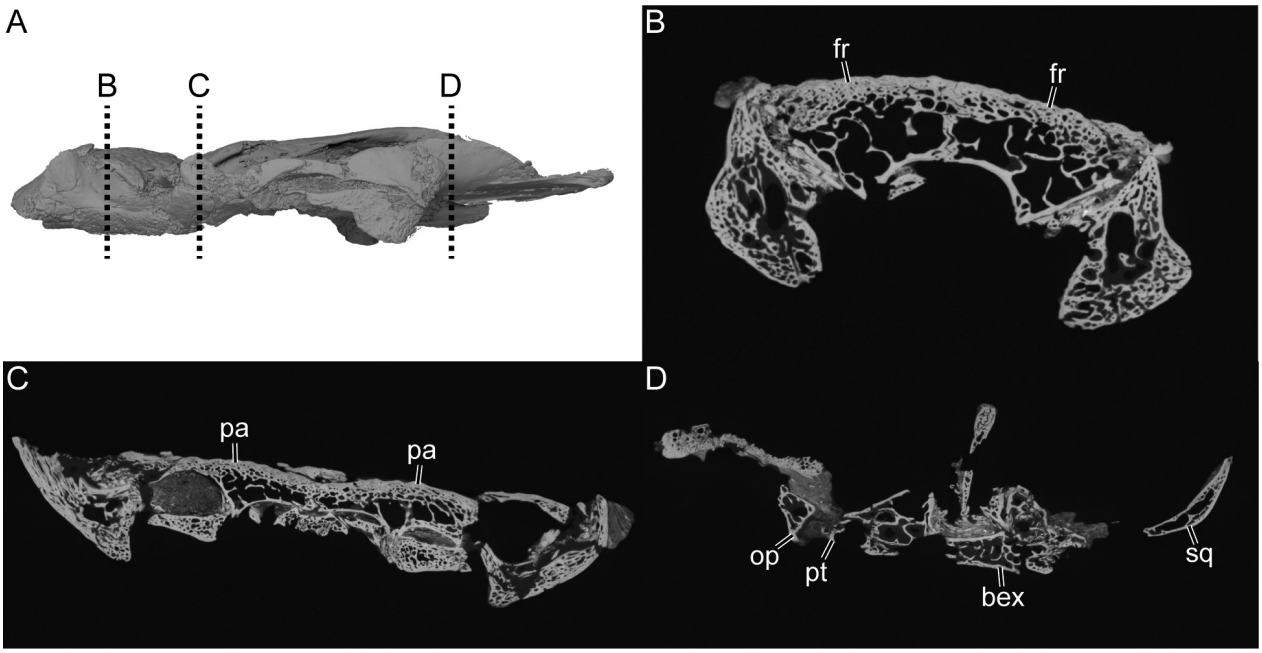


Figure 35. Selection of µCT slices highlighting the great degree of porosity in the cranium of *Allaeochelys crassesculpta* (SMF Me3004). **A.** Three-dimensional rendering of the cranium SMF Me3004, showing the location of the µCT slices in the cranium; **B.** µCT slice 2151; **C.** µCT slice 1818; **D.** µCT slice 907. Abbreviations: bex, basioccipital-exoccipital complex; fr, frontal; op, opisthotic; pa, parietal; pt, pterygoid; sq, squamosal.

Geiseltal, which consists of the tortoise *Pelorochelon*/*Hadrianus eocaenica*, the terrestrial ptychogasterid *Geiselemys ptychogastroides*, the aquatic geoemydid *Palaeoemys messeliana*, and rare occurrences of "*Trionyx*" *messeliana* (Krumbiegel 1962; Krumbiegel et al. 1983; Hervet 2004; Ascarrunz and Joyce 2024). *Allaeochelys crassesculpta* is completely absent, suggesting absence of permanent bodies of water at Geiseltal.

Phylogenetic analyses

Our parsimony phylogenetic analysis under equal-weighting resulted in 34,623 most parsimonious trees with 120 character-state transitions. *Anosteira lingnanica* and *Allaeochelys magnifica* were identified as wildcard taxa using the pruned tree function of TNT and removed prior to the generation of the strict consensus tree, which is shown in Fig. 36. The strict consensus tree is poorly resolved. *Byeoljubuchelys yeosuensis* is retrieved as the earliest branching carettochelyid, as in Kim et al. (2025), and the next less inclusive clade groups *Kizylkumemys* spp. and *Anosteira* spp. into a large polytomy. *Allaeochelys* spp. and *Carettochelys* spp. are grouped together within the latter clade forming an '*Allaeochelys*/*Carettochelys*' lineage, albeit with fully unresolved ingroup relationships, as in previous studies (Havlik et al. 2014; Danilov et al. 2017a; Carbot-Chanona et al. 2020; Kim et al. 2025). In the strict consensus tree, *Carettochelyidae* is supported by two synapomorphies: presence of a midline keel restricted to the pygal and/or suprapygal (character 58, state 1) and a reduced width of the posterior plastral lobe (character 63, state 1). The next less inclusive clade, which unites all carettochelyids but *Byeoljubuchelys yeosuensis*, is supported by four synapomorphies: the presence of paired ventral processes on the nuchal (character 49, state 1), a neural reversal occurring on neural I (character 51, state 0), the location of the most posterior socket for articulation of the hypoplastron with the carapace on the anterior third of peripheral VII (character 55, state 2), and a midline keel that clearly extends onto the neurals (character 58, state 2). The '*Allaeochelys*/*Carettochelys*' clade is supported by 15 synapomorphies: an elongate postorbital-quadratojugal suture (character 5, state 2), a shallow cheek emargination in the form of a small notch (character 8, state 1), the presence of a maxilla-quadratojugal contact (character 9, state 1), the absence of a quadratojugal-squamosal contact (character 10, state 0), the presence of an anterior foramen in the maxilla for the canalis alveolaris superior (character 16, state 1), the presence of an enfolded ridge on the ventral surface of the pterygoid that covers the pterygoid fossa (character 25, state 1), a shallow antrum postoticum (character 29, state 1), the presence of a large quadrate fossa (character 31, state 2), dorsoventral thickening of the quadrate at the level of the processus trochlearis oticum (character 34, state 1), elongate and pointy tuberculum basioccipitale (character 41, state 2), the absence of a subdivision of the triturating surface of the dentary (character 43, state 0), the presence of a midline keel, restricted to the pygal and/or suprapygal (character 58, state 1), the absence of carapacial and plastral scute sulci (character 59, state 3), an entoplastron with lateral sides as long as posterior side (character 62, state 1), and a wide posterior plastral lobe (character 63, state 0).

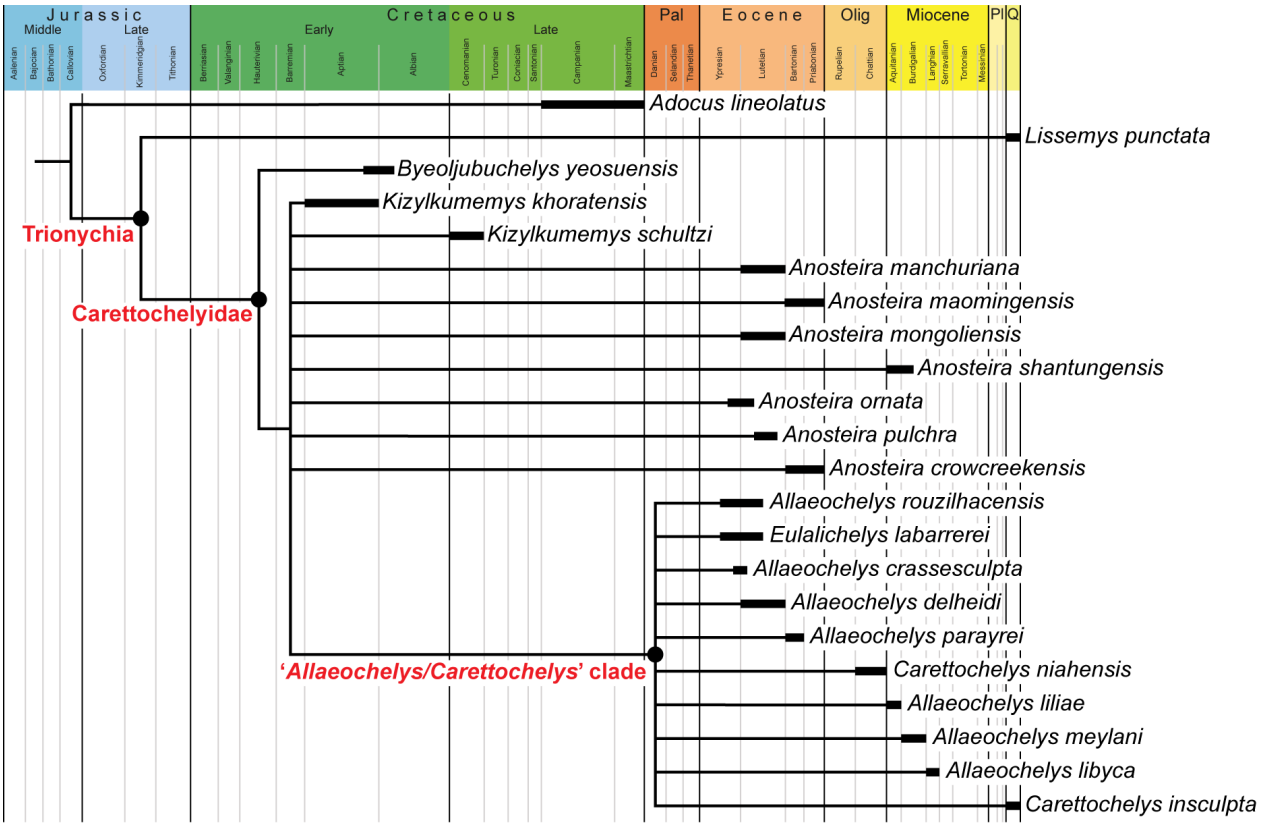


Figure 36. Strict consensus tree obtained from the parsimony analysis. Taxa are scaled to geological time.

In the 50% majority-rule tree, which is shown in Fig. 37, again without *Allaeochelys lingnanica* and *Allaeochelys magnifica*, the relationships are slightly better resolved, as *Anosteira shantungensis* is retrieved as an early branching carettochelyid in a less inclusive position than *Byeoljubuchelys yeosuensis*. *Kizylkumemys schultzi*, *Anosteira crowcreekensis*, *Anosteira ornata*, *Anosteira pulchra*, and *Anosteira mongoliensis* form a monophyletic subclade and this relationship is moderately well-supported as it is recovered in 61% of the most parsimonious trees. In this topology, *Carettochelyidae* are supported by the same two synapomorphies as in the strict consensus tree (see above). The next less inclusive clade (i.e. uniting *Anosteira shantungensis* and all other carettochelyids but *Byeoljubuchelys yeosuensis*) is supported by a single synapomorphy, the presence of a midline keel that extends onto the neurals (character 58, state 2). The following less inclusive clade, which unites all carettochelyids but *Byeoljubuchelys yeosuensis* and *Anosteira shantungensis*, is also supported by a single synapomorphy, the location of the neural reversal on neural I (character 51, state 0). Within the latter clade, the subclade formed by *Kizylkumemys schultzi*, *Anosteira crowcreekensis*, *Anosteira ornata*, *Anosteira pulchra*, and *Anosteira mongoliensis* is supported by two synapomorphies: a foramen posterius canalis carotici interni located near midlevel of the parabasisphenoid (character 26, state 0) and a strongly developed midline keel that resembles the dorsal fin of a shark (character 58, state 3). The '*Allaeochelys*/*Carettochelys*' clade is well-supported, albeit by slightly fewer synapomorphies relative to the strict consensus tree. TNT retrieved 11 synapomorphies rather than 15, in the 50% majority-rule tree: an elongate postorbital-quadratojugal suture (character 5, state 2), a shallow cheek emargination in the form of a small notch (character 8, state 1), the presence of a maxilla-quadratojugal contact (character 9, state 1), the absence of a quadratojugal-squamosal contact (character 10, state 0), the presence of an anterior foramen in the maxilla for the canalis alveolaris superior (character 16, state 1), a dorsoventral thickening of the quadrate at the level of the processus trochlearis oticum (character 34, state 1), elongate and pointy tuberacula basioccipitale (character 41, state 2), the absence of a subdivision of the triturating surface of the dentary (character 43, state 0), the absence of carapacial and plastral scute sulci (character 59, state 3), an entoplastron with lateral sides as long as posterior side (character 62, state 1), and a wide posterior plastral lobe (character 63, state 0). The only difference between the strict consensus and 50% majority-rule trees within the '*Allaeochelys*/*Carettochelys*' subclade is the placement of *Allaeochelys crassesculpta*, which is retrieved as the earliest branching member in the 50% majority-rule tree. This slightly more refined resolution and placement of *Allaeochelys crassesculpta* might be explained by the presence of a mosaic of characters in the latter taxon, which seem to be typical of either earlier branching representatives of *Kizylkumemys* spp. and *Anosteira* spp., or more advanced carettochelyids of the '*Allaeochelys*/*Carettochelys*' lineage. *Allaeochelys crassesculpta* notably shares with earlier branching

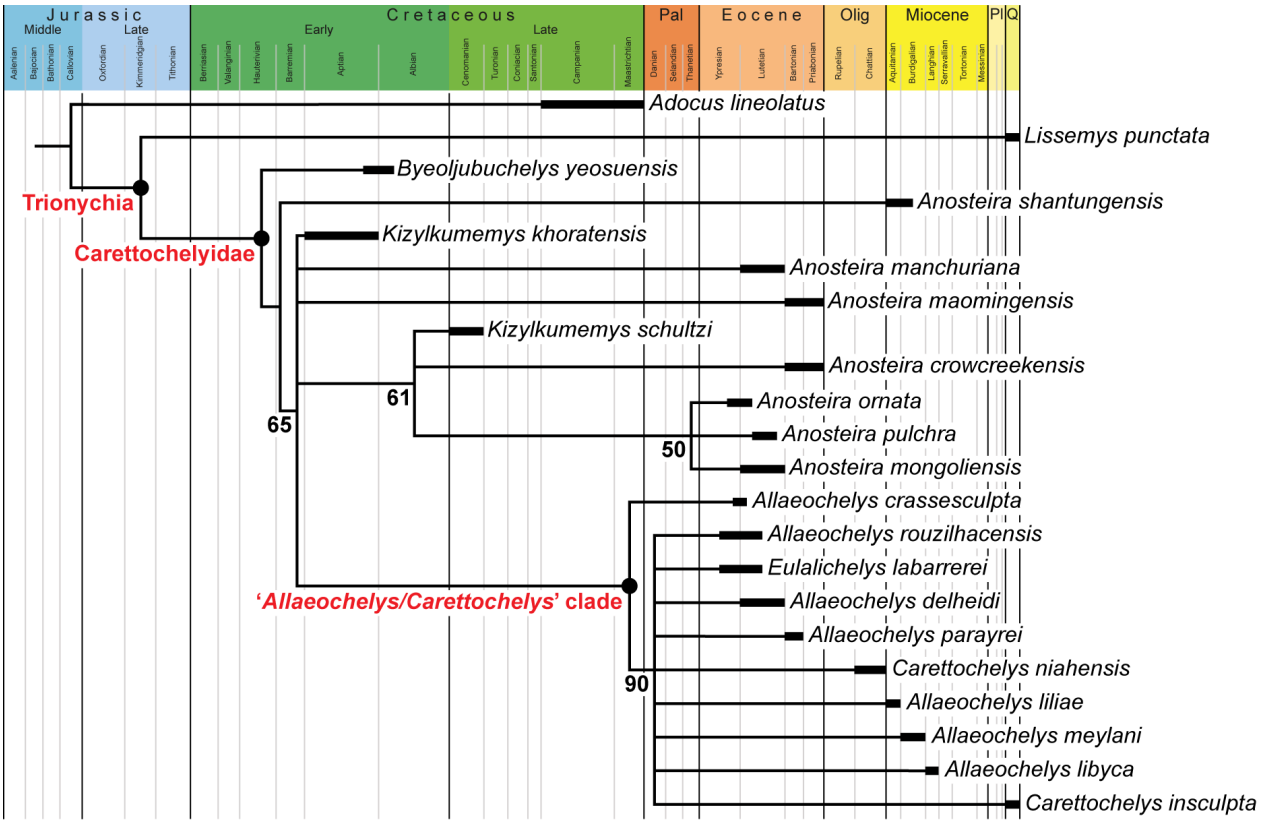


Figure 37. 50% Majority-Rule tree obtained from the parsimony analysis. Taxa are scaled to geological time.

carettochelyids a straight labial margin of the maxilla (wavy in '*Allaeochelys*/*Carettochelys*'), the absence of an enfolded ridge on the ventral surface of the pterygoid that covers the pterygoid fossa (present in '*Allaeochelys*/*Carettochelys*'), a more anteriorly located foramen posterius canalis carotici interni (generally more posteriorly located in '*Allaeochelys*/*Carettochelys*'), and a deeper and larger antrum postoticum (generally reduced or absent in '*Allaeochelys*/*Carettochelys*'), but shares with members of the '*Allaeochelys*/*Carettochelys*' subclade the presence of a contact between the maxilla and quadratojugal that prevents the jugal from contributing to the ventral margin of the cranium (contact is absent in *Anosteira maomingensis* and *Anosteira pulchra*), the absence of contact between the quadratojugal and squamosal above the cavum tympani (contact is present in *Anosteira maomingensis* and *Anosteira pulchra*), the complete absence of carapacial and plastral scute sulci (scute sulci remain present, to varying degrees, in *Byeoljubuchelys yeosuensis*, *Kizylkumemys* spp., and *Anosteira* spp.), an equilateral entoplastron (lateral sides longer than posterior sides in *Byeoljubuchelys yeosuensis* and *Anosteira manchuriana*, *Anosteira maomingensis*, and *Anosteira ornata*), and a wide posterior plastral lobe (narrow or reduced in *Byeoljubuchelys yeosuensis*, *Kizylkumemys* spp., and *Anosteira* spp.).

The tip-dating Bayesian phylogenetic analysis produced an extremely poorly resolved half compatibility tree. In this tree, *Byeoljubuchelys yeosuensis* and *Kizylkumemys khoratensis* are retrieved in a polytomy as the earliest branching carettochelyids, followed in a less inclusive position by *Kizylkumemys schultzi*, which itself is followed by a large polytomy that includes all remaining carettochelyid taxa. As this tree is highly uninformative, we choose to only show the all-compatibility tree herein, which, despite showing low support for most internal nodes and relationships, offers at least room for some comments and putative evolutionary insights (the log file of the Bayesian analysis, including the half compatibility tree, is available in Suppl. material 5). The all-compatibility tree is shown in Fig. 38.

In the all-compatibility tree, *Byeoljubuchelys yeosuensis* is retrieved as the earliest branching carettochelyid, followed in the next more internal node by *Kizylkumemys khoratensis*, and then *Kizylkumemys schultzi*, so that all Cretaceous carettochelyids are retrieved as the earliest branching members of *Carettochelyidae*. *Allaeochelys lingnanica* is retrieved in a less inclusive position than *Kizylkumemys schultzi* and this relationship is the last internal node with a high clade credibility value (i.e., 88). All remaining relationships are poorly supported with clade credibility values of 41 at most and typically only around 10 to 30. Nevertheless, it is notable that, in this topology, the remaining carettochelyid taxa are distributed into two distinct subclades. All *Anosteira* representatives are grouped together, forming a subclade that includes *Allaeochelys magnifica*, which is retrieved as the earliest branching representative of this subclade. The three North American taxa, *Anosteira ornata*, *Anosteira pulchra*, and *Anosteira crowcreekensis*, form a monophyletic subclade,

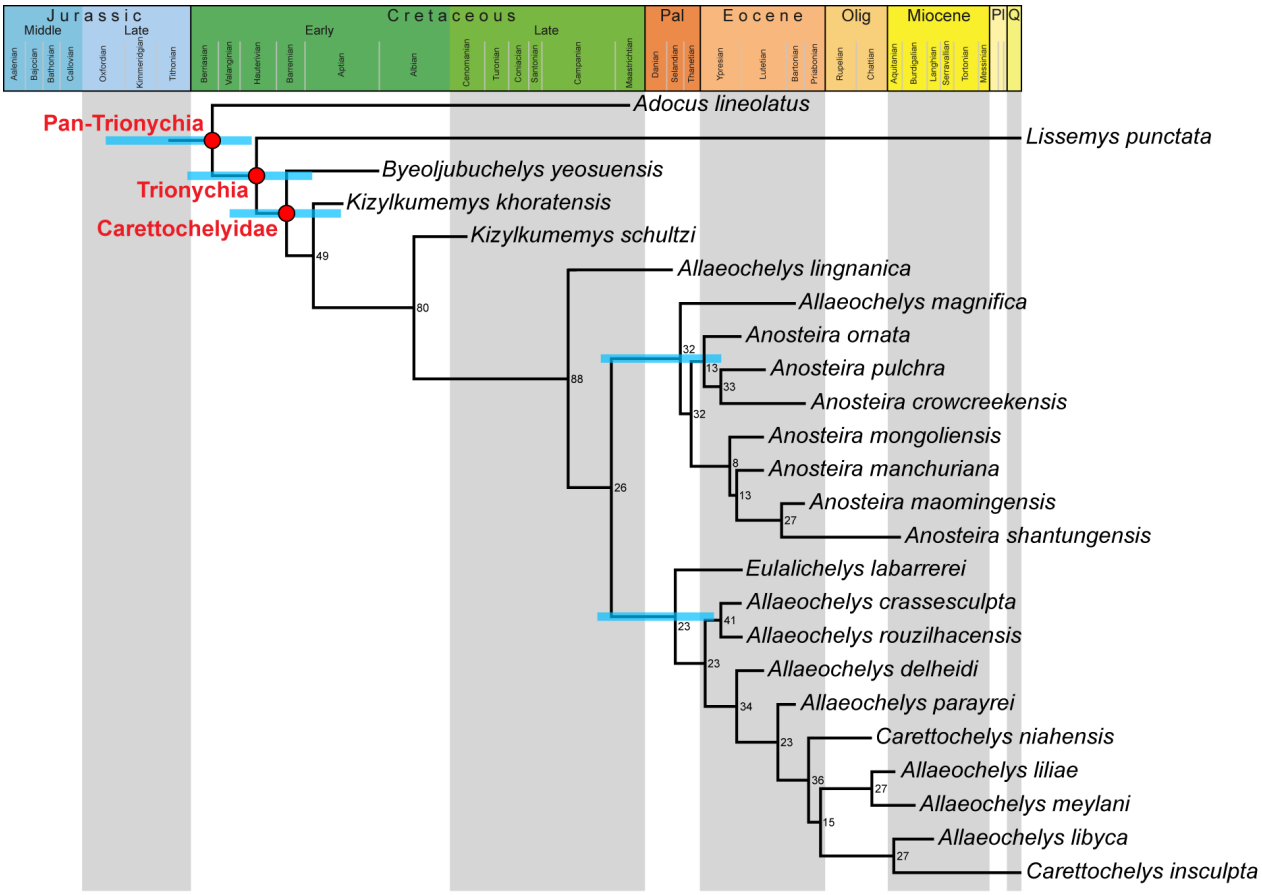


Figure 38. All-compatibility tree retrieved from the Markov Chain Monte Carlo Bayesian tip-dating phylogenetic analysis. The terminal end of the branch for each taxon is scaled to geological time. Major clades are shown with a 95% highest posterior density interval for the estimated node age, indicated by blue bars. Numbers show the clade credibility values. Unlabeled nodes indicate clade credibilities of 100%.

with *Anosteira pulchra* as sister taxon to *Anosteira crowcreekensis*, while all Asian taxa are grouped together as a sister-clade to the North American *Anosteira*. The placement of *Allaeochelys magnifica*, however, should be taken with caution, as this taxon could only be scored for a single character in our matrix. The second major carettochelyid subclade includes all European and African taxa, as well as *Allaeochelys liliae* from the Early Miocene of North America and *Carettochelys niahensis* from the Late Oligocene of Malaysia. Within this subclade, *Eulalichelys labarrerei* is retrieved as the earliest branching representative, followed by *Allaeochelys crassesculpta* as sister taxon to *Allaeochelys rouzilhacensis*.

While *Eulalichelys labarrerei* exhibits clear differences from *Allaeochelys crassesculpta* even if scored for a reduced number of characters, such as a strongly expanded posterior half of the triturating surface and a tall quadrate below the cavum tympani, *Allaeochelys crassesculpta* barely differs from *Allaeochelys rouzilhacensis* and we suspect the latter might be a junior synonym of *Allaeochelys crassesculpta*. In our matrix, the scorings of these terminals differ for three characters. In particular, following our own observations, we scored *Allaeochelys crassesculpta* as having a deep antrum postoticum. However, *Allaeochelys rouzilhacensis* was coded as having a deep or shallow antrum postoticum since we are unable to assess the depth of this feature in this taxon, based on the description of Godinot et al. (2018). The second feature that differs between *Allaeochelys crassesculpta* and *Allaeochelys rouzilhacensis* is the depth of the quadrate fossa. The quadrate fossa is small in *Allaeochelys crassesculpta*, but is described as large in *Allaeochelys rouzilhacensis* (Godinot et al. 2018). However, we cannot assess the size of this feature in the latter taxon, based on the illustrations in Godinot et al. (2018) as a posterior view of the cranium is not provided. The third feature contrasting *Allaeochelys crassesculpta* and *Allaeochelys rouzilhacensis* pertains to the expansion of the supraoccipital crest. In *Allaeochelys crassesculpta*, the supraoccipital crest is developed as a T-shaped expansion of bone that forms a mediolaterally broad sheet along its ventral aspect, extending for the entire length of the supraoccipital crest. However, as this feature is damaged in *Allaeochelys rouzilhacensis*, we scored this taxon as uncertain. Godinot et al. (2018) otherwise reported that the foramen posterius canalis carotici interni is located in the pterygoid posterior to the mandibular condyle in *Allaeochelys rouzilhacensis*, which indeed differs from the more anteriorly located foramen posterius canalis

carotici interni of *Allaeochelys crassesculpta*, but we are not able to replicate this observation with confidence in the former taxon due to damage that affects its basicranium. So, while these two terms are scored differently in our matrix, all reflect uncertainty. We thus urge μCT scanning and digital segmentation of the holotype cranium of *Allaeochelys rouzilhacensis* to clarify the matter.

The phylogenetic relationships of carettochelyids have been studied extensively since the taxonomic review of Joyce (2014). Based on the phylogenetic work of Joyce (2007), Havlik et al. (2014), Danilov et al. (2017a), Carbot-Chanona et al. (2020), and Kim et al. (2025) conducted phylogenetic analyses to accompany their investigation of the anatomy of several carettochelyid taxa. These analyses always yielded either poorly resolved trees, typically uniting '*Anosteira*' and '*Allaeochelys*/*Carettochelys*' taxa into distinct subclades albeit with unresolved ingroup relationships (Havlik et al. 2014; Danilov et al. 2017a; Carbot-Chanona et al. 2020), or phylogenetic trees with low support for most clades retrieved (Kim et al. 2025). Unfortunately, the phylogenetic relationships retrieved herein, despite the assemblage of a new matrix and transcription of many novel anatomical observations into morphological characters, are as poorly resolved as previous investigations. Although the recent use of μCT data and 3D bone-by-bone segmentation clearly improved our understanding of the cranial anatomy of carettochelyids, many carettochelyid taxa remain exclusively known by shell material and our studies so far only focused on members of the '*Allaeochelys*/*Carettochelys'* lineage, limiting the impact of our anatomical investigations to a subclade of advanced carettochelyids. Furthermore, the proportion of missing data in our morphological matrix is still remarkably high for most taxa, with more than 70% missing data for 15 of the 22 carettochelyids included in our study. Nearly 90% of trait data is missing for *Kizylkumemys khoratensis*, *Anosteira crowcreekensis*, *Anosteira manchuriana*, *Anosteira mongoliensis*, *Anosteira shantungensis*, *Allaeochelys lingnanica*, *Allaeochelys magnifica*, *Allaeochelys liliae*, and *Carettochelys niahensis*, which obviously greatly hinders the reconstruction of their relationships. We still believe that many of the newly created characters accurately describe variation among carettochelyids (e.g., contact between the crista cranii and descending process of the prefrontal, additional anterior fossa on the triturating surface, enfolded ridge of the pterygoid ventrally covering the pterygoid fossa, presence and depth of the antrum postoticum, general morphology and anatomy of the quadrate), but that more complete material is needed to have a better picture of carettochelyid anatomy. The classic adage 'more fossils are needed' seems to be more than ever true for carettochelyids, as a better understanding of the shell scute pattern, shell scute reduction, and changes in cranio-mandibular anatomy are crucially needed to untangle and better assess their evolutionary history.

Conclusions

Micro-computed laminography and tomography were used to perform the first detailed investigation of the osteology of *Allaeochelys crassesculpta* from the middle Eocene of Messel, Germany. Digital segmentations of several specimens were used to create high-resolution 3D reconstructions of the cranium, mandible, and fore- and hindlimb, which serve as a basis for detailed anatomical descriptions of this emblematic fossil turtle. The investigation of the anatomy of the appendicular skeleton shows that the forelimb of *Allaeochelys crassesculpta* has a similar morphology to that of the extant pig-nosed turtle *Carettochelys insculpta* and that it shares with the latter features associated with its unique locomotor mode, i.e. 'synchronous rowing,' suggesting this locomotor mode was already employed by *Allaeochelys crassesculpta* and likely evolved from the Late Cretaceous to Paleocene. We incorporated our new anatomical observations and recent insights into carettochelyid morphology into an updated phylogenetic matrix to evaluate their impact on carettochelyid relationships, which remain poorly resolved. Our phylogenetic analyses failed to improve topologies compared to previous studies and we primarily attribute these results to the great amount of missing data within our matrix, as many carettochelyids are known by incomplete or fragmentary material. While well-preserved fossils are critically needed to better understand the evolutionary history of carettochelyids, our work identifies numerous craniomandibular features that had not been reported previously and which document morphological variation among carettochelyids, potentially facilitating future comparative work regarding carettochelyids.

Acknowledgements

We are grateful to Angelica Cecilia and Thomas van de Kamp for technical support at the Karlsruher Institut für Technologie. We are deeply thankful to Léa C. Girard and Yuzheng Ke for sharing pictures, data, and 3D models of trionychids and adocusians. We are also grateful to Guilherme Hermanson for discussions about turtle humeri and assistance with humeral measurements. Minguk Kim is acknowledged for sharing 3D models of *Byeoljubuchelys yeosuensis*. We are also very grateful to Anika Vogel and Krister Smith for access and assistance in the SMF, to Torsten Wappler for access and assistance in the collections of the HLMD, to Julien Kimmig and Jannik Weidtke for access and assistance in the collections of the SMNK, and to Annelise Folie for access and assistance in the collections of the IRSNB. We also thank the United States National Science Foundation for funding the CIPRES online platform. We are grateful to the editor Florian Witzmann and the reviewers Brent Adrian and Igor Danilov for their careful review of the present manuscript and comments, which greatly improved its quality.

References

Adrian B, Holroyd PA, Hutchison JH, Townsend KEB (2020) Additional records and stratigraphic distribution of the middle Eocene carettochelyid turtle *Anosteira pulchra* from the Uinta Formation of Utah, North America. PeerJ 8: e9775. https://doi.org/10.7717/peerj.9775

Albrecht PW (1967) The cranial arteries and cranial arterial foramina of the turtle genera *Chrysemys*, *Sternotherus*, and *Trionyx*: a comparative study with analysis of possible evolutionary implications. Tulane Studies in Zoology 14(3): 81–99.

Alonso Santiago L, Alonso Andrés L (2005) Diferencias anatómicas entre dos formas de *Allaeochelys* del Eoceno de Corrales (Zamora, España). Nueva especie de tortuga, *Allaeochelys jimenezi* nov. sp. Studia Geologica Salmanticensia 41: 103–126.

Alonso Santiago L, Alonso Andrés L, Jiménez Fuentes E (2008) Primer espaldar en conexión anatómica de *Allaeochelys casasecai*. Cazurra: nuevo yacimiento del Eoceno de Zamora (España). Studia Geologica Salamanticensia 44: 177–186.

Ascarrunz E, Joyce WG (2024) A plastron fragment reveals a previously unrecorded turtle species in the Eocene of Messel Pit, Germany. Fossil Record 27(2): 259–264. https://doi.org/10.3897/fr.27.132374

Ascarrunz E, Claude J, Joyce WG (2021) The phylogenetic relationships of geoemydid turtles from the Eocene Messel Pit Quarry: a first assessment using methods for continuous and discrete characters. PeerJ 9: e11805. https://doi.org/10.7717/peerj.11805

Bai B, Wang YQ, Li Q, Wang HB, Mao FY, Gong YX, Meng J (2018) Biostratigraphy and diversity of Paleogene perissodactyls from the Erlian Basin of Inner Mongolia, China. American Museum Novitates 2018(3914): 1–60. https://doi.org/10.1206/3914.1

Batsch AJGC (1788) Versuch einer Anleitung, zur Kenntniß und Geschichte der Thiere und Mineralien. Akademische Buchhandlung, Jena, 528 pp. https://doi.org/10.5962/bhl.title.79854

Baur G (1891) On the relations of *Carettochelys*, Ramsay. American Naturalist 25(295): 631–639. https://doi.org/10.1086/275363

Bergounioux F-M (1931) Le genre *Allaeochelys* et ses caractères adaptifs. Bulletin de la Société d'histoire naturelle de Toulouse 61: 161–181.

Broin F de (1977) Contribution à l'étude des chéloniens: Chéloniens continentaux du Crétacé et du Tertiaire de France. Mémoires du Muséum National d'histoire naturelle (Nouvelle série, Series C, Sciences de la terre 38), Paris (Éditions du museum), 366 pp.

Cadena E (2015) A global phylogeny of Pelomedusoides turtles with new material of *Neochelys franzeni* Schleich, 1993 (Testudines, Podocnemididae) from the middle Eocene, Messel Pit, of Germany. PeerJ 3: e1221. https://doi.org/10.7717/peerj.1221

Cadena E (2016) *Palaeoamyda messeliana* nov. comb. (Testudines, Pan-Trionychidae) from the Eocene Messel Pit and Geiseltal localities, Germany, taxonomic and phylogenetic insights. PeerJ 4: e2647. https://doi.org/10.7717/peerj.2647

Cadena E, Joyce WG, Smith KT (2018) Turtles – armored survivalists. In: Smith KT, Schaal SFK, Habersetzer J (Eds) Messel – An Ancient Greenhouse Ecosystem. Senckenberg-Bücher, Frankfurt am Main, 149–158.

Carbot-Chanona G, Rivera-Velázquez G, Jiménez-Hidalgo E, Reynoso VH (2020) The first Pan-Carettochelys turtle in the Neogene of the American continent and its paleobiogeographical relevance. Journal of South American Earth Sciences 104: 102925. https://doi.org/10.1016/j.jsames.2020.102925

Cheng Z-W (1961) A new anosterine turtle from Linchu, Shantung. Vertebrata Palasiatica 1961: 273–276.

Chow MM, Liu C-I (1955) A new anosterine turtle from Maoming, Kwangtung. Acta Palaeontologica Sinica 3: 275–282.

Clark J (1932) A new anosteirid from the Uinta Eocene. Annals of the Carnegie Museum of Natural History 21: 161–170. https://doi.org/10.5962/p.214559

Claude J, Tong H (2004) Early Eocene testudinoid turtles from Saint-Papoul, France, with comments on the early evolution of modern Testudinoidea. Oryctos 5: 3–45.

Cope ED (1868) On the origin of genera. Proceedings of the Academy of Natural Sciences of Philadelphia 20(1868): 242–300.

Danilov IG, Obraztsova EM (2015) Taxonomic position of *Oxemys gutta* Nessov, 1977, a problematic turtle from the Upper Cretaceous of Uzbekistan, and basisphenoid morphology in some groups of Late Mesozoic turtles of Asia. Paleontological Journal 49(3): 279–292. https://doi.org/10.1134/S003103011503003X

Danilov IG, Obraztsova EM, Chen W, Jianhua J (2017a) The cranial morphology of *Anosteira maomingensis* (Testudines, Pan-Carettochelys) and the evolution of pan-carettochelyid turtles. Journal of Vertebrate Paleontology 37(4): e1335735. https://doi.org/10.1080/02724634.2017.1335735

Danilov IG, Syromyatnikova EV, Sukhanov VB (2017b) Subclass Testudinata. In: Lopatin AV, Zelenkov NV (Eds) Fossil vertebrates of Russia and adjacent countries. Fossil Reptiles and Birds. Part 4. GEOS, Moscow, 27–395. [in Russian]

Delfino M, Fritz U, Sánchez-Villagra MR (2010) Evolutionary and developmental aspects of phalangeal formula variation in pig-nose and soft-shelled turtles (Carettochelyidae and Trionychidae). Organisms Diversity and Evolution 10: 69–79. https://doi.org/10.1007/s13127-010-0019-x

de Stefano G (1902) Un nuovo chelonide della famiglia Trionychidae appartenente all'eocene francese. Bollettino della Società Geologica Italiana 21(2): 389–397.

Dollo L (1886) Première note sur les chéloniens du Bruxellien (Éocène moyen) de la Belgique. Bulletin du Musée royal d'histoire naturelle de Belgique 4: 75–100.

Evers SW, Al Iawati Z (2024) Digital skull anatomy of the Oligocene North American tortoise *Stylemys nebrascensis* with taxonomic comments on the species and comparisons with extant testudinids of the *Gopherus-Manouria* clade. Swiss Journal of Palaeontology 143(1): 12. https://doi.org/10.1186/s13358-024-00311-y

Evers SW, Barrett PM, Benson RB (2019) Anatomy of *Rhinochelys pulchriceps* (Protostegidae) and marine adaptation during the early evolution of chelonioids. PeerJ 7: e6811. https://doi.org/10.7717/peerj.6811

Evers SW, Ponstein J, Jansen MA, Gray JA, Fröbisch J (2022) A systematic compendium of turtle mandibular anatomy using digital dissections of soft tissue and osteology. The Anatomical Record 306(6): 1228–1303. https://doi.org/10.1002/ar.25037

Ezcurra MD, Nesbitt SJ, Bronzati M, Dalla Vecchia FM, Agnolin FL, Benson RBJ, Egli FB, Cabreira SF, Evers SW, Gentil AR, Irmis RB, Martinelli AG, Novas FE, da Silva LR, Smith ND, Stocker MR, Turner AH, Langer MC (2020) Enigmatic dinosaur precursors bridge the gap to the origin of Pterosauria. Nature 588(7838): 445–449. https://doi.org/10.1038/s41586-020-3011-4

Faragó T, Gasilov S, Emslie I, Zuber M, Helfen L, Vogelgesang M, Baumbach T (2022) Tofu: a fast, versatile and user-friendly image processing toolkit for computed tomography. Synchrotron Radiation 29(3): 916–927. https://doi.org/10.1107/S160057752200282X

Foth C, Evers SW, Joyce WG, Volpato VS, Benson RBJ (2019) Comparative analysis of the shape and size of the middle ear cavity of turtles reveals no correlation with habitat ecology. Journal of Anatomy 235: 1078–1097. https://doi.org/10.1111/joa.13071

Gaffney ES (1972) An illustrated glossary of turtle skull nomenclature. American Museum Novitates 2486: 1–33.

Gaffney ES (1990) The comparative osteology of the Triassic turtle *Proganochelys*. Bulletin of the American Museum of Natural History 194: 1–263.

Gaffney ES, Tong H, Meylan PA (2006) Evolution of the side-necked turtles: The families Bothremydidae, Euraxemydidae, and Araripemydidae. Bulletin of the American Museum of Natural History 2006(300): 1–698. https://doi.org/10.1206/0003-0090(2006)300[1:EOTSTT]2.0.CO;2

Gill T (1889) A remarkable tortoise. Annual Report of the Board of Regents of the Smithsonian Institution, for the Year Ending June 30th 1887 Part 1: 509–511.

Gilmore CW (1931) Fossil turtles of Mongolia. Bulletin of the American Museum of Natural History 59: 213–257.

Godinot M, Labarrère HP, Erfurt J, Franzen JL, Lange-Badré B, Lapparent de Broin FD, Vidalenc D (2018) Un nouveau gisement à vertébrés éocènes, Rouzilhac (MP 10-11), dans la série molassique d'Issel (Aude, France). Revue de Paléobiologie 37(1): 141–333.

Goloboff PA, Morales ME (2023) TNT version 1.6, with a graphical interface for MacOS and Linux, including new routines in parallel. Cladistics 39(2): 144–153. https://doi.org/10.1111/cla.12524

Gramann F (1956) Schildkröten aus dem Melanienton von Borken (Niederhessische Senke) (*Trionyx*, *Anosteira*). Notizblatt des hessischen Landesamtes für Bodenforschung zu Wiesbaden 84: 16–20.

Groessens-Van Dyck MC (1978) Etude des tortues et des alligatores de l'Eocène moyen de Messel conservés au musée de la ville de Dortmund. Dortmunder Beiträge zur Landeskunde, Naturwissenschaftliche Mitteilungen 12: 79–95.

Haines RW (1946) A revision of the movements of the forearm in tetrapods. Journal of Anatomy 80: 1–11.

Harrassowitz H (1922) Die Schildkrötengattung *Anosteira* von Messel bei Darmstadt und ihre stammesgeschichtliche Bedeutung. Abhandlungen der Hessischen Geologischen Landesanstalt 6: 132–239.

Havlik PE, Joyce WG, Böhme M (2014) *Allaeochelys libyca*, a new carettochelyine turtle from the Middle Miocene (Langhian) of Libya. Bulletin of the Peabody Museum of Natural History 55(2): 201–214. https://doi.org/10.3374/014.055.0207

Hay OP (1906) On two interesting genera of Eocene turtles, *Chisternon* Leidy and *Anosteira* Leidy. Bulletin of the American Museum of Natural History 22: 155–160.

Hay OP (1908) The Fossil Turtles of North America. Carnegie Institute of Washington publication 75: 1–568. https://doi.org/10.5962/bhl.title.21745

He H, Deng C, Pan Y, Deng T, Luo Z, Sun J, Zhu R (2011) New $^{40}Ar/^{39}Ar$ dating results from the Shanwang Basin, eastern China: Constraints on the age of the Shanwang Formation and associated biota. Physics of the Earth and Planetary Interiors 187(1–2): 66–75. https://doi.org/10.1016/j.pepi.2011.05.002

Heaphy LJ (1990) The ecology of the pig nosed turtle, *Carettochelys insculpta*, in Northern Australia. PhD Thesis, University of New South Wales, Sydney, Australia.

Hendrickson JR (1980) The ecological strategies of sea turtles. American Zoologist 20(3): 597–608. https://doi.org/10.1093/icb/20.3.597

Hermanson G, Arnal FA, Szczygielski T, Evers SW (2024) A systematic comparative description of extant turtle humeri, with comments on humerus disparity and evolution based on fossil comparisons. The Anatomical Record 307(11): 3437–3505. https://doi.org/10.1002/ar.25450

Hervet S (2004) Systématique du groupe «*Palaeochelys* sensu lato – *Mauremys*» (Chelonii, Testudinoidea) du Tertiaire d'Europe occidentale: principaux résultats. Annales de Paléontologie 90: 13–78. https://doi.org/10.1016/j.annpal.2003.12.002

Hutchison JH, Holroyd PA, Ciochon RL (2004) Preliminary report on Southeast Asia's oldest Cenozoic turtle fauna from the late middle Eocene Pondaung Formation, Myanmar. Asiatic Herpetological Research 10: 38–52.

Hutchison JH, Westgate JW (2024) Reptiles from the late Eocene Jackson group of Arkansas. Paleobios 41(4): 1–11. https://doi.org/10.5070/P941438517

Jiménez Fuentes E (1971) Primer *Pseudotrionyx* español: *Allaeochelys casasecai*, nov. sp. del Luteciense de Corrales (Zamora). Estudios Geologicos 27: 153–166.

Jiménez Fuentes E (1992) Quelonios fósiles de Castilla y León. In: Jiménez Fuentes E (Ed.) Vertebrados fósiles de Castilla y León. Museo de Salamanca, Salamanca, 71–100.

Joyce WG (2007) Phylogenetic relationships of Mesozoic turtles. Bulletin of the Peabody Museum of Natural History 48(1): 3–102. https://doi.org/10.3374/0079-032X(2007)48[3:PROMT]2.0.CO;2

Joyce WG (2014) A review of the fossil record of turtles of the clade Pan-Carettochelys. Bulletin of the Peabody Museum of Natural History 55(1): 3–33. https://doi.org/10.3374/014.055.0102

Joyce WG, Gauthier JA (2004) Palaeoecology of Triassic stem turtles sheds new light on turtle origins. Proceedings of the Royal Society of London, Series B: Biological Sciences 271(1534): 1–5. https://doi.org/10.1098/rspb.2003.2523

Joyce WG, Micklich N, Schaal SF, Scheyer TM (2012) Caught in the act: the first record of copulating fossil vertebrates. Biology Letters 8(5): 846–848. https://doi.org/10.1098/rsbl.2012.0361

Joyce WG, Parham JF, Lyson TR, Warnock RC, Donoghue PC (2013) A divergence dating analysis of turtles using fossil calibrations: an example of best practices. Journal of Paleontology 87(4): 612–634. https://doi.org/10.1666/12-149

Joyce WG, Sterli J, Chapman SD (2014) The skeletal morphology of the solemydid turtle *Naomichelys speciosa* from the Early Cretaceous of Texas. Journal of Paleontology 88(6): 1257–1287. https://doi.org/10.1666/14-002

Joyce WG, Volpato VS, Rollot Y (2018) The skull of the carettochelyid turtle *Anosteira pulchra* from the Eocene (Uintan) of Wyoming and the carotid canal system of carettochelyid turtles. Fossil Record 21(2): 301–310. https://doi.org/10.5194/fr-21-301-2018

Kim M, Jung J, Joyce WG, Park JI, Jung HY, Jo H, Huh M (2025) A new, Early Cretaceous carettochelyid turtle from South Korea provides insights into softshell evolution and aquatic ecology. Swiss Journal of Palaeontology 144(1): 75. https://doi.org/10.1186/s13358-025-00415-z

Krahl A (2021) The locomotory apparatus and paraxial swimming in fossil and living marine reptiles: comparing Nothosauroidea, Plesiosauria, and Chelonioidea. Paläontologische Zeitschrift 95(3): 483–501. https://doi.org/10.1007/s12542-021-00563-w

Krahl A, Werneburg I (2023) Deep-time invention and hydrodynamic convergences through amniote flipper evolution. The Anatomical Record 306(6): 1323–1355. https://doi.org/10.1002/ar.25119

Krahl A, Lipphaus A, Sander MP, Mafucci F, Hochscheid S, Witzel U (2020) Humerus osteology, myology, and finite element structure analysis of Cheloniidae. The Anatomical Record 303(8): 2177–2191. https://doi.org/10.1002/ar.24311

Krumbiegel G (1962) Die Fossilfundstellen der mitteleozänen Braunkohle des Geiseltales. Wissenschaftliche Zeitschrift der Martin-Luther-Universität Halle-Wittenberg 11: 745–762.

Krumbiegel G, Rüffle L, Haubold H (1983) Das eozäne Geiseltal. A. Ziemsen Verlag, Wittenberg Lutherstadt, Germany, 227 pp.

Leidy J (1873) Contributions to the extinct Vertebrata fauna of the western territories. In: Hayden FV (Ed.) Report of the United States Geological Survey of the Territories, Volume 1, Part 1. Govt. Print. Off, Washington, 1–358.

Lepage T, Bryant D, Philippe H, Lartillot N (2007) A general comparison of relaxed molecular clock models. Molecular Biology and Evolution 24(12): 2669–2680. https://doi.org/10.1093/molbev/msm193

Lewis PO (2001) A likelihood approach to estimating phylogeny from discrete morphological character data. Systematic Biology 50(6): 913–925. https://doi.org/10.1080/106351501753462876

Lydekker R (1889) Catalogue of the Fossil Reptilia and Amphibia in the British Museum (Natural History). Part 3, Chelonia. Longmans, London, 239 pp.

Marzola M (2019) The Late Triassic vertebrate fauna of the Jameson Land Basin, East Greenland: description, phylogeny, and paleoenvironmental implications. PhD thesis, Universidade Nova de Lisboa, Lisbon, Portugal.

Meylan PA (1987) The phylogenetic relationships of soft-shelled turtles (Family Trionychidae). Bulletin of the American Museum of Natural History 186: 1–101.

Miller MA, Pfeiffer W, Schwartz T (2010) Creating the CIPRES Science Gateway for Inference of Large Phylogenetic Trees. In: 2010 Gateway Computing Environments Workshop (GCE), New Orleans LA (USA), November 2010. IEEE Computer Society, Washington, 1–8. https://doi.org/10.1109/GCE.2010.5676129

Motani R, Vermeij GJ (2021) Ecophysiological steps of marine adaptation in extant and extinct non-avian tetrapods. Biological Reviews 96(5): 1769–1798. https://doi.org/10.1111/brv.12724

Nessov LA (1976) On the systematics and phylogeny of two clawed turtles. Vestnik Leningradeskogo Universiteta 9: 7–17.

Nessov LA (1977) A new genus of pitted-shelled turtle from the Upper Cretaceous of Karakalpakia. Paleontological Journal 10: 96–107.

Nessov LA (1986) Some Late Mesozoic and Paleocene turtles of Soviet Middle Asia. Studia Geologica Salmanticensia 2: 7–22.

Nessov LA (1987) On some Mesozoic turtles of the Soviet Union, Mongolia and China, with comments on systematics. Studia Palaeocheloniologica 2: 87–102.

Noulet JB (1867) Nouveau genre de tortues fossiles proposé sous le nom d'*Allaeochelys*. Mémoires de l'Académie Impériale des Sciences, Inscriptions et Belles-Lettres de Toulouse 5: 172–177.

Pereira AG, Sterli J, Moreira FRR, Schrago CG (2017) Multilocus phylogeny and statistical biogeography clarify the evolutionary history of major lineages of turtles. Molecular Phylogenetics and Evolution 113: 59–66. https://doi.org/10.1016/j.ympev.2017.05.008

Ramsay EP (1887) On a new genus and species of fresh water tortoise from the Fly River, New Guinea. Proceedings of the Linnaean Society of New South Wales 2nd series 1: 158–162. https://doi.org/10.5962/bhl.part.29176

Reinach AV (1900) Schildkrötenreste im Mainzer Tertiärbecken und in benachbarten ungefähr gleichaltrigen Ablagerungen. Abhandlungen der Senckenbergischen Naturforschenden Gesellschaft 28: 11–35.

Rivera AR, Rivera G, Blob RW (2013) Forelimb kinematics during swimming in the pig-nosed turtle, *Carettochelys insculpta*, compared with other turtle taxa: rowing versus flapping, convergence versus intermediacy. Journal of Experimental Biology 216(4): 668–680. https://doi.org/10.1242/jeb.079715

Rollot Y, Evers SW, Joyce WG (2021) A review of the carotid artery and facial nerve canal systems in extant turtles. PeerJ 8: e10475. https://doi.org/10.7717/peerj.10475

Rollot Y, Evers SW, Joyce WG (2024a) A digital redescription of the Middle Miocene (Langhian) carettochelyid turtle *Allaeochelys libyca*. Fossil Record 27(1): 13–28. https://doi.org/10.3897/fr.27.115046

Rollot Y, Evers SW, Ferreira GS, Girard LC, Werneburg I, Joyce WG (2024b) Skull osteology, neuroanatomy, and jaw-related myology of the pig-nosed turtle *Carettochelys insculpta* (Cryptodira, Trionychia). The Anatomical Record 307(9): 2966–3020. https://doi.org/10.1002/ar.25411

Rollot Y, AbdelGawad MK, Hamdan MA, El-Barkooky AN, Hassan SM, Joyce WG (2025) Trionychian turtles from the Early Miocene (Burdigalian) Moghra Formation, Egypt, including a new species of Carettochelyidae. Swiss Journal of Palaeontology 144(1): 30. https://doi.org/10.1186/s13358-025-00358-5

Ronquist F, van der Mark FP, Huelsenbeck JP (2009) Bayesian phylogenetic analysis using Mr Bayes. In: Lemey P, Salemi M, van Damme AM (Eds) The phylogenetic handbook: a Practical Approach to Phylogenetic Analysis and Hypothesis Testing. Cambridge University Press, Cambridge, 210–266. https://doi.org/10.1017/CBO9780511819049.009

Schaal SFK, Ziegler W (1992) Messel—an insight into the history of life and of the earth. Clarendon Press, Oxford, 322 pp.

Scheyer TM, Danilov IG, Sukhanov VB, Syromyatnikova EV (2014) The shell bone histology of fossil and extant marine turtles revisited. Biological Journal of the Linnean Society 112(4): 701–718. https://doi.org/10.1111/bij.12265

Schleich HH (1993) *Neochelys franzeni* n. sp., the first pleurodiran turtle from Messel. Kaupia, Darmstädter Beiträge zur Naturgeschichte 3: 15–21.

Smith KT, Schaal SFK, Habersetzer J (2018) Messel: An ancient greenhouse ecosystem. Schweizerbart Science Publishers, Stuttgart, 355 pp.

Sterli J, de la Fuente MS, Rougier GW (2007) Anatomy and relationships of *Palaeochersis talampayensis*, a Late Triassic turtle from Argentina. Palaeontographica Abteilung A 281: 1–61. https://doi.org/10.1127/pala/281/2007/1

Sun QG, Collinson ME, Li CS, Wang YF, Beerling DJ (2002) Quantitative reconstruction of palaeoclimate from the Middle Miocene Shanwang flora, eastern China. Palaeogeography, Palaeoclimatology, Palaeoecology 180(4): 315–329. https://doi.org/10.1016/S0031-0182(01)00433-3

Szczygielski T, Piechowski R (2023) Limb anatomy of the Triassic turtles: appendicular osteology of *Proterochersis* (Testudinata,

Proterochersidae). Zoological Journal of the Linnean Society 199(3): 771–831. https://doi.org/10.1093/zoolinnean/zlad057

Tada S, Tsuihiji T, Morgan DJ, Witmer LM, Werneburg I (2025) Evolution of the rostral vasculature in turtles. Swiss Journal of Palaeontology 144(1): 64. https://doi.org/10.1186/s13358-025-00403-3

Thomson RC, Spinks PQ, Shaffer HB (2021) A global phylogeny of turtles reveals a burst of climate-associated diversification on continental margins. Proceedings of the National Academy of Sciences 118(7): e2012215118. https://doi.org/10.1073/pnas.2012215118

Tong H, Suteethorn V, Claude J, Buffetaut E, Jintasakul P (2005) The turtle fauna from the Khok Kruat Formation (Early Cretaceous) of Thailand. In: Proceedings of the International Conference on Geology, Geotechnology and Mineral Resources of Indochina (GEOINDO 2005), Khon Kaen (Thailand), November 2005. Khon Kaen University, Khon Kaen, 610–614.

Tong H, Zhang JY, Li JL (2010) *Anosteira maomingensis* (Testudines: Carettochelyidae) from the Late Eocene of Maoming, Guangdong, southern China: New material and re-description. Neues Jahrbuch fur Geologie und Palaontologie Abhandlungen 256(3): 279–290. https://doi.org/10.1127/0077-7749/2010/0053

TTWG [Turtle Taxonomy Working Group: Rhodin AGJ, Iverson JB, Fritz U, Gallego-García N, Georges A, Shaffer HB, van Dijk PP] (2025) Turtles of the World: Annotated Checklist and Atlas of Taxonomy, Synonymy, Distribution, and Conservation Status (10th Ed.). Chelonian Research Monographs 10: 1–575. https://doi.org/10.3854/crm.10.checklist.atlas.v10.2025

Waite ER (1905) The osteology of the New Guinea turtle (*Carettochelys insculpta* Ramsay). Records of the Australia Museum 6: 110–118. https://doi.org/10.3853/j.0067-1975.6.1905.994

Walker WF (1973) The locomotor apparatus of Testudines. In: Gans C, Parsons TS (Eds) Biology of the Reptilia. Volume 4. Morphology D. Academic Press, London and New York, 1–100.

Walther WG (1922) Die Neu-Guinea Schildkröte *Carettochelys insculpta* Ramsay. Nova Guinea (Zoology) 13: 607–704. https://doi.org/10.5962/bhl.title.11842

Wang YQ, Meng J, Jin X (2012) Comments on Paleogene localities and stratigraphy in the Erlian basin, Nei Mongol, China. Vertebrata Palasiatica 50(3): 181–203.

Wang Y, Li Q, Bai B, Jin X, Mao F, Meng J (2019) Paleogene integrative stratigraphy and timescale of China. Science China Earth Sciences 62(1): 287–309. https://doi.org/10.1007/s11430-018-9305-y

Weitzel K (1949) Neue Wirbeltiere (Rodentia, Insectivora, Testudinata) aus dem Mitteleozän von Messel bei Darmstadt. Abhandlungen der Senckenbergischen Naturforschenden Gesellschaft 480: 1–24.

Werneburg I (2011) The cranial musculature of turtles. Palaeontologia Electronica 14(2): 1–99.

White AW, Archer M, Hand SJ, Godthelp H, Gillespie AK (2023) A new broad-snouted fossil carettochelyid turtle from a previously unknown Caenozoic deposit in Sarawak, Malaysia. Alcheringa: An Australasian Journal of Palaeontology 47(2): 1–10. https://doi.org/10.1080/03115518.2023.2243503

Young CC, Chow MC (1962) Some reptilian fossils from the "red beds" of Kwangtung and Chekiang. Vertebrata Palasiatica 6(2): 130–135.

Yu J, Pang X, Fu W, Hilton J, Liang M, Jiang Z, Zhao X, Qiao W, Shi S, Zhang D, Cao H, Jia H, Wang Y, Hu X, Zhang R (2021) A high-resolution timescale for the Miocene Shanwang diatomaceous shale lagerstätte (China): development of Wavelet Scale Series Analysis for cyclostratigraphy. Geosciences Journal 25(5): 561–574. https://doi.org/10.1007/s12303-020-0055-2

Zangerl R (1947) A new anosteirine turtle from Manchuria. Fieldiana Geology 10: 13–21. https://doi.org/10.5962/bhl.title.3270

Zhang C (2016) Molecular clock dating using MrBayes. arXiv.

Zuber M, Laaß M, Hamann E, Kretschmer S, Hauschke N, van de Kamp T, Baumbach T, Koenig T (2017) Augmented laminography, a correlative 3D imaging method for revealing the inner structure of compressed fossils. Scientific Reports 7(1): 41413. https://doi.org/10.1038/srep41413

Zug GR (1971) Buoyancy, locomotion, morphology of the pelvic girdle and hindlimb, and systematics of cryptodiran turtles. Miscellaneous publications (University of Michigan Museum of Zoology) 142: 1–98.

Additional information

Conflict of interest

The authors have declared that no competing interests exist.

Ethical statement

No ethical statement was reported.

Artificial Intelligence (AI) use

The authors accept full responsibility for the content of the manuscript, including the disclosure of any use of AI.
No AI tools were used in the preparation of this manuscript.

Funding

This work was funded by the SNSF grants 200021_207377 and P500PB_230713.

Author contributions

YR photographed the specimens, digitally segmented the specimens, generated the 3D models, prepared the figures, performed the phylogenetic analyses, and wrote the text. MZ performed µCT and µCL scanning and wrote the text. EH performed µCT and µCL scanning and wrote the text. WGJ photographed the specimens, prepared the figures, and wrote the text.

Author ORCIDs

Y. Rollot https://orcid.org/0000-0002-2020-9456
M. Zuber https://orcid.org/0000-0002-2429-6171
E. Hamann https://orcid.org/0000-0002-0623-9069
W.G. Joyce https://orcid.org/0000-0003-4726-2449

Data availability

The µCT scans and associated 3D models that served for this study are available at MorphoSource in the project entitled 'Rollot et al. 2026. CT scans and 3D models of *Allaeochelys crassesculpta*' (https://www.morphosource.org/projects/000839347).

Supplementary material 1

Additional specimens

Authors: Yann Rollot, Marcus Zuber, Elias Hamann, Walter G. Joyce
Data type: pdf
Explanation note: This supplementary file contains pictures of additional specimens that we used to study the anatomy of *Allaeochelys crassesculpta* and score our morphological matrix.
Copyright notice: This dataset is made available under the Open Database License (http://opendatacommons.org/licenses/odbl/1.0). The Open Database License (ODbL) is a license agreement intended to allow users to freely share, modify, and use this Dataset while maintaining this same freedom for others, provided that the original source and author(s) are credited.
Link: https://doi.org/10.3897/fr.29.195537.suppl1

Supplementary material 2

List of phylogenetic characters

Authors: Yann Rollot, Marcus Zuber, Elias Hamann, Walter G. Joyce
Data type: docx
Explanation note: This supplementary file contains the lists of taxa and characters used in our study.
Copyright notice: This dataset is made available under the Open Database License (http://opendatacommons.org/licenses/odbl/1.0). The Open Database License (ODbL) is a license agreement intended to allow users to freely share, modify, and use this Dataset while maintaining this same freedom for others, provided that the original source and author(s) are credited.
Link: https://doi.org/10.3897/fr.29.195537.suppl2

Supplementary material 3

Mesquite matrix

Authors: Yann Rollot, Marcus Zuber, Elias Hamann, Walter G. Joyce
Data type: nex
Explanation note: This supplementary file contains our morphological matrix made in Mesquite.
Copyright notice: This dataset is made available under the Open Database License (http://opendatacommons.org/licenses/odbl/1.0). The Open Database License (ODbL) is a license agreement intended to allow users to freely share, modify, and use this Dataset while maintaining this same freedom for others, provided that the original source and author(s) are credited.
Link: https://doi.org/10.3897/fr.29.195537.suppl3

Supplementary material 4

MrBayes file

Authors: Yann Rollot, Marcus Zuber, Elias Hamann, Walter G. Joyce
Data type: txt
Explanation note: This supplementary file contains the MrBayes file used to run the Bayesian tip-dating analysis.
Copyright notice: This dataset is made available under the Open Database License (http://opendatacommons.org/licenses/odbl/1.0). The Open Database License (ODbL) is a license agreement intended to allow users to freely share, modify, and use this Dataset while maintaining this same freedom for others, provided that the original source and author(s) are credited.
Link: https://doi.org/10.3897/fr.29.195537.suppl4

Supplementary material 5

Log file Bayesian analysis

Authors: Yann Rollot, Marcus Zuber, Elias Hamann, Walter G. Joyce
Data type: txt
Explanation note: This supplementary file contains the log file resulting from the Bayesian tip-dating analysis.
Copyright notice: This dataset is made available under the Open Database License (http://opendatacommons.org/licenses/odbl/1.0). The Open Database License (ODbL) is a license agreement intended to allow users to freely share, modify, and use this Dataset while maintaining this same freedom for others, provided that the original source and author(s) are credited.
Link: https://doi.org/10.3897/fr.29.195537.suppl5